SLAC-PUB-944
(TH) and (EXP)
August 1971

INCLUSIVE PROCESSES AT HIGH TRANSVERSE MOMENTUM†

S. M. Berman, J. D. Bjorken and J. B. Kogut
Stanford Linear Accelerator Center, Stanford University, Stanford, California 94305

ABSTRACT

We calculate the distribution of secondary particles C in processes $A+B \to C+$ anything at very high energies when (1) particle C has transverse momentum p_T far in excess of 1 GeV/c, (2) the basic reaction mechanism is presumed to be a deep-inelastic electromagnetic process, and (3) particles A, B and C are either lepton (ℓ), photon (γ), or hadron (h). We find that such distribution functions possess a scaling behavior, as governed by dimensional analysis. Furthermore, the typical behavior even for A, B and C all hadrons, is a power law decrease in yield with increasing p_T, implying measurable yields at NAL of hadrons, leptons, and photons produced in 400 GeV pp collisions even when the observed secondary-particle p_T exceeds 8 GeV/c. There are similar implications for particle yields from $e^{\pm} - e^{-}$ colliding-beam experiments and for hadron yields in deep-inelastic electroproduction (or neutrino processes). Among the processes discussed in some detail are $\ell\ell \to h$, $\gamma\gamma \to h$, $\ell h \to h$, $\gamma h \to h$, $\gamma h \to \ell$, as well as $hh \to \ell$, $hh \to \gamma$, $hh \to W$, and $W \to h$, where W is the conjectured weak-interaction intermediate boson. The basis of the calculation is an extension of the parton model. The new ingredient necessary to calculate the processes of interest is the inclusive probability for finding a hadron emerging from a parton struck in a deep-inelastic collision. This probability is taken to have a form similar to that generally presumed for finding a parton in an energetic hadron. We study the dependence of our conclusions on the validity of the

---

† Work supported by the U. S. Atomic Energy Commission.

(Submitted to Phys. Rev.)

parton model, and conclude that they follow mainly from kinematics, duality arguments a la Bloom and Gilman, and the crucial assumption that multiplicities in such reactions grow slowly with energy. The picture we obtain generalizes the concept of deep-inelastic process, and predicts the existence of "multiple cores" in such reactions. We speculate on the possibility of strong, non-electromagnetic deep-inelastic processes. If such exist, our predictions of particle yields for $hh \to h$ could be up to 4 orders of magnitude too low, and for $\gamma h \to h$ and $hh \to \gamma$ up to 2 orders of magnitude too low.

I. Introduction

It is often said that the fundamental reason for building particle accelerators of increasingly higher energy is to probe matter at increasingly small distances.[1] However, what is said is often not what is done. The connection between longitudinal momentum and longitudinal distances is, if anything, the opposite; as the energy increases the important longitudinal distances increase.[2] The connection between transverse momentum and transverse distances, indeed, is likely to be that given by the Heisenberg uncertainty relations. Nevertheless, the extensively studied two-body and quasi-two-body processes are dominated by impact parameters of order 1 fermi, independent of incident energy. Distributions of secondary particles in strong interactions are dominated by low $p_T \lesssim 0.5$ GeV corresponding again to the same distances ~ 1 F, of the order of the physical extension of the particles. Indeed, these distributions fall so precipitously with increasing p_T, with empirical fits typically of the form $\exp(-a p_T)$ or $\exp(-b p_T^2)$, that one is not sure whether there will be measurable production of very high p_T (> 5 GeV) particles in strong interaction processes.

On the other hand, high-energy tests of pure quantum electrodynamics do exhibit a sensitivity to small distances, and more recently deep inelastic electroproduction experiments and high-energy neutrino processes have opened up a new class of processes which indeed appear to be sensitive to small transverse distances. It is the purpose of this paper to explore as systematically as possible the implications of this class of processes in hadron-hadron and other kinds of collisions. Specifically, we examine inclusive processes initiated by high-energy hadron, photon, or lepton projectiles in which the observed particle has large transverse momentum, i.e., greater than several GeV. If the exponential transverse momentum dependence

associated with pure hadronic interactions remains valid for somewhat larger values of transverse momentum, then the differential cross sections will decrease sufficiently so that electromagnetic interactions could become important. In fact, we find that the known deep-inelastic electromagnetic mechanism is sufficient to provide a population of the high p_T region of phase space which falls off (at sufficiently high energy) roughly as a power, not as an exponential of p_T.

In order to estimate the contribution to inclusive processes from an electromagnetic effect, we use an extension of the parton model[3] where the basic process is the electromagnetic interaction between the constituent partons. While the parton model is, to be sure, of dubious quality, we believe that most of our qualitative conclusions follow (within, say, a factor 10 accuracy) from two general considerations. These are, firstly, the overall kinematics; and secondly, the presumption that the mean multiplicity for these high-p_T processes grows slowly with increasing incident energy, final $p_{\|}$ and p_T; say, more slowly than a power of these variables. This will be discussed in more detail in Section IV and in the conclusion of the paper.

To compare with the extrapolations of the hadronic reactions, we consider as an example the inclusive process A + B → C + anything where A, B, and C are hadrons. The graphs in Figure 1 compare our parton model calculation of the differential cross-section to observe particle C at 90° in the c.m. system with a conservative extrapolation[4] ($d\sigma/dp_T^2 \sim e^{-6p_T}$) of the purely hadronic background for an N.A.L. condition of $s = 800\ \text{GeV}^2$. In particular, the comparison shows that in the neighborhood of $p_T \approx 5$ GeV there should be an abrupt flattening of the slope of the observed cross-section. For smaller angles this could occur at an even smaller value of p_T.

Of course, the extrapolation in p_T of the form $\exp(-6p_T)$ to such large values could be quite erroneous. On the other hand, the electromagnetic process must be present and thus our results based on electromagnetic contributions may be viewed as a lower bound on the real cross-sections at large p_T.

It may even be that the electromagnetic contribution to such a process is never dominant. Such a case exists in the model of Wu and Yang[5] which describes elastic proton-proton scattering data reasonably well. In the Wu-Yang model, partons interact strongly with each other via a current-current coupling, such as would arise from exchange of a $J = 1$ "gluon". If such an analogy to the vector electromagnetic interaction should hold true for the inelastic case,[6] then because of the slow fall-off with respect to q^2 of the electromagnetic structure function a similar weak dependence would be expected for the analogous large momentum transfer hadronic reaction. In this case we would expect similar distributions to the examples given here, but increased in order of magnitude by a factor of $\lesssim 10^4$ since the factor of α^2 would be absent. This emphasizes our point of view that the purely electromagnetic processes provide only lower limits to the real differential cross-sections.

However, while the interpretation of inelastic electron scattering supports the fact that the photon-parton couplings exist, only vague speculations can be made regarding the pure strong parton vertices. We will thus confine ourselves to only those processes where the scattering vertices occur through photon emission or absorption and thus expect only a lower limit on the possible size of these processes.

In any case, this lower limit shows a reasonable magnitude for the expected large transverse momentum cross-section, indicating that study of these processes

is not only of considerable theoretical interest but also definitely within the realm of experimental feasibility.

The main body of this paper is divided into four sections. In Section II we introduce the parton model used in the calculations and generalize the notion of deep inelastic processes to encompass a wide class of scattering processes. Our parton model is specified by two differential probabilities: the first, called F(x), describes the constitution of an energetic hadron as an ensemble of partons and a second, G(x), describes the decay of a parton isolated in phase space into a system of hadrons. The existence and properties of G are motivated on the basis of our experience with hadron-hadron processes. Two forms for G are proposed which should bracket the true function which will be measured in colliding beam experiments.

In Section III we sketch the calculations of the inclusive differential cross-sections of interest. We find that they can be written in a universal form consisting of two factors, $4\pi\alpha^2/p_T^4$ characteristic of single photon exchange and a form factor $\mathscr{F}(-\frac{u}{s}, -\frac{t}{s})$. The numerous calculations are organized into several subsections according to the presence of hadrons in the initial or final states. We make detailed numerical estimates of these form factors and present the results in numerous graphs. In a final subsection we consider weak processes, including the production of the W boson, which might be observable in hadron-hadron collisions.

In Section IV we discuss in more detail the physics underlying our assumptions concerning the function G. Invoking two familiar sum rules and a generalization of an argument due to Bloom and Gilman,[7] we motivate our guesses for the functional form of G which were used in the numerical estimates. We finally consider the sensitivity of our predictions to the possible failure of these various speculative ideas.

In Section V we summarize our conclusions and major experimental predictions.

Details underlying the calculations contained in Sections II-IV are contained in four lengthy appendices.

II. Definition and Properties of Deep Inelastic Processes from the Parton Viewpoint

In the parton model an energetic physical particle is viewed at any instant as composed of a collection of pointlike constituents, the partons. They are the quanta of H_0, where H_0 is the kinetic energy portion of the hamiltonian. For our purposes, a physical photon or physical lepton is predominantly composed of one parton, the bare photon or bare lepton, with perturbation theory sufficient to obtain the corrections. The parton composition of hadrons is certainly more complex. From the observed behavior of hadron collisions , i. e. the approximate dx/x dependence of the inclusive differential cross-section, the probability of finding a hadronic parton in some region of momentum-space is presumed to be roughly constant per unit of log $p_{\|}$ and rapidly decreasing as p_T increases.

In a collision process the parton distributions of target and projectile are modified by their interaction. In quantum electrodynamics, the coulomb interaction between charged partons predominates at high energy. Also possible is low momentum transfer exchange of partons in those regions of phase space where the parton distributions of target and projectile overlap.

In hadron processes, Feynman[3] views this latter mechanism as the predominant interaction in ordinary collisions. On the other hand, we shall define deep inelastic processes as those relatively rare processes where at least one parton is produced in the final state a large distance in momentum-space from all initial-state target or projectile partons. In particular, this requires such a final parton to have high p_T, since for small p_T longitudinal phase-space is generally well-populated with partons. Because deep inelastic processes are rare, it is reasonable to assume that one elementary process involving a very small

number of initial-state partons is responsible for production of high p_T partons in the final state. Division of one parton into two high-p_T partons is not possible if the partons are light or massless (as we shall assume) except as a highly virtual intermediate state. Therefore, the simplest elementary process is high-p_T parton-parton scattering, and the simplest coupling[8] the point Yukawa coupling of Figure 2. This celebrated diagram is to be taken here with point vertices, and only when the exchanged p_T is large and the net amplitude small.

It will prove convenient to catalog these possible elementary processes on the basis of the types of partons (bare leptons, bare photons, hadronic partons) present in a particular diagram. The possible diagrams are shown in Figure 3. In each case the vertices and propagators are taken as pointlike. Processes (a) and (b) are pure quantum electrodynamics of leptons and photons in lowest order. Process (c) exists to the extent that the parton model is a correct (or at least kinematically adequate) description of deep inelastic electroproduction. Existence of (d) is assured from the existence of (c). Process (e), parton Compton scattering, requires the concept of a highly virtual hadronic parton, but otherwise no unknown couplings. Thus, while less compelling than (a)-(d), its existence is at least plausible. Processes (f) and (g) require strong pointlike trilinear couplings of partons to each other. These are presumably the unrenormalized vertices and may possibly be $\infty^{-1} = 0$. These elementary processes have no or one power of e rather than two for the others. They would, if present, be expected to dominate various high p_T processes.

We have little evidence on which hadronic partons exist (indeed, whether the concept is correct). We feel it is relatively futile at this stage to speculate wildly about the nature of strong parton-parton interactions. Therefore, we consider mainly the elementary electromagnetic processes (a)-(e). The results we obtain, as

mentioned earlier, should be regarded only as rough lower bounds, especially for those processes for which one can identify possible mechanisms of the type (f) and (g).

After defining the fundamental scattering event in the infinite momentum frame as the interaction between the constituent partons, the calculation requires two additional elements. These are the connections between the initial physical state and the parton system, and, after the interaction, the return of the parton system to the observed final physical state.

The first is the probability that a hadron of type a is a collection of partons, one of which, with fraction x of the total momentum, interacts with a photon. This probability is given by $(F_{ai}(x)/e_i^2 x)$ for the i^{th} parton of charge e_i. The function $F_{ai}(x)$ depends in general on both the type of parton and hadron. For inelastic electron scattering where the hadron is a proton, it was shown by Feynman[9,10] that summing over all partons gives

$$\sum_i F_{pi}(x) = \nu W_2^{(p)}(x) \qquad \text{(II.1)}$$

where $x = Q^2/2m\nu$.

The second element is the determination of the probability of finding a hadron of a certain four momentum in the final state, given the configuration of partons produced by the deep-inelastic process. Here we make the following guesses, motivated by the reciprocal analogy to the nature of the first element:

1. If a deep-inelastic parton of high-p_T has four-momentum p_μ ($p^2 \approx 0$), then any member of the final system of hadrons of high p_T has four-momentum $p'_\mu \approx xp_\mu$; in other words, there is a limited p_T exchange between the parton and such observed hadrons.

2. The differential probability, dP_{ic}, of finding a hadron c associated with the produced parton i and having fraction x of the parton longitudinal momentum is

$$dP_{ic} = \frac{dx}{x} G_{ic}(x) \tag{II.2}$$

This probability is independent of the rest of the environment; e.g., the incident energy, incident particles, or other partons.

These guesses, which we expect the reader to find somewhat arbitrary, are motivated in Section IV, where, in addition, many properties of the function G are derived.

Two of these properties which are useful in suggesting a definite functional form for G are the following sum rules:

1. Integrating $G_{ic}(x)/x$ over all x counts the contribution of the hadrons of type c repeatedly $\bar{n}_{i,c}$ times over and thus,

$$\int_{m_c/E_0}^{1} G_{ic}(x) \frac{dx}{x} = \bar{n}_{i,c} \ , \tag{II.3}$$

where $\bar{n}_{i,c}$ is the mean multiplicity of particle type c of mass m_c emerging from parent parton of type i and energy E_0.

2. Conservation of energy in the parton decay into hadrons requires

$$\sum_c \int G_{ic}(x)\, dx = 1 \tag{II.4}$$

independent of i (the type of parton).

The latter sum rule suggests the approximation that G_{ic} is independent of i, the type of parton. Further, since in our calculations we allow any hadron to be

observed, we define

$$\sum_c G_{ic}(x) = G_i(x) \approx G(x) \ . \qquad \text{(II.5)}$$

Intuitively we expect G(x) to be similar to the longitudinal momentum distributions in purely hadronic inclusive reactions in which a leading particle is observed. For example, the longitudinal momentum distribution G(x)/x of the observed proton in P + P → P + anything is essentially flat for a large range in x. Further, we show in Section 4 that a power law behavior in (1-x) is expected for G(x) when x is in the vicinity of unity. This is qualitatively the same kind of functional dependence as νW_2 and so, in the absence of any more precise knowledge, we will take G(x) proportional to νW_2 with the constant of proportionality chosen to satisfy (II.4). This approximation should be sufficient for the kind of order of magnitude estimations of interest here.

We test the sensitivity of our calculations to the explicit choice of the function G(x) by considering a second possibility of the form G(x) = 2(1-x) which is also commensurate with our intuition, the sum rules and the power law nature of G(x) near the endpoint x = 1. In the numerical estimates here this choice can yield nearly an order of magnitude larger values for our expected cross-sections and thus gives an estimation of the sensitivity of our results to G(x).

We will see in Sections III and IV that if one accepts our parton model, the function G(x) can be directly related to the colliding beam experiments and to electroproduction of hadrons. The data which will soon be available will eliminate our uncertainty concerning the character of G(x).

To give experimental support for the existence of the function G(x) as well as to test for the presence of strong parton-parton interactions, it is important to search

for other experimental consequences of deep-inelastic processes. We briefly digress to discuss what general characteristics they would probably have. Consider proton-proton scattering in the center-of-mass frame under CERN ISR conditions. In phase-space a typical initial-state parton distribution is shown in Fig. 4a. Suppose the partons with longitudinal momenta -9 and +16 suffer a deep-inelastic scatter through 90^{o} in their center-of-mass, producing intermediate state (b) in Fig. 4. This state may further evolve through final-state interactions which predominantly would not be expected to also be deep-inelastic. At the very minimum, the isolated high-p_T partons will communicate with the wee partons by cascade emission of partons. If only low p_T mechanisms are involved in the cascade, the resultant parton-four-momenta (approximately null) will be proportional to the parent parton four momentum. The result is Fig. 4c. The hadron distribution would also be similar to Fig. 4c, and the loci of all phase-points in momentum space of secondary hadrons in such an event would lie along three straight lines with perhaps a dispersion Δp_T of order 0.3 GeV. This is, in cosmic-ray parlance, the phenomenon of "multiple cores." Measurements of the total energy of the cores and their angles determine the center-of-mass energy of the parton-parton system and also the center-of-mass scattering angle. Such information would shed much light on the nature of the most basic elements of strong interaction dynamics, despite the fact that the parton charge, spin, etc., are not directly observed.

III. Cross-Sections for the Various Processes

A. Kinematics

In the limit of high energy and high transverse momentum, we assume that we may neglect all hadron masses, parton masses, and parton or hadron transverse-momentum exchange in the structure factors F and G, as discussed in Section II. Thus no intrinsic dimensions remain and all cross-sections we discuss will exhibit a scaling behavior. It behooves us to introduce scaling variables in terms of which the cross-section formulae are concisely written. With the notation of Figure 5, we choose

$$x_1 = -\frac{(p_b - p_c)^2}{(p_a + p_b)^2} = \frac{-u}{s}$$
$$x_2 = -\frac{(p_a - p_c)^2}{(p_a + p_b)^2} = \frac{-t}{s} \qquad \text{(III.1)}$$

which satisfy

$$x_1 + x_2 \leq 1 . \qquad \text{(III.2)}$$

In the laboratory frame (b at rest)

$$x_1 = \frac{E_c}{E_a} , \qquad \text{(III.3)}$$

and thus x_1 is the customary longitudinal fraction. In any collinear frame

$$x_1 x_2 = \frac{p_T^2}{s} \qquad \text{(III.4)}$$

where p_T is the transverse momentum of the produced particle c. Also (for any collinear frame)

$$\frac{x_1}{x_2} = \frac{E_b + |p_b| \cos\theta}{E_a - |p_a| \cos\theta} = \begin{cases} \cot^2 \frac{\theta}{2} & \text{(center of mass frame)} \\ (M_p/2E_a) \csc^2 \frac{\theta}{2} & \text{(laboratory frame)} \end{cases} \tag{III.5}$$

where θ is the angle between $\underset{\sim}{p}_a$ and $\underset{\sim}{p}_c$.

From dimensional analysis, and in accord with our specific calculations, we write for the laboratory differential cross-section for the inclusive process a + b— c + anything

$$\pi E_c \frac{d\sigma}{d^3 p_c} = E_c \frac{d\sigma}{dp_T^2 \, dp_{\| c}} = \frac{4\pi\alpha^2}{p_T^4} \mathscr{F}(x_1, x_2) \tag{III.6a}$$

or

$$\frac{d\sigma}{dx_1 dx_2} = \frac{4\pi\alpha^2}{s x_1^2 x_2^2} \mathscr{F}(x_1, x_2) \tag{III.6b}$$

Tabulation of $\mathscr{F}(x_1, x_2)$ then determines the value of the cross-sections at all incident energies, secondary energies, and angles. We consider these processes a + b → c + anything in turn for the generic cases of a, b, and c either γ, lepton (e or μ) or hadron. The 18 such cases are classified according to four categories discussed in subsections B through E. A few comments regarding weak-interaction processes are reserved for subsection F. To guide the reader through the maze of processes, cross-section formulae, and curves to come, the following table of contents outlines which high-p_T processes are discussed in detail:

Subsection B: no hadrons in initial or final states:

(i) We write down $\mathcal{F}(x_1, x_2)$ for the processes $\gamma\gamma \to \ell\bar{\ell}$, $\gamma\ell \to \gamma\ell$, $\ell\ell \to \ell\ell$.

(ii) We show that Compton-scattering of an electron at high p_T is feasible and interesting in high-energy $e^- - e^\pm$ storage ring experiments.

Subsection C: no hadrons in the initial state; hadron in the final state:

(i) $e^+e^- \to h$ (+ anything) via one-photon exchange.

(ii) $\gamma\gamma \to h$ via parton-antiparton pair production; remotely possible to measure in $e^- - e^\pm$ storage rings.

(iii) $e\gamma \to e$ + anything, or $e\gamma \to h$ + anything; this is deep-inelastic electroproduction from a photon target[11]; again it is possibly measurable in $e^- - e^\pm$ storage rings.

Subsection D: one and only one hadron in the initial state:

(i) Hadron distributions in deep-inelastic electroproduction.

(ii) Hadron distributions in deep-inelastic Compton scattering.

(iii) $\gamma h \to \mu$ + anything; the virtual muon flux in the incident photon state Coulomb-scatters deep-inelastically from the target.

Subsection E: two hadrons in the initial state:

(i) $hh \to \ell$ (+ anything); this is the experiment of Christensen et al.[12], as interpreted by Drell and Yan.[13]

(ii) $hh \to \gamma$; this is similar to (i) but with the parton-antiparton pair annihilating into two photons.

(iii) $hh \to h$ via deep-inelastic photon exchange.

Subsection F: weak processes and W-production:

(i) Total cross-section for hh → W + anything via Drell-Yan[13] parton-antiparton annihilation mechanism.

(ii) Decay of W into hadrons and leptons.

B. No Hadrons in the Initial or Final State

This class includes well-known tests of pure quantum electrodynamics; the dominant reactions are

$$\gamma + \gamma \to \ell + \bar{\ell} \tag{III.7}$$

$$\gamma + \ell \to \gamma + \ell \tag{III.8}$$

$$\ell + \ell \to \ell + \ell \tag{III.9}$$

$$\gamma + \gamma \to \gamma + \text{anything} \tag{III.10}$$

Reaction (III.10) is not very interesting, being dominated by routine radiative corrections to (III.7). For future convenience we record $\mathscr{F}(a\,b \to c)$ for reactions (III.7), (III.8), and (III.9) in our scaling variables x_1, x_2:

$$\mathscr{F}(\ell\bar{\ell} \to \gamma) = \mathscr{F}(\gamma\gamma \to \ell) = \tfrac{1}{2} x_1 x_2 (1-2x_1x_2)\delta(x_1 + x_2 - 1) \tag{III.11}$$

$$\mathscr{F}(\gamma\ell \to \gamma) = \tfrac{1}{2} x_1 x_2^2 (1 + x_1^2)\delta(x_1 + x_2 - 1) \tag{III.12}$$

$$\mathscr{F}(\gamma\ell \to \ell) = \tfrac{1}{2} x_1^2 x_2 (1 + x_2^2)\delta(x_1 + x_2 - 1) \tag{III.13}$$

$$\mathscr{F}(e\mu \to e) = \tfrac{1}{2} x_1^2 (1 + x_1^2)\delta(x_1 + x_2 - 1) \tag{III.14}$$

(Coulomb diagram)

$$\mathscr{F}(e\bar{e} \to \mu) = \tfrac{1}{2} x_1^2 x_2^2 (1 - 2x_1x_2)\delta(x_1 + x_2 - 1) \tag{III.15}$$

(annihilation diagram)

Reactions (III.7) and (III.9) are prominent channels in e^+e^- colliding beam experiments and need no discussion here. Reaction (III.8) is of interest in high energy e^+e^- or e^-e^- colliding beam experiments as a test of the electron propagator in the timelike region (e.g. production of e* resonances). The quantum electrodynamic cross-section for γe elastic scattering through angles greater than 45^o in the center-of-mass frame is

$$\sigma_{\gamma e} \cong \frac{2\pi\alpha^2}{s} \log\frac{\sqrt{2}+1}{\sqrt{2}-1} \cong \frac{2.5\times 10^{-31}\,\mathrm{cm}^2}{s(\mathrm{GeV})^2} \tag{III.16}$$

Upon taking $s = (10\ \mathrm{GeV})^2$ and a probability of 4% that an electron contain a sufficiently energetic Weizsacker-Williams virtual photon to initiate the process, this still gives a cross-section of order $10^{-34}\ \mathrm{cm}^2$; perhaps within the limits of feasibility.

For later convenience we also record the result of folding (III.12) over the equivalent-photon spectrum[14] $\epsilon(dk/k)\left[1-\frac{k}{E}+\frac{1}{2}\left(\frac{k}{E}\right)^2\right]$ carried by an electron. The single photon spectrum for process (III.12) then has the form

$$\begin{aligned}\mathscr{F}_{ee\to(e)\gamma\to\gamma+\ldots} &= \epsilon\int_0^1 \frac{du}{u}\left(1-u+\frac{u^2}{2}\right)\left\{\mathscr{F}_{\gamma e\to\gamma e}\left(\frac{x_1}{u},x_2\right)+(x_1\longleftrightarrow x_2)\right\} \\ &= \epsilon x_2^2(1-x_2+\tfrac{1}{2}x_2^2)\left[1-\left(\frac{x_1}{1-x_2}\right)+\tfrac{1}{2}\left(\frac{x_1}{1-x_2}\right)^2\right]+(x_1\longleftrightarrow x_2)\end{aligned} \tag{III.17}$$

where $\epsilon = \frac{2\alpha}{\pi}\log\frac{E_{eff}}{m_e}$ is the probability of finding a virtual photon in the electron, typically ~ 0.04. Equation (III.17) is plotted in Figure 6 for $\epsilon = 0.04$.

C. No hadrons in the initial state; hadron in the final state

This class of reactions includes

$$\ell + \bar{\ell} \rightarrow h + \text{anything (via single photon exchange)} \tag{III.18}$$

$$\gamma + \gamma \rightarrow h + \text{anything} \tag{III.19}$$

$$\ell + \gamma \rightarrow h + \text{anything} \tag{III.20}$$

They are all of interest, and we discuss then in turn. Process (III.18), illustrated in Figure 7, is of great importance in the current $e^+ - e^-$ colliding beam experiments. We may compute the cross-section in our simple model[15] by convoluting the point cross-section for production of a parton-antiparton pair ($q\bar{q}$) with the probability dP_{ia} for production of a hadron of type a possessing four-momentum xp_μ in dx from a parton i of four-momentum p_μ. As discussed in Section II, this differential probability is assumed to be given by

$$dP_{ia} = \frac{dx}{x} G_{ia}(x) \tag{III.21}$$

independent of the rest of the environment in the reaction. In the center-of-mass frame, the point cross-section is

$$\frac{d\sigma}{d\Omega} = \frac{\pi\alpha^2}{s} (1 + \cos^2\theta) \tag{III.22}$$

Therefore the cross-section for process (III.18) for production of a hadron of type a and momentum p is

$$p\frac{d\sigma_a}{d\Omega\, dp} = \frac{\pi\alpha^2}{s}(1+\cos^2\theta)\sum_i e_i^2\, G_{ia}\left(\frac{2p}{\sqrt{s}}\right) \tag{III.23}$$

and where e_i is the charge of the i^{th} parton (or antiparton) type, assumed here to be spin $\frac{1}{2}$. In general, for the purposes of estimating yields we shall in this paper

a) sum over hadron channels a

b) assume the only charged partons have quark quantum numbers

c) assume $\sum_a G_{ia}(x)$ is independent of the parent parton type i.

As discussed in Sections II and IV, this third assumption is made more plausible by the observation that, independent of i,

$$\sum_a \int_0^1 dx\, G_{ia}(x) = 1 \tag{III.24}$$

Thus we hereafter put

$$\sum_a G_{ia}(x) \cong G(x) \tag{III.25}$$

Equation (III.23) can easily be cast in the standard form (III.6), with the form factor $\mathscr{F}$ given by

$$\mathscr{F}(x_1, x_2) = \tfrac{1}{2}\sum_i e_i^2 \frac{x_1^2 x_2^2}{(x_1+x_2)^4}(x_1^2+x_2^2)\, G(x_1+x_2) \tag{III.26}$$

$$\left(\sum_i e_i^2 = 4/3;\ \text{the sum is over q and } \bar{q}\right)$$

In order to continue, a form is needed for G(x). As mentioned in Section II, and as will be further discussed in Section IV, we have the conditions

$$\int_{m/E}^{1} \frac{dx}{x} G(x) = \bar{n} = \text{mean multiplicity of jet}$$

$$\int_{0}^{1} dx\, G(x) = 1 \tag{III.27}$$

$$G(x) \sim (1-x)^{p} \qquad x \approx 1$$

where p is related to the form factors F_i for exclusive processes in such a way that p probably lies in the range 1 to 3. We therefore choose as extreme cases

$$G(x) = 2(1-x) \tag{III.28}$$

$$G(x) = 6.84\, F(x) \tag{III.29}$$

with

$$F(x) = 0.56\,(1-x)^3 + 2.2\,(1-x)^4 - 2.6\,(1-x)^5 \tag{III.30}$$

an empirical fit to the electroproduction data.[16]

With these choices $\mathscr{F}_{\ell\bar{\ell}\to h}(x_1, x_2)$ is plotted in Figure 8 and Figure 9. In addition, we plot, in Figure 10 and Figure 11, $p(d\sigma/d\Omega\, dp)_{cm}$ at $\theta_{cm} = 90^{o}$ for center-of-mass energies of 5 and 8 GeV, along with the background of low p_T secondaries computed in Appendix D. This background is estimated according to ρ-dominance; the hadron production expected from ρ^{o}-ρ^{o} collisions is multiplied by $(250)^{-2}$ and folded into the Weizsacker-Williams virtual photon spectrum as in (III.35).

The process $\gamma + \gamma \rightarrow h + \text{anything}$, (III.19), is measurable in principle in colliding-beam experiments at high energies via the collision of the virtual photons carried by the leptons. As shown in Figure 12, parton-antiparton pair production, $\gamma + \gamma \rightarrow q + \bar{q}$, provides a mechanism for producing hadrons of high p_T. To compute the production cross-section consequent from the mechanism of Figure 12, we observe that for the lepton processes

$$\left(\frac{d\sigma}{d\Omega_{cm}}\right)_{e^+e^- \leftrightarrow \gamma\gamma} \Big/ \left(\frac{d\sigma}{d\Omega_{cm}}\right)_{e^+e^- \leftrightarrow \mu^+\mu^-} = \frac{4}{\sin^2\theta_{cm}} \tag{III.32}$$

Therefore, from (III.23) and (III.25)

$$\left(p\,\frac{d\sigma}{d\Omega_{cm}dp}\right)_{\gamma\gamma \rightarrow h} = \frac{4\pi\alpha^2}{s}\left(\frac{1+\cos^2\theta_{cm}}{\sin^2\theta_{cm}}\right)\left(\sum_i e_i^4\right) G\left(\frac{2p}{\sqrt{s}}\right)$$

$$\left(\sum_i e_i^4 = 4/9\right) \tag{III.33}$$

or in terms of the form-factor

$$\mathscr{F}(x_1, x_2)_{\gamma\gamma \rightarrow h} = \tfrac{1}{2}\,\frac{x_1 x_2}{(x_1 + x_2)^2}\,(x_1^2 + x_2^2)\sum_i e_i^4\, G(x_1 + x_2) \tag{III.34}$$

$\mathscr{F}$ is plotted in Figures 13 and 14, along with a modified form in Figures 15 and 16 suitable for colliding-beam experiments, obtained by folding (III.34) over the spectrum of equivalent photons, as described in Appendix A.

$$\mathscr{F}(x_1, x_2)_{ee \rightarrow \gamma\gamma \rightarrow h} = \epsilon^2 \int_0^1\int_0^1 \frac{du_1}{u_1}\,\frac{du_2}{u_2}\left(1 - u_1 + \frac{u_1^2}{2}\right)\left(1 - u_2 + \frac{u_2^2}{2}\right)\mathscr{F}\left(\frac{x_1}{u_1}, \frac{x_2}{u_2}\right)_{\gamma\gamma \rightarrow h} \tag{III.35}$$

$\epsilon^2 \approx \left(\frac{2\alpha}{\pi} \log \frac{E_{eff}}{m_e}\right)^2$ is again the probability of finding photons in the leptons and is set equal to 1.6×10^{-3} in Fig. 15 and 16. The cross section for the high-p_T process ($e^{\pm} e^{-} \longrightarrow e^{\pm} e^{-} h + \ldots$) typically is $\sim 10^{-2}$ to 10^{-3} as large as the corresponding lepton annihilation process. Therefore it appears that the prospects for measuring this channel, e.g., in high-energy $e^{-}e^{-}$ collisions, are rather remote but not unthinkable.

The third process (III.20) is deep-inelastic scattering of a lepton from the vector hadron states coupled to a real photon.[11] It can be estimated in terms of the process $\ell + \rho^{o} \longrightarrow h$ + anything, as discussed below in Subsection D. One must remember that the meson electromagnetic vertices may not fall as rapidly with increasing Q^2 as nucleon electromagnetic vertices. Then by the Drell-Yan[17] or Bloom-Gilman[7] argument (Section IV), the structure function F(x) may not fall as rapidly near $x = 1$ as νW_2 does for the nucleons. In other words, for meson targets F(x) may look more like $2(1-x)$ and less like νW_2. But in any case this mechanism is $0(\alpha^4)$ and thus the net yield for this process is not much better than for the deep-inelastic $\gamma\gamma$ process (III.19).

D. One and only one hadron in the initial state

The initial states of interest here include γp, μp, ep, and νp, although the latter is outside the scope of these considerations. Our results, however, are readily adaptable to that case as well. The generic inclusive processes are

$$\ell + h \rightarrow \ell + \text{anything} \tag{III.36}$$

$$\ell + h \rightarrow h + \text{anything} \tag{III.37}$$

$$\ell + h \rightarrow \gamma + \text{anything} \tag{III.38}$$

$$\gamma + h \rightarrow \gamma + \text{anything} \tag{III.39}$$

$$\gamma + h \rightarrow h + \text{anything} \tag{III.40}$$

$$\gamma + h \rightarrow \ell + \text{anything} \tag{III.41}$$

Process (III.36) is the original deep-inelastic channel of electroproduction and needs no elaboration here.[10] We only record $\mathscr{F}(x_1, x_2)$ in order to provide a simple basis for comparison with other secondary distributions

$$\mathscr{F}(x_1, x_2)_{\ell h \rightarrow \ell} = \tfrac{1}{2} \frac{x_1^2}{1-x_1} (1 + x_1^2) F\left(\frac{x_2}{1-x_1}\right) . \tag{III.42}$$

It is plotted in Figure 17, using Eq. (III.30) for F ($F = \nu W_2$).

The distribution of secondary hadrons in electroproduction, channel (III.37), is of considerable current interest. The model we use here asserts that the hadron distribution in this reaction will be closely related to that found in the very high energy colliding-beam processes. The mechanism is illustrated in Figure 18. In terms of the G(x) defined in the previous section, the distribution of longitudinal momentum p of produced energetic hadrons of type a in the laboratory frame is given by

$$\frac{d\sigma_a}{dQ^2 d\nu\, dp} = \frac{4\pi\alpha^2}{Q^4\nu}\left(1-\frac{\nu}{E}+\frac{\nu^2}{2E^2}\right)\sum_i F_i\left(\frac{Q^2}{2M\nu}\right)\left[\frac{1}{p}G_{ia}\left(\frac{p}{\nu}\right)\right] \quad , \qquad \text{(III.43)}$$

where the sum is over produced parton types i, and F_i is the contribution to νW_2 from partons of type i. The rest of the variables are defined as in reference 10. Upon summing over a and assuming as before that $\sum_a G_{ia} = G$ independent of i, we find simply that the distribution of energetic hadrons has the same functional dependence as in colliding beam experiments:[18]

$$\frac{dN}{dp} = \frac{1}{p}G\left(\frac{p}{\nu}\right) \qquad \text{electroproduction}$$

$$\frac{dN}{dp} = \frac{2}{p}G\left(\frac{2p}{\sqrt{s}}\right) \qquad \text{colliding beams} \qquad \text{(III.44)}$$

Again, small p_T relative to the direction of the virtual photon for the emerging hadrons has been assumed; this is discussed more in Section IV. We record $\mathscr{F}(x_1, x_2)_{\ell h \to h}$ below and plot it in Figures 19 and 20:

$$\mathscr{F}_a(x_1, x_2)_{\ell h \to h} = \tfrac{1}{2}\sum_i \int \frac{dy\, y}{(1-y)^3} x_1^2 (1+y^2) F_i\left(\frac{x_2(1-y)}{x_1 y}\right) G_{ia}\left(\frac{x_1}{1-y}\right)$$

$$(\mathscr{F} = \sum_a \mathscr{F}_a) \qquad \text{(III.45)}$$

Turning now to process (III.38), $\ell h \to \gamma$, it appears to be useful, at best, as a way of testing quantum electrodynamics by wide-angle bremsstrahlung[19]; i. e. Compton scattering of the Coulomb field of the hadron by the incoming lepton. We shall not discuss this rather familiar process further.

Process (III.39) has been already discussed in the literature from the parton point of view.[9] It is related, for the quark distribution-functions assumed in this paper, to electroproduction by the simple formula (laboratory variables)

$$\left(\frac{d\sigma}{dp^2\, dp_\parallel}\right)_{\gamma h \to \gamma} \Bigg/ \left(\frac{d\sigma}{dp^2\, dp_\parallel}\right)_{\ell h \to \ell} = \frac{(E_a - E_c)^2}{E_a E_c} \frac{\langle \Sigma e_i^4 \rangle}{\langle \Sigma e_i^2 \rangle} \qquad \text{(III.46)}$$

$$\approx 0.3 \frac{(E_a - E_c)^2}{E_a E_c}$$

In terms of $\mathscr{F}_{\gamma h \to \gamma}$, we have

$$\mathscr{F}(x_1, x_2)_{\gamma h \to \gamma} = \tfrac{1}{2} x_1 (1 - x_1)(1 + x_1^2) \sum_i e_i^2 F_i\left(\frac{x_2}{1 - x_1}\right) . \qquad \text{(III.47)}$$

The sum over the F_i weighted in a different way from the sum for νW_2 requires a model for the parton distributions which is elaborated in Appendix B. We plot $\mathscr{F}_{\gamma h \to \gamma}$ in Figure 21 using the form-factors F_i described in Appendix A. We emphasize that the elementary process for deep inelastic Compton scattering involves exchange of a very virtual parton [Figure 3e]. We must therefore consider this calculation less reliable than the corresponding calculation for electroproduction.[21]

The discussion of the hadron channel (III.40) in deep-inelastic Compton scattering directly parallels that for electroproduction; Eq. (III.44) remains true and (III.43), appropriately modified using (III.46), survives as well. As usual we record $\mathscr{F}$ for this case and plot it in Figures 22 and 23 for the two assumed forms for G(x).

$$\mathscr{F}(x_1, x_2)_{\gamma h \to h} = \tfrac{1}{2} \int \frac{dy}{1 - y} x_1^2 (1 + y^2) \sum_i e_i^2 F_i\left(\frac{x_2 (1 - y)}{x_1 y}\right) G\left(\frac{x_1}{1 - y}\right) . \qquad \text{(III.48)}$$

One may question whether, in addition to the $0(\alpha^2)$ process we have considered (shown in Figure 24a) there exists an $0(\alpha)$ process (shown in Figure 24b) which is associated with an elementary deep-inelastic process involving a strong parton vertex (as in Figure 3f). If the lower strong parton vertex exists, then copious numbers of high-p_T secondaries might result. If the final unobserved parton at the lower vertex (Figure 24b) is a $J = 1^{\pm}$ gluon, then the distribution function (III.48) multiplied by a factor $\lesssim 100$ may roughly represent the expected distribution.

We now consider process (III.41), electromagnetic pair-production, which is a well-known test of quantum electrodynamics. But another aspect of this process, perhaps useful at electron accelerators, emerges at very high energies. This is to consider the virtual muons in the γ-rays as an effective muon beam. One percent of the time there is a virtual muon in a high energy γ-ray, while typically only $< 10^{-4}$ real muons per γ can be obtained by converting photons in a target. By looking at secondary muons at very high p_T, one might observe deep-inelastic muon-nucleon scattering with a flux ~ 100 times greater than otherwise obtainable. The flux of virtual muons of given charge per incident photon is approximately represented by the formula

$$\frac{dN}{dx} \cong \left(\frac{\alpha}{2\pi} \log \frac{E_\gamma}{m_\mu}\right)\left[x^2 + (1-x)^2\right] \qquad \text{(III.49)}$$

$$x = E_\mu / E_\gamma$$

When this distribution is folded against the deep-inelastic formula (III.42), we find for the secondary distribution of muons of given charge:

$$\mathscr{F}(x_1, x_2)_{\gamma h \to \mu} \cong \left(\frac{\alpha}{4\pi} \log \frac{E_\gamma}{m_\mu}\right) \int \frac{dy}{y^3} \left[y^2 + (1-y)^2 \frac{x_1^2 (y^2 + x_1^2)}{y - x_1} F\left(\frac{x_2 y}{y - x_1}\right)\right] . \qquad \text{(III.50)}$$

This is plotted in Figure 25.

E. Two hadrons in the initial state

The final three processes are all relevant to experiments at the CERN intersecting storage rings as well as to measurements of single-particle distributions at NAL. They are

$$h + h \to \ell + \text{anything} \qquad \text{(III.51)}$$

$$h + h \to \gamma + \text{anything} \qquad \text{(III.52)}$$

$$h + h \to h + \text{anything} \qquad \text{(III.53)}$$

Process (III.51) has been measured by Christensen et al.[12] and calculated in the parton model by Drell and Yan[13] and many others[20]. We here consider the Drell-Yan model, where the process goes only via parton-antiparton annihilation, as shown in Figure 26. The function $\mathscr{F}$ is in our notation given by

$$\mathscr{F}(x_1, x_2)_{hh \to \ell} = \tfrac{1}{2} \int dy\, y(1-y)\left[1 - 2y(1-y)\right] \sum_i \frac{1}{e_i^2} F_{a\,i}\left(\frac{x_1}{y}\right) F_{b\,\bar{i}}\left(\frac{x_2}{1-y}\right) \qquad \text{(III.54)}$$

where the sum over i goes over all parton (and antiparton) types. For protons incident and for the quark distributions we have been using (described in Appendix B), $\mathscr{F}_{hh \to \ell}$ is plotted in Figure 27.

Process (III.52) describes production of $\gamma\gamma$ pairs via parton-antiparton annihilation, as in Figure 28. The elementary deep-inelastic process [Figure 3d] involves strong parton exchange and is therefore on less firm ground than the

previous process, being in the same category as inelastic Compton scattering and deep-inelastic hadron production in $\gamma\gamma$ collisions.[21] Given this caveat, the computation follows that of (III.54), and the answer is

$$\mathscr{F}(x_1, x_2)_{hh \to \gamma} = \tfrac{1}{2}\int dy[1-2y(1-y)] \sum_i F_{a\,i}\left(\frac{x_1}{y}\right) F_{b\,\bar{i}}\left(\frac{x_2}{1-y}\right) \qquad \text{(III.55)}$$

Equation (III.55) is plotted in Figure 29 for the quark-model choices of structure-functions described in Appendix B.

In this reaction, one may again question whether a process of lower order in α might play the dominant role. The elementary deep inelastic parton process is the same [Figure 3f] as in the $\gamma h \to h$ process discussed in the previous section; we illustrate the mechanism in Figure 30. Again, if the unobserved high-p_T parton is a gluon, the photon yield may be estimated by multiplying $\mathscr{F}_{hh \to \gamma}$ as given in (III.55) by a factor $\lesssim 100$. This mechanism is, of course, even more speculative than that of Figure 28.

The final reaction (III.53) of hadron production is of special interest. Photon exchange (Figure 31a) between the incident hadrons (or partons therein) is a sure mechanism for populating the high-p_T region, and the contribution is readily calculated from our assumptions. The result is

$$\mathscr{F}(x_1, x_2)^{\text{Coulomb}}_{hh \to h} = \tfrac{1}{2}\int \frac{dy_1 dy_2 x_1^2 (y_1^2 y_2^2 + x_1^2)}{y_1^4 (y_1 y_2 - x_1) y_2^2} \sum_i \bar{F}_{a\,i}(y_1) G_{i\bar{c}}(y_2) F_b\left(\frac{x_2 y_1}{y_1 y_2 - x_1}\right) \qquad \text{(III.56)}$$

This contribution is plotted in Figures 32 and 33 for the quark-model choices of form factors F and G discussed in Appendix B. The Drell-Yan parton-anti-parton annihilation mechanism [Figure 31b] provides an additional contribution

$$\mathscr{F}(x_1, x_2)^{\text{Annihilation}}_{hh \to h} = \tfrac{1}{2} \int \frac{dy_1 dy_2}{y_1^3} x_1^2 y_2 (1-y_2) [1-2y_2(1-y_2)]$$

$$\times \sum_{i,j} \frac{e_j^2}{e_i^2} F_{a\,i}\left(\frac{y_1}{y_2}\right) F_{b\,\bar{i}}\left(\frac{x_2 y_1}{x_1(1-y_2)}\right) G_{j\,c}\left(\frac{x_1}{y_1}\right) \quad . \tag{III.57}$$

It is plotted in Figures 34 and 35. One sees that it is generally small enough compared to the Coulomb contribution that it may be ignored.

In addition to these $0(\alpha^2)$ mechanisms there are elementary deep-inelastic parton processes involving possible strong parton vertices which may conceivably be present and give contributions of $0(\alpha)$ or 0(1). The 0(1) contribution associated with J = 1 gluon-exchange is the most serious possibility and was discussed previously in the introduction. Should the mechanism exist, one multiplies $\mathscr{F}_{hh \to h}$ as defined in (III.56) by a factor $\lesssim 10^4$. If the mechanism exists, one should observe at the CERN ISR secondary hadrons with p_T in excess of 8 GeV.

F. Weak-interaction processes

Before leaving this section, it is appropriate to mention the role of weak interactions in these considerations. Given the conventional local or intermediate-vector-boson current-current couplings, it follows[22] that particle-production via virtual-W-exchange processes (or even the direct Fermi couplings) will be much smaller than electromagnetic processes because $(G\sqrt{2})^2 << 4\pi\alpha^2 p_T^{-4}$ for $p_T << 100$ GeV. However, this is not the case for processes involving production of the W.[23] In the process h + h → W + anything, calculated via the Drell-Yan parton-antiparton annihilation mechanism one finds

$$\sigma = \pi G\sqrt{2} \int_{\frac{m_W^2}{s}}^{1} \frac{dx}{x} \sum_i \frac{1}{e_i^4} F_{a\,i}(x)\, F_{b\,\bar{i}'}\left(\frac{m_W^2}{xs}\right) \tag{III.58}$$

where $\sum_i$ is a sum over parton-antiparton pairs i, $\bar{i}'$ with the quantum numbers of the W. This cross-section is $\sim 4 \times 10^{-33} \text{cm}^2$ for $s >> m_W^2$ and is plotted for the wave-functions we use in Figure 36. The decay branching ratios are, in the parton model, 1/3 for $e\bar{\nu}$, $\mu\bar{\nu}$, and hadrons. The hadron distribution in the rest-frame of the W should be very similar to that for e^+e^- annihilation, Eq. (III.23) or (III.24), with appropriate isotopic-spin modifications. The transverse-momentum distribution of the decay leptons is spectacular; it is the same as for a W at rest:

$$\frac{dN}{dp_T^2} = \frac{3}{m_W^2} \frac{\left(2 - \frac{4p_T^2}{m_W^2}\right)}{\sqrt{1 - \frac{4p_T^2}{m_W^2}}} \tag{III.59}$$

Single-W production in other processes we have discussed requires knowledge of the electromagnetic vertex of the W and will not be considered here.

Neutrino-induced processes, as is well known, share such similar features with electroproduction (because of CVC) that we need not dwell on them here.

IV. The Relation between the Intermediate Parton State and the Final Hadron State; Properties of G(x)

A basic ingredient in our calculations is the parton model as practised in the interpretation of deep inelastic electroproduction. This approach gives a description of the initial hadronic system of colliding particles in terms of constituent partons summarized by the structure function $F(x) = \nu W_2(x)$. We have attempted in a similar fashion to relate the intermediate parton system existing after the deep inelastic interaction to the final system of produced particles as summarized by our use of the function G(x).

In this section we critically discuss this latter step; in particular, the degree of plausibility of the assumptions, the conditions necessary for their validity, and the consequences to our predictions if the assumptions fail.

Given the assumptions leading to G(x) as approximately correct, a great deal may be inferred about its properties using the sum rules (II.3) and (II.4). Furthermore, a generalization of the connection between inclusive and exclusive processes as discussed by Drell and Yan,[17] Feynman,[3] Bloom and Gilman,[7] and others may be derived.

To begin let us look again at the configuration of partons in phase space immediately after the deep inelastic interaction for the generic processes of a) $e^+e^- \rightarrow$ hadrons, b) $ep \rightarrow e +$ hadrons, and c) $pp \rightarrow$ hadrons, as shown in Figure 37. The collision is depicted in the overall center-of-mass system with the beam axis along the z direction and the deep inelastic parton-parton collision defining the x-z plane.

Our problem is to guess which final state hadron configurations have the largest overlap with the post-reaction parton configurations. The most significant consideration in this regard is that a parton which has been given a large p_T by the interaction ("active parton") has a large subenergy when combined with any other parton in the configuration. It is generally assumed in the parton model that the condition of large subenergy of two partons implies little or no correlation or interaction between them, i. e. the evolution of a parton which is distantly removed in phase space from the rest of the partons should be independent of them. Supposing that this is indeed the case, the problem is reduced to following the evolution of each active parton.

To this end we recognize that deep inelastic reactions are relatively rare in hadron physics, and thus, the subsequent evolution of a parton should be dominated by a succession of the usual small p_T "ordinary" reactions. This condition means no large subenergies will be created in the cascading division of the active parton into other partons. The resulting parton configurations in Figure 37 then have evolved into those shown in Figure 38, consisting of several jets of partons with tails pointing back to the origin in momentum space. The parton configuration resulting from an ordinary hadron-hadron collision (Figure 39) is also a pair of such jets. Feynman conjectures[24] that for such a configuration, the resulting hadron distribution will be similar to the parton distribution. Applied to our case, this conjecture implies that the distributions of final hadrons will also be as shown in Figure 38.

The eventual disposition of the possible fractional charge carried by the active parton is related to the manner in which the tail connects up with the other partons at the origin.[25] At this point the relative subenergy between the relevant

partons will be small and there will be considerable interaction with the tails of the other jets present in the final state. Thus, it is not inconsistent that the parton jet have fractional charge and the associated hadron jet integral charge.

These qualitative considerations lead us to three essential assumptions which motivate the existence of the function G(x).

1. The dynamics of the high p_T component of the state factors out from that of the rest of the environment.

2. The $< p_T >$ in the parton cascade (e. g. the width of the band of phase points in Figure 38) is the usual 300 MeV/c characteristic of the dominant hadron reactions.

3. The parton multiplicity and momentum distribution in each jet are, respectively log p and dp/p.

These assumptions allow us to infer further properties of G(x) which we now elucidate.

We first consider the sum rules (II.3) and (II.4)

$$\int_{x_{min}}^{1} \frac{dx}{x} G_{ic}(x) = \bar{n}_{ic} \approx G_{ic}(0) \log E_0 + \text{const.} \tag{IV.1}$$

and

$$\int_0^1 dx\, G_{ic}(x) = \epsilon_c, \quad \Sigma_c \epsilon_c = 1 \tag{IV.2}$$

where ϵ_c is the fraction of the total energy E_0 of the jet carried by hadrons of type c. We derive these relations in Appendix C. However, to make them more familiar, we may take the basic definition of $G(x) = \Sigma_c G_{ic}(x)$, as used in

Sections II and III, to be the longitudinal momentum distribution, in the laboratory frame, for hadrons produced in process (b), the deep inelastic electroproduction process. Because, as viewed in the laboratory frame, the active parton i has absorbed all the energy ν of the virtual photon, the function G(y) is just proportional to the inclusive distribution function as customarily defined for projectile fragments. In that case the two sum rules (IV.1) and (IV.2) are the well-known ones expressing probability conservation[26] and energy conservation,[27] respectively.

The factorization property (the first of the three essential assumptions) tells us that the laboratory distribution of hadrons in deep inelastic electroproduction is essentially the same as the colliding beam process (a). Provided $p_{\parallel} >> p_T$ for the fast hadrons in the deep inelastic electroproduction process (b), then the colliding beam distribution function for fast secondary hadrons is easily related to that of deep inelastic electroproduction by

$$\left(p \frac{dN}{dp}\right)_{e^+e^- \to h + "x"} = 2\left(p_{\parallel} \frac{dN}{dp_{\parallel}}\right)_{ep \to e + h + "x"} \qquad \text{(IV.3)}$$

where dN/dp is the mean number of hadrons produced in momentum interval dp per collision, and ν for process (b) is set equal to $\frac{1}{2}\sqrt{s}$ for process (a).

The sum rules (IV.1) and (IV.2) are extremely useful in both normalizing the function G(x) as well as for inferring the behavior of G(x) near the origin. Assuming no more than a logarithmic rise of multiplicity with increasing ν in deep inelastic electroproduction implies that $G(x_{min})$ is bounded as $x \to x_{min} \sim \text{const}/\nu$ (a result familiar[27] from hadronic processes). The finiteness

of G(x) near $x \approx 0$, used with the energy conservation sum rule (IV.2), then provides a reliable normalization for G(x).

Finally, we note that it is possible to relate the inclusive distribution functions near $x \approx 1$ to the elastic electromagnetic form factors in a manner similar to the connections between inelastic and elastic form factors discussed by Drell and Yan[17] and Bloom and Gilman,[7] and many others. This argument is most easily carried out for the colliding beam process $e^+e^- \to \pi + "x"$. As the π energy approaches its maximum energy E_0, the missing mass m of the unobserved system decreases until at E_0 it is just the mass of a single π. In terms of the energy E of the observed pion, we have that

$$\frac{m^2}{4E_0^2} \approx 1-x = 1 - \frac{E}{E_0} \qquad \text{(IV.4)}$$

When $m < 2$ GeV we may expect to see resonant behavior in the pion distribution function G(x) corresponding to the two body channels such as πA, $\pi\omega$, $\pi\rho$, and at $x = 1$, $\pi\pi$. We assume that whatever the dynamics responsible for the inclusive distribution, it extrapolates smoothly into this "resonance" region. Then, provided the interaction radius is $\lesssim 1$ F, the number of angular momentum channels available to the recoiling system when $m \leq 2$ GeV is bounded. We now decompose the multiparticle amplitudes which build G(x) into this finite number of angular momentum channels, a finite fraction of which are resonant. The amplitudes in the resonant channels should be enhanced by a finite factor given roughly by the Breit-Wigner resonance formula. Consequently, the contribution of the resonances should be a finite fraction of the total contribution to G(x) in the resonance region i. e.

$$\int_{1-\frac{m^2}{4E_0^2}}^{1} dx\, G(x) \sim \text{sum of resonances} \gtrsim F_\pi^2 (4E_0^2) \qquad \text{(IV.5)}$$

where $\sim$ means "of the same order of magnitude, independent of E_0". If $F_\pi(q^2) \sim (q^2)^{-p}$, then as found by Drell and Yan, and developed by Bloom and Gilman, (IV.5) implies that $G(x) \sim (1-x)^{2p-1}$. It is almost unthinkable that F_π be smaller than the nucleon form factor. Thus, $p \leq 2$. It is even more unthinkable that $F_\pi > 0$ as $q^2 \to \infty$. Therefore, $p > 0$ and more probably $p \geq 1$. For $p = 2$, $G(x)$ has all the qualitative features of the famous electroproduction structure function νW_2, and this motivates our choice of the "minimum" $G(x) = 6.84\, \nu W_2(x)$ in Section III. The "maximum" $G(x)$ we take to be $2(1-x)$, corresponding to $F_\pi(q^2) \sim q^{-2}$ as $q^2 \to \infty$, and consider it unlikely that $G(x)$ is larger than this for large y. Thus these two choices for $G(x)$ could provide reasonable upper and lower bounds to the true situation.

We are now in a position to return to the three assumptions we posed earlier in this section and ask what consequences follow if they were not true.

1. If "factorization" were false, there would be considerable interaction between partons of large subenergy and Feynman's picture of the dynamics would have to be abandoned. The most incisive experimental test of "factorization" is the comparison of secondary hadron distributions in e^+e^- colliding beam processes (at very high energies) with the hadron distributions in deep inelastic electroproduction as given by (IV.3). They should be very similar.

2. If the longitudinal momentum distribution is held fixed and $< p_T >$ is allowed to grow, the p_T distributions calculated in Section III would broaden even

further. Thus our choice of low $< p_T >$ is the most conservative we could make. The cleanest experimental test of this assumption is to measure $< p_T >$ as a function of $p_{\|}$ and ν in electroproduction processes, especially for energetic secondaries.

3. The assumption of low multiplicity is crucial for the calculations of Section III. We believe it unlikely that the hadron multiplicity $\bar{n}$ at photon energy ν in deep inelastic electroproduction is smaller than that for photoproduction at the same ν. But $\bar{n}$ might be larger, and the sum rules make it clear that in such a case G(x) increases for small y, and decreases for large y, possibly becoming, for infinite energy, zero execpt at $y \cong 0$. Such a situation,[28] of course, would drastically reduce the yield of high p_T particles from what we have estimated. While we cannot rule this out, we find such a possibility somewhat unattractive, because this would mean a very small yield of high-momentum particles in the colliding beam process. However, the power law fall-off of electromagnetic form factors and their successful integration into the electroproduction scaling function by Bloom and Gilman strongly suggest a large yield of high-momentum particles in the colliding beam process. Again, the measurement of hadron distributions in electroproduction, ν-processes, and colliding beam experiments will provide clear answers as well as well-defined input functions for the calculations of hadron-hadron processes.

We hope that this discussion makes our use of the functions G(x) more plausible. We have also attempted to demonstrate that our estimates actually depend rather weakly on the details of the parton model, but rely mostly upon kinematics and the crucial assumption that multiplicities in the deep inelastic processes grow

slowly with increasing energy and p_T (more slowly than a power). This latter assumption, while perhaps the most popular option around at present, is anything but compelling. However, it is susceptible to test, and if wrong, opens up a very new and most interesting kind of dynamics itself.

V. Conclusion

We list here some of the more salient features and results as obtained from our analysis.

(1) Particle Production Rates

For inclusive processes initiated by hadrons, photons or leptons and where a final hadron is observed with large transverse momentum we expect several orders of magnitude increase in cross-section over what might be expected from an extrapolation of existing data with the extrapolating form $\exp(-6p_T)$. This means that for both the ISR and NAL machines there will be high transverse momentum particles sufficiently copious to warrant a systematic study of high transverse momentum processes.

Typical cross-sections deduced here vary roughly as a power law in p_T rather than as an exponential in p_T. In particular, Figure 1 shows the expected cross-sections for NAL with a beam energy of 400 GeV.

These cross-sections, which are of order α^2, are based on the assumption that the scattering at high p_T is the result of an electromagnetic interaction. Based on our experience with the deep inelastic electron scattering we expect these results to yield the correct order of magnitude in a model independent manner, and thereby to provide a reliable lower bound to the expected cross sections.

The explicit numerical results given here in the various graphs are obtained using a parton constituent model of hadrons which also yields relations among the many different processes listed in Section III. Within this model our main quantitative uncertainty is in the relation between the intermediate constituent parton system and the final observed hadron system. This uncertainty can be eliminated

when data becomes available on the spectrum of final hadrons in either deep inelastic electron scattering or colliding beam experiments.

(2) Scaling Behavior

Since all masses are neglected in our calculations it is natural that the cross-sections at large energy and high p_T have a scaling property which is given explicitly by (III.6a) and (III.6b). This property is independent of details of our constituent model. Except for the factor p_T^{-4}, characteristic of single photon exchange, we expect that the cross-sections will depend on two scaling variables x_1 and x_2 as defined by (III.1, 2). This is in contrast to the observed behavior at smaller values of p_T (< 1 GeV/ c) where the p_T distribution is roughly independent of $p_{\|}$ and s.

The parton constituent model further predicts that the charge ratios for final hadrons in Section III.E) should be similar to the charge ratios for final hadrons in processes initiated by leptons or photons as in Sections (III.C) and (III.D).

(3) Cores and Multiple Cores

In Section IV we have described the decay evolution of an active parton and motivated the existence of a function G(x) which gives the probability of decay of the intermediate parton into the final observed hadron. This function is proposed to depend only on the ratio x of hadron to parent parton energies and further assumes that the emerging hadron is confined to have only small p_T with respect to the active parton direction. Thus in electroproduction of hadrons, the longitudinal momentum distribution should depend only on ν independent of Q^2 (to the extent that the parent parton distribution has only a weak dependence on ω). The final hadrons are therefore expected to emerge in a core-like distribution along the virtual photon direction.

This kind of behavior is expected also in colliding beam processes as well as in hadron-hadron collisions where the subsequent hadron distributions should collect into multiple core-like distributions as discussed in more detail in Section IV. This kind of distribution is in sharp contrast to a statistical model in which the distributions are essentially uniform.

(4) Similarity of Hadron Distributions in ep and e^+e^- Processes

The existence of the function G(x) suggests an equality between the number distribution of the final observed hadrons in the processes $e + p \rightarrow h +$ anything and $e^+ + e^- \rightarrow h +$ anything. Corroboration of this result is fundamental to the arguments given here and behooves prompt experimental verification or rejection.

Acknowledgment

It is a pleasure to acknowledge a very helpful conversation with R. P. Feynman. We also benefitted from discussions with H. Harari and many colleagues at SLAC.

APPENDIX A

Derivations of Cross-section Formulae

We will derive here the differential cross sections for the processes discussed in the text. This material is obtained most efficiently by considering the simple quantum electrodynamic processes first and building the hadronic cross sections from these parts. Furthermore, after starting the calculations by quoting certain familiar formulas for quantum electrodynamic processes written in terms of conventional variables such as scattering angle, we will convert to the scaling variables x_1 and x_2 and use these almost exclusively from then on.

Consider

$$\ell + \bar{\ell} \rightarrow \ell + \text{'X'} \quad \text{(annihilation)}$$

for which the differential cross section in the center of mass reads,

$$\frac{d\sigma}{dE d\Omega} = \frac{\alpha^2}{16E^2}(1 + \cos^2\theta)\delta(E - E_0) \tag{A.1}$$

where E_0 is the energy of one of the incident leptons. In order to identify $\mathscr{F}_{\ell+\bar{\ell}\rightarrow\ell}(x_1, x_2)$ for this process, we should write (A.1) in the form of Eq. (II.6a). Changing variables,

$$E\frac{d\sigma}{dp_{\|}\, dp_T^2} = \frac{\pi\alpha^2}{16E^3}(1 + \cos^2\theta)\delta(E - E_0) \tag{A.2}$$

where

$$p_T = E\sin\theta\,, \qquad p_{\|} = E\cos\theta$$

Recalling that the center of mass expressions for x_1 and x_2 read,

$$x_1 = \tfrac{1}{2}\frac{E}{E_0}(1+\cos\theta)\,, \qquad x_2 = \tfrac{1}{2}\frac{E}{E_0}(1-\cos\theta) \tag{A.3}$$

we can easily rewrite (A.2) in the form,

$$E\frac{d\sigma}{dp_{\|}\,dp_T^2} = \frac{4\pi\alpha^2}{p_T^4}\,\mathscr{F}_{\substack{\ell+\bar{\ell}\to\ell \\ (\text{ann.})}}(x_1, x_2) \tag{A.4}$$

and identify

$$\mathscr{F}_{\substack{\ell+\bar{\ell}\to\ell \\ (\text{ann.})}}(x_1, x_2) = \tfrac{1}{2}x_1^2x_2^2(1-2x_1x_2)\delta(x_1+x_2-1) \tag{A.5}$$

The corresponding formula for the processes

$$\gamma+\gamma\to\ell+\text{'X'} \qquad \ell+\bar{\ell}\to\gamma+\text{'X'}$$

is simply obtained from this result by recalling their differential cross section

$$\frac{d\sigma}{dE\,d\Omega} = \frac{\alpha^2}{4E^2}\,\frac{(1+\cos^2\theta)}{\sin^2\theta}\,\delta(E-E_0) \tag{A.6}$$

So, if we multiply (A.5) by

$$\frac{4}{\sin^2\theta} = \frac{1}{x_1x_2}$$

we obtain the $\mathscr{F}(x_1, x_2)$ for these processes,

$$\mathscr{F}_{\gamma+\gamma\to\ell}(x_1, x_2) = \tfrac{1}{2}x_1x_2(1-2x_1x_2)\delta(x_1+x_2-1) \tag{A.7}$$

The differential cross section for the scattering

$$\ell + \bar{\ell} \to \ell + \text{'X'} \quad \text{(scattering channel)}$$

reads,

$$\frac{d\sigma}{d\Omega} = \frac{\alpha^2}{8E^2}\left(\frac{1+\cos^4(\theta/2)}{\sin^4(\theta/2)}\right) \tag{A.8}$$

which can be rewritten by the same manipulations as above as

$$E\frac{d\sigma}{dp_{\|}dp_T^2} = \frac{4\pi\alpha^2}{p_T^4}\,\mathcal{F}_{\substack{\ell\bar{\ell}\to\ell \\ (\text{sca.})}}(x_1, x_2)$$

$$\mathcal{F}_{\substack{\ell\bar{\ell}\to\ell \\ (\text{sca.})}}(x_1, x_2) = \tfrac{1}{2}\,x_1^2(1+x_1^2)\,\delta(x_1+x_2-1) \tag{A.9}$$

Finally, the differential cross section for Compton scattering

$$\gamma + \ell \to \gamma + \text{"X"}$$

is given by the familiar Klein-Nishina formula

$$\frac{d\sigma}{dt} = -\frac{2\pi\alpha^2}{s}\left(\frac{u}{s}+\frac{s}{u}\right) \tag{A.10}$$

Since the scaling variables are

$$x_1 = -\frac{u}{s}\,, \qquad x_2 = -\frac{t}{s}\,, \tag{A.11}$$

it is particularly simple to rewrite (A.10) in our standard form,

$$\frac{d\sigma}{dx_1 dx_2} = \frac{4\pi\alpha^2}{s x_1^2 x_2^2} \mathscr{F}_{\gamma\ell \to \gamma}(x_1, x_2)$$

$$\mathscr{F}_{\gamma\ell \to \gamma}(x_1, x_2) = \tfrac{1}{2} x_1 x_2^2 (1 + x_1^2)\delta(x_1 + x_2 - 1) \tag{A.12}$$

The differential cross section for observing the recoil lepton in Compton scattering

$$\gamma + \ell \to \ell + \text{'X'}$$

is obtained from (A.12) by interchanging the labels 1 and 2. So,

$$\mathscr{F}_{\gamma\ell \to \ell}(x_1, x_2) = \tfrac{1}{2} x_2 x_1^2 (1 + x_2^2)\delta(x_1 + x_2 - 1) \tag{A.13}$$

With these results we can go on to progressively more complicated processes involving hadrons. We begin with the colliding beam reaction,

$$\ell + \bar{\ell} \to h + \text{'X'}$$

which is visualized in Figure 7 . The differential cross section is given by the product of the differential cross section for the parton event ($\ell + \bar{\ell} \to \gamma \to q\bar{q}$) with the probability that a hadron of type "c" emerge from a parton of type "i". As discussed in the text, this probability is assumed to have the form

$$dP_{ic} = G_{ic}(x) \frac{dx}{x} \tag{A.14}$$

where x is the ratio between the 4 momentum of hadron c, p_c, and the 4 momentum of parton i, p_i. The cross section for $\ell + \bar{\ell} \to h$ is then

$$d\sigma = \sum_i e_i^2 \int \frac{4\pi\alpha^2}{\hat{s}\hat{x}_1^2\hat{x}_2^2} \tfrac{1}{2}\hat{x}_1^2\hat{x}_2^2(1-2\hat{x}_1\hat{x}_2)\delta(\hat{x}_1+\hat{x}_2-1)G_{ic}(x)\frac{dx}{x} \tag{A.15}$$

where the careted variables refer to the parton event. Since the $\hat{x}_2$ integral is trivial, we are left with a function of $\hat{x}_1$ and x. However, to arrive at our conventional form for the differential cross section we really want to treat x_1 and x_2 as independent variables. This change of variables is easily done by recalling the definitions (II.1):

$$\begin{aligned} \hat{x}_1 &= -\frac{(\bar{p}-p_i)^2}{(p+\bar{p})^2}, \quad \hat{x}_2 = -\frac{(p-p_i)^2}{(p+\bar{p})^2} \\ x_1 &= -\frac{(\bar{p}-p_c)^2}{(p+\bar{p})^2}, \quad x_2 = -\frac{(p-p_c)^2}{(p+\bar{p})^2} \end{aligned} \tag{A.16}$$

Treating all the four-vectors as lightlike we easily read off from these relations that,

$$\hat{x}_1 = \frac{x_1}{x_1+x_2}, \quad \hat{x}_2 = \frac{x_2}{x_1+x_2}, \quad x = x_1+x_2 \tag{A.17}$$

Finally, substituting this change of variables into (A.15), we find after some algebra,

$$\begin{aligned} \frac{d\sigma}{dx_1dx_2} &= \frac{4\pi\alpha^2}{s x_1^2 x_2^2}\,\mathscr{F}_{\ell\bar{\ell}\to h}(x_1,x_2) \\ \mathscr{F}_{\ell\bar{\ell}\to h}(x_1,x_2) &= \tfrac{1}{2}\sum_i e_i^2 \frac{x_1^2x_2^2}{(x_1+x_2)^4}(x_1^2+x_2^2)\,G_{ic}(x_1+x_2) \end{aligned} \tag{A.18}$$

From (A.5) and (A.7) we see that the form factor for the process

$$\gamma + \gamma \rightarrow h + \text{'X'}$$

is obtained from (A.18) by multiplication with

$$e_i^2 \frac{1}{\hat{x}_1 \hat{x}_2} = e_i^2 \frac{(x_1 + x_2)^2}{x_1 x_2}$$

So,

$$\mathcal{F}_{\gamma\gamma \rightarrow h}(x_1, x_2) = \tfrac{1}{2} \sum_i e_i^2 \frac{x_1 x_2}{(x_1 + x_2)^2} (x_1^2 + x_2^2) G_{ic}(x_1 + x_2) \tag{A.19}$$

Now we turn to deep inelastic electron scattering

$$\ell + h \rightarrow \ell + \text{'X'}$$

shown in Figure 40 . The cross section for this reaction is obtained in the parton model by multiplying the cross section for scattering of a lepton off a pointlike parton times the probability that parton i of longitudinal fraction x appears in hadron a,

$$dP_{ai} = \frac{1}{e_i^2} F_{ai}(x) \frac{dx}{x} \tag{A.20}$$

And if we observe only the outgoing lepton we must sum over the constituents i and integrate over x,

$$d\sigma = \sum_i \int \frac{4\pi\alpha^2}{\hat{s} \hat{x}_1^2 \hat{x}_2^2} \tfrac{1}{2} \hat{x}_1^2 (1 + \hat{x}_1^2) \delta(\hat{x}_1 + \hat{x}_2 - 1) d\hat{x}_1 d\hat{x}_2 \frac{F_{ai}(x)}{x} dx \tag{A.21}$$

Of course $\sum_i F_{ai}(x)$ is just the structure function νW_2 for hadron of type a. We will, for the sake of consistent notation, denote it

$$F_a(x) = \sum_i F_{ai}(x) \tag{A.22}$$

To convert (A.21) to our conventional form we must find the relation between x, $\hat{x}_1$ and x_1, x_2. Using (II.1)

$$\begin{aligned} \hat{x}_1 &= -\frac{(xP-p')^2}{(xP+p)^2}, \qquad \hat{x}_2 = -\frac{(p-p')^2}{(xP+p)^2} \\ x_1 &= -\frac{(P-p')^2}{(P+p)^2}, \qquad x_2 = -\frac{(p-p')^2}{(P+p)^2} \end{aligned} \tag{A.23}$$

We read off from these relations that,

$$\hat{x}_1 = x_1, \qquad x = \frac{x_2}{1-x_1} \tag{A.24}$$

Furthermore, the square of the center of mass energy for the parton event, $\hat{s}$, is related to the overall s by,

$$\hat{s} = (xP+p)^2 = xs = \frac{x_2}{1-x_1}\, s \tag{A.25}$$

Inserting (A.24) and (A.25) into our expression for $d\sigma$, we have

$$\frac{d\sigma}{dx_1 dx_2} = \frac{4\pi\alpha^2}{s\, x_1^2 x_2^2}\, \mathscr{F}_{\ell h \to \ell}(x_1, x_2) \tag{A.26}$$

$$\mathscr{F}_{\ell h \to \ell}(x_1, x_2) = \tfrac{1}{2} \frac{x_1^2}{1-x_1} (1+x_1^2)\, F_a\left(\frac{x_2}{1-x_1}\right)$$

We obtain the form factor for deep inelastic Compton scattering

$$\gamma + h \rightarrow \gamma + \text{'X'}$$

by the now familiar trick of noticing that this reaction is related to deep inelastic lepton scattering via the multiplicative factor,

$$\frac{\hat{x}_2^2}{\hat{x}_1} e_i^2 = \frac{(1-x_1)^2}{x_1} e_i^2 \tag{A.27}$$

We have

$$\mathcal{F}_{\gamma h \rightarrow \gamma}(x_1, x_2) = \tfrac{1}{2} x_1 (1-x_1)(1+x_1^2) \sum_i e_i^2 F_{ai}\left(\frac{x_2}{1-x_1}\right) \tag{A.28}$$

Now consider the cross section for observing the recoil hadron in deep inelastic electron scattering,

$$\ell + h \rightarrow h + \text{'X'}$$

The process is visualized and its kinematics defined in Figure 18 . We use three ingredients in order to obtain the differential cross section: the cross section for lepton parton scattering, the probability that a parton of longitudinal fraction x exists in the incident hadron, and the probability that hadron c emerges from the final state interaction with longitudinal fraction $\bar{x}$ (measured relative to parton p_i'). So,

$$d\sigma = \sum_i \int \left(\frac{4\pi\alpha^2}{\hat{s}\hat{x}_1^2\hat{x}_2^2} \tfrac{1}{2} \hat{x}_1^2 (1+\hat{x}_1^2) \delta(\hat{x}_1 + \hat{x}_2 - 1) d\hat{x}_1 d\hat{x}_2\right)\left(\frac{F_{ai}(x)}{x} dx\right)\left(\frac{G_{ic}(\bar{x})}{\bar{x}} d\bar{x}\right) \tag{A.29}$$

We are faced now with the usual exercise of changing from the variables x and $\bar{x}$ to the more meaningful pair x_1, x_2. Writing the definitions,

$$\hat{x}_1 = -\frac{(p_i - p')^2}{(p_i + p)^2} , \qquad \hat{x}_2 = -\frac{(p - p')^2}{(p_i + p)^2}$$

$$x_1 = -\frac{(P_a - P_c)^2}{(P_a + p)^2} , \qquad x_2 = -\frac{(p - P_c)^2}{(P_a + p)^2} \tag{A.30}$$

Furthermore,

$$p_i = xP_a , \qquad P_c = \bar{x}p_i' \tag{A.31}$$

So, (A.30) can be simplified,

$$\hat{x}_1 = \frac{P_a \cdot p'}{P_a \cdot p} , \qquad \hat{x}_2 = \frac{1}{x}\,\frac{p \cdot p'}{P_a \cdot p}$$

$$x_1 = \bar{x}\,\frac{P_a \cdot p_i'}{P_a \cdot p} , \qquad x_2 = \bar{x}\,\frac{p \cdot p_i'}{P_a \cdot p} \tag{A.32}$$

Momentum conservation reads,

$$p - p' = p_i' - p_i$$

which will allow us to identify relations among several of the scaling variables. In particular,

$$\hat{x}_2 = -\frac{(p_i' - p_i)^2}{(p_i + p)^2} = -\frac{(xP_a - p_i')^2}{(xP_a + p)^2} = \frac{P_a \cdot p_i'}{P_a \cdot p}$$

Inserting this into the invariant expression for x_1, and recalling the delta function in (A.29), we can solve for $\bar{x}$,

$$\bar{x} = \frac{x_1}{\hat{x}_2} = \frac{x_1}{1-\hat{x}_1} \tag{A.33}$$

If we now use momentum conservation to eliminate p_i' from the equation for x_2, we have

$$x_2 = \bar{x}\ \frac{p\cdot(xP_a - p')}{P_a\cdot p} = \bar{x}(x - x\hat{x}_2) = \left(\frac{x_1}{1-\hat{x}_1}\right)\hat{x}_1 x \tag{A.34}$$

So, we can obtain x,

$$x = \frac{x_2(1-\hat{x}_1)}{x_1\hat{x}_1} \tag{A.35}$$

Eliminating x and $\bar{x}$ in (A.29) in favor of the pair x_1, x_2, we have now,

$$\frac{d\sigma}{dx_1 dx_2} = \frac{4\pi\alpha^2}{s x_1^2 x_2^2}\,\mathscr{F}_{\ell h\to h}(x_1, x_2)$$

$$\mathscr{F}_{\ell h\to h}(x_1, x_2) = \tfrac{1}{2}\int \sum_i \frac{dy}{(1-y)^3}\, y x_1^2 (1+y^2)\, F_{ai}\left(\frac{x_2(1-y)}{x_1 y}\right)\, G_{ic}\left(\frac{x_1}{1-y}\right) \tag{A.36}$$

where we have renamed $\hat{x}_1 = y$ to conform with the notation in the text.

The form factor for the hadron distribution in deep inelastic Compton scattering

$$\gamma + h \to h + \text{'X'}$$

is obtained from (A.36) by multiplication with the factor

$$\frac{\hat{x}_2^2}{\hat{x}_1} e_i^2 = \frac{(1-y)^2}{y} e_i^2$$

So,

$$\mathcal{F}_{\gamma h \to h}(x_1, x_2) = \tfrac{1}{2}\int \sum_i \frac{dy}{(1-y)} x_1^2 (1+y^2) e_i^2 F_{ai}\left(\frac{x_2(1-y)}{x_1 y}\right) G_{ib}\left(\frac{x_1}{1-y}\right) \tag{A.37}$$

We now turn to processes involving two hadrons in the initial state. First there is lepton production

$$h + h \to \ell + 'X'$$

whose kinematics are defined in Figure 26. By our usual reasoning the cross section is the probability that parton i with longitudinal fraction y_i exists in hadron a, times the probability that an anti-parton $\bar{i}$ with longitudinal fraction $y_{\bar{i}}$ exists in hadron b, times the cross section for the parton event. Finally, a sum over the types of partons i must be done giving

$$d\sigma = \sum_i \frac{1}{e_i^2} \frac{F_{ia}(y_1)}{y_1} dy_1 \left[\frac{4\pi\alpha^2}{\hat{s}\hat{x}_1^2\hat{x}_2^2} \tfrac{1}{2} \hat{x}_1^2\hat{x}_2^2 (1-2\hat{x}_1\hat{x}_2)\delta(\hat{x}_1+\hat{x}_2-1) d\hat{x}_1 d\hat{x}_2\right] \times \frac{F_{b\bar{i}}(y_2)}{y_2} dy_2 \tag{A.38}$$

Using the invariant expressions for the scaling variables,

$$\hat{x}_1 = -\frac{(y_2 P_b - p)^2}{(y_2 P_b + y_1 P_a)^2}, \quad \hat{x}_2 = -\frac{(y_1 P_a - p)^2}{(y_2 P_b + y_1 P_a)^2}$$

$$x_1 = -\frac{(P_b - p)^2}{(P_a + P_b)^2}, \quad x_2 = -\frac{(P_a - p)^2}{(P_a + P_b)^2} \tag{A.39}$$

and the fact that $\hat{x}_1 + \hat{x}_2 = 1$, we easily read off from these relations,

$$y_1 = \frac{x_1}{\hat{x}_1}, \quad y_2 = \frac{x_2}{1-\hat{x}_1}, \quad \hat{s} = y_1 y_2 s \tag{A.40}$$

Now (A.38) can be written in terms of the experimentally meaningful variables x_1 and x_2,

$$\frac{d\sigma}{dx_1 dx_2} = \frac{4\pi\alpha^2}{s x_1^2 x_2^2} \mathscr{F}_{hh\to\ell}(x_1, x_2)$$

$$\mathscr{F}_{hh\to\ell}(x_1, x_2) = \tfrac{1}{2} \sum_i \int y(1-y)\left[1-2y(1-y)\right] \frac{1}{e_i^2} F_{ai}\left(\frac{x_1}{y}\right) F_{b\bar{i}}\left(\frac{x_2}{1-y}\right) dy \tag{A.41}$$

where we have renamed the dummy variable $\hat{x}_1$ to conform with the notation of the text.

The cross section

$$h + h \to \gamma + \text{'X'}$$

is obtained from (A.41) by multiplying with

$$e_i^2 \frac{1}{\hat{x}_1 \hat{x}_2} = e_i^2 \frac{1}{y(1-y)}$$

So,

$$\mathscr{F}_{hh\to\gamma}(x_1, x_2) = \tfrac{1}{2} \sum_i \int \left[1-2y(1-y)\right] F_{ai}\left(\frac{x_1}{y}\right) F_{b\bar{i}}\left(\frac{x_2}{1-y}\right) dy \tag{A.42}$$

Parton annihilation processes also provide a potentially important mechanism for the production of the W boson,

$$h + h \to W + \text{'X'}$$

Using a slight modification of the argument preceding (A.38), we have the production cross section,

$$\sigma = \sum_i \frac{1}{e_i^2} \frac{1}{e_{\bar{i}W}^2} \int \frac{F_{ai}(y_1)}{y_1} dy_1 \left[\sigma_{i\bar{i}_W}(\hat{s})\right] \frac{F_{a\bar{i}_W}(y_2)}{y_2} dy_2 \tag{A.43}$$

where $\sigma_{i\bar{i}_W}(s)$ is the production cross section for W's in the annihilation of two partons having appropriate quantum numbers. An elementary calculation gives,

$$\sigma_{i\bar{i}_W}(\hat{s}) = 2\pi g_W^2 \delta(\hat{s} - m_W^2)$$

$$\hat{s} = y_1 y_2 s \tag{A.44}$$

where m_W is the mass of the W, g_W is the bare coupling of the W to the weak parton current. We have made the natural assumptions here that the hadronic partons couple to the W just as the leptons do

$$\left(g_W^2 / m_W^2 = G/\sqrt{2}\right),$$

and, for the simplicity of our numerical estimates, the Cabibbo angle can be set to zero. Then, (A.43) can be simplified to

$$\sigma = \sqrt{2}\,\pi G \sum_i \int \frac{dy}{y} \frac{1}{e_i^2} \frac{1}{e_{\bar{i}W}^2} F_{ai}(y) F_{b\bar{i}_W}\left(\frac{m_W^2}{ys}\right) \tag{A.45}$$

Next there is the production of hadrons of large transverse momentum in hadron-hadron collisions

$$h + h \rightarrow h + \text{'X'} \quad \text{(scattering channel)}$$

which is drawn in Figure 31a. By the now familiar reasoning we can write the differential cross section

$$d\sigma = \sum_i \int \frac{F_b(x_j)}{x_j}\, dx_j \; \frac{F_{ai}(x_i)}{x_i}\, dx_i \left[\frac{4\pi\alpha^2}{\hat{s}\hat{x}_1^2\hat{x}_2^2} \tfrac{1}{2}\hat{x}_1^2(1+\hat{x}_1^2)\delta(\hat{x}_1+\hat{x}_2-1)d\hat{x}_1 d\hat{x}_2\right]$$
$$\times \frac{G_{ic}(x)}{x}\, dx \qquad \text{(A.46)}$$

where the scaling variables are defined by

$$p_j = x_j P_b, \quad p_i = x_i P_a, \quad P_c = x p_i' \qquad \text{(A.47)}$$

The variables $\hat{x}_1$ and x may be replaced in favor of x_1 and x_2 without difficulty. If we write out the definitions

$$\hat{x}_1 = -\frac{(p_j - p_i')^2}{(p_i + p_j)^2}, \quad \hat{x}_2 = -\frac{(p_i - p_i')^2}{(p_i + p_j)^2}$$
$$x_1 = -\frac{(P_b - P_c)^2}{(P_a + P_b)^2}, \quad x_2 = -\frac{(P_a - P_c)^2}{(P_a + P_b)^2} \qquad \text{(A.48)}$$

we can identify the relations

$$\hat{x}_1 = \frac{1}{x x_i} x_1, \qquad \hat{x}_2 = \frac{1}{x x_j} x_2 \qquad \text{(A.49)}$$

and solve for x_j,

$$x_j = \frac{x_2 x_i}{x x_i - x_1} \qquad \text{(A.50)}$$

Finally, the $\hat{s}$ for the parton event is related to the overall hadron-hadron s by,

$$\hat{s} = (p_i + p_j)^2 = (x_i P_a + x_j P_b)^2 = x_i x_j s = \frac{x_2 x_i^2}{x x_i - x_1} s \tag{A.51}$$

It is now straightforward to write (A.46) in terms of x_1, x_2, x, and x_i. We obtain

$$\frac{d\sigma}{dx_1 dx_2} = \frac{4\pi\alpha^2}{s x_1^2 x_2^2}\left[\mathscr{F}_{hh\to h}(x_1, x_2) + \mathscr{F}_{hh\to h}(x_2, x_1)\right]$$

$$\mathscr{F}_{hh\to h}(x_1, x_2) = \sum_i \int \frac{x_1^2}{y_1^2 (y_1 y_2 - x_1)}\left[\tfrac{1}{2} + \tfrac{1}{2}\frac{x_1^2}{y_1^2 y_2^2}\right] F_b\left(\frac{y_1 y_2}{y_1 y_2 - x_1}\right) F_{ai}(y_1) G_{ic}(y_2)\, dy_1 dy_2 \tag{A.52}$$

where we have renamed the dummy integration variables in the usual way and included the exchange term coming from u-channel photon exchange. Interference between t-channel and u-channel exchange amplitudes are neglected. At most they increase the cross-section by less than a factor of 2 at 90^o in the center of mass.

Hadrons at large transverse momentum can also be produced through the annihilation channel shown in Figure 31b. The derivation of the cross section for this process is similar to the one just done, but since it is numerically much smaller we just quote the result,

$$\mathscr{F}_{\substack{hh\to h \\ (ann.)}}(x_1, x_2) = \int \sum_{ij} \frac{x_1^2}{2y_1^3}\, y_2(1-y_2)\left[1-2y_2(1-y_2)\right]\frac{e_j^2}{e_i^2} F_{ai}\left(\frac{y_1}{y_2}\right) F_{b\bar{i}}\left(\frac{x_2 y_1}{x_1(1-y_2)}\right) G_{jc}\left(\frac{x_1}{y_1}\right) dy_1 dy_2 \tag{A.53}$$

Another class of processes considered in the text is the colliding electron-electron beam reactions. Simplest of all is

$$e + e \longrightarrow \gamma + \text{'X'}$$

which will provide a test of pure QED. The kinematics for the reaction are defined in Figure 41. We will evaluate the high energy limit of this cross section using the Weizsacker-Williams technique which states that the probability for the initial electron of energy E to have a photon of energy ω around it is

$$\frac{2\alpha}{\pi}\left[1-\frac{\omega}{E}+\tfrac{1}{2}\frac{\omega^2}{E^2}\right]\log\left(\frac{E}{m_e}\right)\frac{d\omega}{\omega} \tag{A.54}$$

So, the differential cross section of interest is the product of this probability times the cross section for Compton scattering off the electron of momentum p_b,

$$d\sigma = \epsilon\int'\frac{d\omega}{\omega}\left[1-\frac{\omega}{E_a}+\tfrac{1}{2}\frac{\omega^2}{E_a^2}\right]\frac{4\pi\alpha^2}{s\hat{x}_1^2\hat{x}_2^2}\,\mathscr{F}_{\gamma\ell\to\gamma}(\hat{x}_1,\hat{x}_2)d\hat{x}_1d\hat{x}_2 \tag{A.55}$$

where

$$\epsilon = \frac{2\alpha}{\pi}\log\left(\frac{E_a}{m_e}\right)$$

and the careted quantities and the form factor $\mathscr{F}$ refer to the Compton process. The differential cross section also receives a contribution from the possibility that the photon of momentum p_c emerged from the other electron. This contribution differs from (A.55) only by the interchange $x_1 \rightleftharpoons x_2$ and will be added into the final expression. Now we must rewrite (A.55) in terms of variables which refer to the external particles. Since the Weizsacker-Williams photon is approximately parallel to the incident electron,

$$k = up_a \quad (0 \le u \le 1)$$

and so,

$$\hat{s} = (k + p_b)^2 = (u p_a + p_b)^2 = u s$$

$$\hat{x}_1 = - \frac{(p_b - p_c)^2}{(k + p_b)^2} = \frac{1}{u} x_1 , \quad \hat{x}_2 = - \frac{(k - p_c)^2}{(k + p_b)^2} = x_2 \tag{A.56}$$

So, the differential cross section for the process of interest can be written,

$$\frac{d\sigma}{dx_1 dx_2} = \frac{4\pi\alpha^2}{s x_1^2 x_2^2} \left\{ \epsilon \int_0^1 \frac{du}{u} \left[1 - u + \tfrac{1}{2} u^2 \right] \left[\mathcal{F}_{\gamma \ell \to \gamma} (\frac{x_1}{u}, x_2) + \mathcal{F}_{\gamma \ell \to \gamma} (x_1, \frac{x_2}{u}) \right] \right\} \tag{A.57}$$

Inserting the explicit form factor for Compton scattering, we have the form factor for $e + e \to \gamma$,

$$\mathcal{F}_{ee \to \gamma} (x_1, x_2) = \epsilon x_2^2 \left| 1 - (\frac{x_1}{1 - x_2}) + \tfrac{1}{2} (\frac{x_1}{1 - x_2})^2 \right] \left[1 - x_2 + \tfrac{1}{2} x_2^2 \right] +$$

$$\epsilon x_1^2 \left[1 - (\frac{x_2}{1 - x_1}) + \tfrac{1}{2} (\frac{x_2}{1 - x_1})^2 \right] \left[1 - x_1 + \tfrac{1}{2} x_1^2 \right] . \tag{A.58}$$

Hadrons at large transverse momentum can also be produced in e-e colliding beams via the reaction diagrammed in Figure 42 . In this case, the Weizsacker-Williams photon converts into a vector meson which then acts as the target for deep inelastic electron scattering by the electron of momentum p_b. The derivation of the form factor for this process parallels the derivation of (A.34) and we obtain

$$\mathcal{F}_{ee\to\gamma e\to h}(x_1,x_2) = \epsilon\int_0^1 \frac{du}{u}\left[1-u+\tfrac{1}{2}u^2\right]\left[\mathcal{F}_{\gamma\ell\to h}(\frac{x_1}{u},x_2) + \mathcal{F}_{\gamma\ell\to h}(x_1,\frac{x_2}{u})\right] \quad (A.59)$$

where the form factors on the right hand side are given by (A.36), multiplied by the probability that the Weizsacker-Williams photon is a vector meson ($\sim\frac{1}{250}$).

There is also the possibility that hadrons are produced in a process involving two Weizsacker-Williams photons shown in Figure [43]. In fact, this reaction proves to be somewhat more probable than (A.59). The reasoning which resulted in (A.57) may be applied here, and it is a simple exercise to find the differential cross section,

$$\frac{d\sigma}{dx_1dx_2} = \frac{4\pi\alpha^2}{s\,x_1^2x_2^2}\,\mathcal{F}_{ee\to\gamma\gamma\to h}(x_1,x_2) \quad (A.60)$$

$$\mathcal{F}_{ee\to\gamma\gamma\to h}(x_1,x_2) = \epsilon^2\cdot\frac{du}{u}\,\frac{dv}{v}(1-u+\tfrac{1}{2}u^2)(1-v+\tfrac{1}{2}v^2)\,\mathcal{F}_{\gamma\gamma\to h}(\frac{x_1}{u},\frac{x_2}{v})$$

where $\mathcal{F}_{\gamma\gamma\to h}$ is given in (A.19).

APPENDIX B

Parton Distribution Functions

The processes considered in the text which involve parton-antiparton annihilation cannot be calculated explicitly until some assumptions are made concerning the distribution of types of partons in the hadron. We will assume here that a hadron in the infinite momentum frame can be viewed as consisting of valence quarks plus a neutral sea of $q-\bar{q}$ pairs plus, possibly, additional neutral gluons.[29] This means that we can write,

$$\nu W_2(x) = C(x) + V(x) \tag{B.1}$$

where $C(x)$ describes the distribution of the quarks in the sea and $V(x)$ describes the valence quarks. Furthermore, it will prove convenient to separate νW_2 into two other terms, one due to partons and the other due to antipartons,

$$\nu W_2(x) = P(x) + \overline{P}(x) \tag{B.2}$$

If we also assume that the sea of $q-\bar{q}$ pairs consists of an equal mixture of bare quarks of all types we have for the proton

$$\begin{aligned} P(x) &= \tfrac{1}{2} C(x) + V(x) \\ \overline{P}(x) &= \tfrac{1}{2} C(x) \end{aligned} \tag{B.3}$$

The model used in the text and described in reference 29 predicts

$$\begin{aligned} C(x) &= 0.30\ (1-x)^{7/2} \\ V(x) &= 1.1\sqrt{x}\,(1-x)^3 \end{aligned} \tag{B.4}$$

which roughly fits the electroproduction data.

Now let us ask for the distribution functions for partons of various types within a proton. We denote P_p, P_n, and P_λ as the distribution functions for p-quarks, n-quarks, and λ-quarks, respectively. Then, recalling that each quark contributes to the distribution functions through the square of its charge, we can write

$$\begin{aligned} P_p(x) &= c(\tfrac{2}{3})^2 C(x) + 2d(\tfrac{2}{3})^2 V(x) \\ P_n(x) &= c(\tfrac{1}{3})^2 C(x) + d(\tfrac{1}{3})^2 V(x) \\ P_\lambda(x) &= c(\tfrac{1}{3})^2 C(x) \end{aligned} \tag{B.5}$$

The fact that the same constant c appears in each equation reflects our assumption that the sea is an equal mixture of quarks of all types. The constants c and d are determined from the requirement

$$P = P_p + P_n + P_\lambda = \tfrac{1}{2} C(x) + V(x) \tag{B.6}$$

and we find

$$c = \tfrac{3}{4}, \quad d = 1 \tag{B.7}$$

In summary,

$$\begin{aligned} P_p &= \frac{2}{3}\overline{P} + \frac{8}{9} V \\ P_n &= \frac{1}{6}\overline{P} + \frac{1}{9} V \\ P_\lambda &= \frac{1}{6}\overline{P} \end{aligned} \tag{B.8}$$

A similar exercise gives the antiparton distribution functions,

$$\begin{aligned} P_{\bar{p}} &= \frac{2}{3}\overline{P} \\ P_{\bar{n}} &= \frac{1}{6}\overline{P} \\ P_{\bar{\lambda}} &= \frac{1}{6}\overline{P} \end{aligned} \tag{B.9}$$

With these preliminaries complete it is a simple exercise to write the form factors for processes involving parton-antiparton annihilation in terms of C(x) and V(x). Let us choose the reaction $h + h \to \ell + \text{"x"}$ as an example,

$$\begin{aligned} \sum_i \frac{1}{e_i^2} F_{ci}(z_1)\, F_{c\bar{i}}(z_2) &= \frac{1}{(\frac{2}{3})^2} P_p(z_1) P_{\bar{p}}(z_2) + \frac{1}{(\frac{1}{3})^2} P_n(z_1) P_{\bar{n}}(z_2) + \frac{1}{(\frac{1}{3})^2} P_\lambda(z_1) P_{\bar{\lambda}}(z_2) \\ &\quad + (\text{same terms with arguments interchanged}) \\ &= (\tfrac{3}{2})^2 \left(\tfrac{2}{3}\overline{P}(z_1) + \tfrac{8}{9}V(z_1)\right) \tfrac{2}{3}\overline{P}(z_2) \\ &\quad + 3^2 \left(\tfrac{1}{6}\overline{P}(z_1) + \tfrac{1}{9}V(z_1)\right) \tfrac{2}{3}\overline{P}(z_2) + 3^2 \frac{1}{6^2}\overline{P}(z_1)\overline{P}(z_2) + \ldots \\ &= \left(\tfrac{2}{3}\overline{P}(z_1) + \tfrac{3}{2}V(z_1)\right)\overline{P}(z_2) + \ldots \\ &= \tfrac{2}{3}\left(\overline{P}(z_1) P(z_2) + P(z_1)\overline{P}(z_2)\right) \end{aligned} \tag{B.10}$$

Other processes involving similar sums are computed in the same way. We simply collect the results here and leave the verifications to the reader,

1. $\gamma + h \to \gamma + \text{"x"} \quad \sum_i e_i^2 F_{ai}(z_1) = \frac{2}{3}\overline{P}(z_1) + \frac{11}{27} V(z_1)$

2. $h + h \to \gamma + \text{"x"} \quad \sum_i F_{ai}(z_1) F_{b\bar{i}}(z_2) = \overline{P}(z_1)\left(\frac{1}{2}\overline{P}(z_2) + \frac{11}{18} V(z_2)\right)$

$$+ P(z_2)\left(\frac{1}{2}\overline{P}(z_1) + \frac{11}{18} V(z_1)\right) \qquad \text{(B.11)}$$

3. $h + h \to \ell + \text{"x"} \quad \sum_i \frac{1}{e_i^2} F_{ai}(z_1) F_{b\bar{i}}(z_2) = \frac{3}{2}\left(\overline{P}(z_1)P(z_2) + P(z_1)\overline{P}(z_2)\right)$

4. $h + h \to W + \text{"x"} \quad \sum_i \frac{1}{e_i^2} \frac{1}{e_{\bar{i}_W}^2} F_{ai}(z_1) F_{b\bar{i}_W}(z_2) = \frac{9}{2}\left(\overline{P}(z_1) P(z_2) + P(z_1)\overline{P}(z_2)\right)$

For those processes involving a hadron in the final state the form factors involve the additional structure function $G_{ia}(x)$. As remarked in the text our cross sections include the summation over the types of observed hadrons and so involve only the sum $\Sigma_c G_{ic}(x)$. We also argued on the basis of sum rules and our ignorance of the precise mechanism governing final state interactions, that it is not unreasonable to let this sum be independent of parton type i,

$$\Sigma_c G_{ic}(x) = G(x) \qquad \text{(B.12)}$$

Accepting this, we can calculate the form factor for $h + h \to h$ (annihilation channel),

$$\sum_{ijc} \frac{e_j^2}{e_i^2} F_{ai}(z_1) F_{b\bar{i}}(z_2) G_{jc}(Z_3) = \left(\sum_i \frac{1}{e_i^2} F_{ai}(z_1) F_{b\bar{i}}(z_2)\right)\left(\Sigma_j e_j^2\right) G(z_3)$$

$$= \frac{3}{2}\left(P(z_1)\overline{P}(z_2) + P(z_2)\overline{P}(z_1)\right) 2 \left[\left(\tfrac{2}{3}\right)^2 + \left(\tfrac{1}{3}\right)^2 + \left(\tfrac{1}{3}\right)^2\right] G(z_3) \qquad \text{(B.13)}$$

$$= 2\left(P(z_1)\overline{P}(z_2) + P(z_2)\overline{P}(z_1)\right) G(z_3)$$

where we used Eq. (C.10). The remaining sums involving final state interactions are computed similarly. We list the results for the reader's convenience,

$$
\begin{aligned}
&5.\ \ell + \ell \to h + \text{"x"} \quad \sum_{ic} e_i^2 G_{ic}(z_1) = \frac{4}{3} G(z_1) \\
&6.\ \gamma + \gamma \to h + \text{"x"} \quad \sum_{ic} e_i^4 G_{ic}(z_1) = \frac{4}{9} G(z_1) \\
&7.\ \gamma + h \to h + \text{"x"} \quad \sum_{ic} e_i^2 F_{a\bar{i}}(z_1) G_{ic}(z_2) = \left(\tfrac{2}{3}\overline{P}(z_1) + \frac{11}{27} V(z_1)\right) G(z_2) \\
&8.\ h + h \to h + \text{"x"} \quad \sum_{ijc} \frac{e_j^2}{e_i^2} F_{ai}(z_1) F_{b\bar{i}}(z_2) G_{jc}(z_3) = 2\Big(P(z_1)\overline{P}(z_2) + \overline{P}(z_1) P(z_2)\Big) G(z_3) .
\end{aligned}
\tag{B.14}
$$

In all these applications the incident and target hadrons have been chosen to be protons simply because this is the experimentally simplest possibility. The results of this Appendix, of course, depend upon this choice. The reader may, for instance, consider $\pi^{\pm} + p \to h$ and calculate the cross section for this process along the same lines as discussed here. A more detailed study of this type may very well be worthwhile since the results are sensitive to the charges of the valence partons making up the various hadrons.

APPENDIX C

Sum Rules

Here we derive the sum rules (II.3) and (II.4) discussed in the text. Consider first the case $e^+ + e^- \to$ hadrons or $\gamma + \gamma \to$ hadrons. We write the fully differential cross-section for producing n_1 hadrons of type 1, n_2 hadrons of type 2, etc.)

$$d\sigma = F(p_{rs})(dp_{11}\cdots dp_{1n_1})(dp_{21}\cdots dp_{2n_2})\cdots(dp_{a1}\cdots dp_{an_a})$$

$$d\sigma = F(p)\,\lceil dp\rceil \tag{C.1}$$

where $F(p_{rs})$ is symmetric in s for fixed hadron type r. The phase-space element dp may stand for d^3p or some larger element (such as $d|\underset{\sim}{p}|$). The partial cross-section $\sigma(n_1\cdots n_a)$ is obtained by integration over all of phase-space after division by the combinatorial factor $\lceil n_1!\, n_2!\cdots n_a!\rceil$

$$\sigma(n_1\cdots n_a) = \frac{F(p)}{n_1!\, n_2!\cdots n_a!}\,[dp] \tag{C.2}$$

The partial single-particle distribution function $\frac{d\sigma}{dp_r}(n_1\cdots n_a) \equiv \frac{d\sigma}{dp_{r1}}(n_1\cdots n_a)$ is obtained by summing over all the available phase space when p_{r1} is held fixed. The combinatorial factor $(n_r-1)!$ is evidently required instead of $n_r!$ Thus,

$$\frac{d\sigma}{dp_r}(n_1\cdots n_a) = \int \frac{n_r F(p)}{n_1!\, n_2!\cdots n_a!}\,\frac{[dp]}{dp_{r1}} \tag{C.3}$$

So,

$$\int \frac{d\sigma}{dp_r}\,dp_r = n_r\sigma(n_1\cdots n_a) \tag{C.4}$$

Hence, upon summation over $n_1 \ldots n_a$ to obtain the total cross-section and the single particle distribution function, it follows that the mean multiplicity for hadrons of type 1 is,

$$\bar{n}_1 \equiv \frac{\sum_{n_1 \ldots n_a} n_1 \sigma(n_1 \ldots n_a)}{\sum_{n_1 \ldots n_a} \sigma(n_1 \ldots n_a)} = \frac{1}{\sigma_{tot}} \int \frac{d\sigma}{dp_1} dp_1 \tag{C.5}$$

which is the first sum-rule.

The second sum-rule is obtained by starting with,

$$E d\sigma = \sum_{r=1}^{a} \sum_{s=1}^{n_r} E_{rs} F(p_{rs}) [dp] \tag{C.6}$$

for fixed $n_1 \ldots n_a$, and fixed (total) energy E released to the hadrons. Integrating to obtain the total cross-section gives, using the symmetry possessed by $F(p_{rs})$,

$$\begin{aligned} E \int d\sigma &= \int (n_1 E_{11} + n_2 E_{22} + \ldots + n_a E_{a1}) \frac{F(p_{rs})}{n_1! \ldots n_a!} [dp] \\ &= \int \left(E_{11} \frac{d\sigma}{dp_{11}} dp_{11} + E_{21} \frac{d\sigma}{dp_{21}} dp_{21} + \ldots + E_{a1} \frac{d\sigma}{dp_{a1}} dp_{a1} \right) \\ &= \sum_r \int E_r \frac{d\sigma}{dp_r} (n_1 \ldots n_a) dp_r \ . \end{aligned} \tag{C.7}$$

Summation over final channels $n_1 \ldots n_a$ yields the energy conservation sum-rule (II.4). The same argument evidently can be made with a component of p replacing E.

Application to electroproduction and deep-inelastic Compton scattering is straightforward. For electroproduction the same argument holds for the laboratory hadron distributions, where E is replaced by $\nu + m_p$, in the standard notation.

To apply the sum-rules to the function $G(x)$ involving an initial parton, we need only invoke longitudinal momentum conservation in the interaction coupling the virtual parton to the final physical hadrons. The argument then follows as in the other cases provided the momentum of the parton is sufficiently high.

APPENDIX D

Estimation of Background

In this appendix we estimate hadron backgrounds coming from ordinary hadron reactions. There exists a wide variety of fits to hadronic diffraction peaks for $p_T \lesssim 1$ GeV/c. These include exponentials, $\exp(-ap_T)$, gaussians, $\exp(-bp_T^2)$, and combinations, $\exp(-cp_T - dp_T^2)$. For typical values of the parameters a-d the simple exponential is many orders of magnitude larger than the gaussian fits for $p_T \gtrsim 3$ GeV/c. We will be conservative and estimate our background in h + h → h + "anything" reactions with,

$$E \frac{d\sigma}{dp_T^2 \, dp_\parallel} = c\, e^{-6p_T} \tag{D.1}$$

although all of the present fits may fail miserably when extrapolated to large values of p_T.

In order to determine the constant appearing in (D.1) we recall the expression for the mean multiplicity in inclusive hadronic reactions obtained in Appendix C,

$$\begin{aligned} \bar{n}(s)\, \sigma_{\text{tot, inel.}}(s) &= d\sigma \\ &\approx c \int_{\sim m}^{s} \frac{dp_\parallel}{E} \int e^{-6p_T} \, dp_T^2 \\ &= \frac{c}{18} \ell n\, s \end{aligned} \tag{D.2}$$

However, in proton-proton collisions

$$\sigma_{\text{tot., inel.}}(s) \approx 30 \text{ mb.}$$
$$\bar{n}(s) \approx 1.1 \ell n\, s + \text{const.} \tag{D.3}$$

so the constant of interest is crudely,

$$c \approx 1.6 \cdot 10^3 \tag{D.4}$$

This result then gives the background curve noted in Figure 1.

We can also write the background in terms of a structure function

$$E \frac{d\sigma}{dp_T^2\, dp_\parallel} = \frac{4\pi\alpha^2}{p_T^4} \mathscr{F}_{hh\to h}^{\text{background}}(x_1 x_2 s) \tag{D.5}$$

We identify from (D.1) and (D.4),

$$\mathscr{F}_{hh\to h}^{\text{background}}(x_1 x_2 s) = \frac{c}{4\pi\alpha^2} p_T^4 e^{-6p_T} = 2.3 \cdot 10^6 \times x_1^2 x_2^2 s^2 e^{-6\sqrt{x_1 x_2 s}} \tag{D.6}$$

The diffractive background present in colliding beam processes can be estimated by imagining the two virtual photons of Figure 43 converting to two rho mesons which scatter strongly from each other. According to (A.60) the structure function for this process is simply,

$$\mathscr{F}_{ee\to h}^{\text{backgr ound}}(x_1, x_2, s) = \left(\frac{\epsilon}{250}\right)^2 \int \frac{du}{u}\frac{dv}{v}(1-u+\tfrac{1}{2}u^2)(1-v+\tfrac{1}{2}v^2)\mathscr{F}_{hh\to h}^{\text{background}}\left(\frac{x_1}{u}, \frac{x_2}{v}, uvs\right)$$

$$\mathscr{F}_{ee\to h}^{\text{background}}(x_1, x_2, s) = \left(\frac{\epsilon}{250}\right)^2 \mathscr{F}_{hh\to h}^{\text{background}}(x_1 x_2 s) \int_{\sim \frac{m_p}{E}}^{1} \frac{du}{u}(1-u+\tfrac{1}{2}u^2) \int_{\sim \frac{m_p}{E}}^{1} \frac{dv}{v}(1-v+\tfrac{1}{2}v^2)$$

$$\approx \left[\frac{\epsilon \log \frac{\sqrt{s}}{2m_p}}{250}\right]^2 \mathscr{F}_{hh\to h}^{\text{background}}(x_1 x_2 s) \tag{D.7}$$

where $\epsilon \approx 0.04$ and we have estimated the probability that a photon is a rho meson to be $(\frac{1}{250})$ and have approximated the secondary distribution for $\rho\rho$ scattering by the secondary distribution of proton-proton scattering. (D.7) then leads to the background curve plotted in Figures 10 and 11.

Footnotes

1. E. G., AEC Authorizing Legislation FY1965, Part 3, pg. 1701.
2. We may cite here coherent bremsstrahlung from crystals, or coherent production of ρ by γ, Al by π, etc. See, e.g. V. Gribov, B. Ioffe, and I. Pomeranchuk, Soviet Journal of Physics 2, 549 (1966).
3. R. P. Feynman, Phys. Rev. Letters 23, 1415 (1969).
4. This dependence on p_T is given by G. Cocconi, L. Koester and D. Perkins, UCRL-10022, 1961, p. 167, based on the average p_T dependence in inelastic hadronic reactions. N. Bali, Lowell Brown, R. Peccei, and A. Pignotti, Phys. Rev. Letters 25, 557 (1970) have fitted the pion p_T dependence in the specific inclusive reaction $p + p \rightarrow \pi + \text{"x"}$ with the form $\exp -2.44(p_T + p_T^2)$ which falls even more rapidly for large p_T than the choice plotted in Figure 1.
5. T. T. Wu and C. N. Yang, Phys. Rev. 137, B708 (1965).
6. S. M. Berman and M. Jacob, Phys. Rev. Letters 25, 1683 (1970).
7. E. D. Bloom and F. J. Gilman, Phys. Rev. Letters 25, 1140 (1970).
8. One may, of course, envisage local quartic couplings of partons as well; we neglect this possibility here, as well as higher order couplings, on grounds of simplicity.
9. J. D. Bjorken and E. A. Paschos, Phys. Rev. 185, 1975 (1969).
10. F. J. Gilman, Proceedings of the Fourth International Conference on Electron and Photon Interactions at High Energies, Daresbury Nuclear Physics Laboratory, 1969.
11. S. J. Brodsky, T. Kinoshita, and H. Terazawa, Cornell University preprint, May 1971.

12. J. H. Christenson, G. S. Hicks, L. M. Lederman, P. J. Limon, and B. G. Pope, Phys. Rev. Letters 25, 1523 (1970).

13. S. D. Drell and T. M. Yan, Phys. Rev. Letters 25, 316 (1970).

14. R. H. Dalitz and D. R. Yennie, Phys. Rev. 105, 1598 (1957).

15. A very similar mechanism has been considered by N. Cabibbo, G. Parisi, and M. Testa, Lett. Nuovo Cimento 4, 35 (1970).

16. G. Miller, thesis, SLAC Report 129, January 1971.

17. S. D. Drell and T. M. Yan, Phys. Rev. Letters 24, 181 (1970).

18. The relative overall factor of two occurs because there are two cores produced per event in the colliding beams process and only one in electroproduction.

19. R. Siemann, W. Ash, K. Berkelman, D. Hartill, G. Lichtenstein, and R. Littauer, Phys. Rev. Letters 22, 421 (1969).

20. S. M. Berman, D. J. Levy, and T. L. Neff, Phys. Rev. Letters 23, 1363 (1969). G. Altarelli et al., Phys. Rev. Letters 26, 42 (1971). A. I. Sanda and M. Suzuki, Columbia University preprint, November 1971.

21. S. J. Brodsky and P. Roy, Phys. Rev. D3, 2914 (1971).

22. Y. Yamaguchi, Prog. Theo. Phys. 23, 1117 (1960).

23. L. M. Lederman and B. G. Pope, Columbia University preprint, July 1971.

24. R. P. Feynman, in Proceedings of the Third Topical Conference on High Energy Collisions of Hadrons, edited by C. N. Yang (Gordon and Breach, New York, 1969).

25. The question of the ultimate fate of the fractional charge may be a difficulty of the quark-parton model. B. Ioffe (Phys. Letters 30B, 123 (1960)) estimates z, the important longitudinal distances in configuration space for electroproduction, to be of the order $M_p^{-1}\,\omega$, where ω is the usual scaling variable. This may imply that the active parton tends to travel a considerable distance without interaction before disintegrating into a jet of hadrons. Thus, there

can be a separation of fractional charge over large distances in configuration space as well as momentum space. However, this does not mean that partons must "backflow" that distance to provide the necessary neutralization of fractional charge. This can be accomplished, for example, by a polarization current created by parton-antiparton pairs created from the vacuum by the field of the active parton. This is also related to a problem raised by R. Dashen (cf M. Gell-Mann, invited talk at the International Conference on Duality and Symmetry in Hadron Physics, Tel Aviv, Israel, April 5-7, 1971).

26. For example, see N. Bali, Lowell Brown, R. Peccei, and A. Pignotti, reference 4.

27. L. Caneschi, C. H. Mehto, and H. J. Yesian, Stanford University preprint, March 1971.

28. This happens, for example, with the CKP distribution (cf G. Cocconi, L. Koester, and D. Perkins, op. cit.)

29. J. D. Bjorken, invited talk at the International Conference on Duality and Symmetry in Hadron Physics, Tel Aviv, April 5-7, 1971. This particular quark-parton model has also been discussed and used in several calculations by J. Kuti and V. Weisskopf, MIT preprint, May 1971.

Figure Captions

Fig. 1 - Secondary particle distributions as calculated in the parton model and compared to diffractive backgrounds for typical NAL conditions.

Fig. 2 - Pointlike Yukawa coupling between partons.

Fig. 3 - A catalog of pointlike couplings among partons.

Fig. 4 - A momentum space visualization of hadron-hadron deep inelastic scattering occurring in three steps.

Fig. 5 - Kinematics for inclusive processes.

Fig. 6 - $\mathscr{F}(x_1, x_2)$ for the process $e + e \rightarrow \gamma + e + e$

Fig. 7 - Mechanism for the process $e^+ + e^- \rightarrow$ hadrons + anything

Fig. 8 - $\mathscr{F}(x_1, x_2)$ for the process $\ell + \ell \rightarrow h$ + anything; $G(x) = 2(1-x)$

Fig. 9 - $\mathscr{F}(x_1, x_2)$ for the process $\ell + \ell \rightarrow h$ + anything; $G(x) = 6.84\ \nu W_2(x)$

Fig. 10 - $p \frac{d\sigma}{d\Omega dp}_{\theta=90}$ for the process $\ell + \ell \rightarrow h$ + anything; $\sqrt{s} = 5$ GeV

Fig. 11 - $p \frac{d\sigma}{d\Omega dp}_{\theta=90}$ for the process $\ell + \ell \rightarrow h$ + anything; $\sqrt{s} = 5$ GeV

Fig. 12 - Mechanism for the process $\gamma + \gamma \rightarrow$ hadrons + anything

Fig. 13 - $\mathscr{F}(x_1, x_2)$ for the process $\gamma + \gamma \rightarrow h$ + anything; $G(x) = 2(1-x)$

Fig. 14 - $\mathscr{F}(x_1, x_2)$ for the process $\gamma + \gamma \rightarrow h$ + anything; $G(x) = 6.84\ \nu W_2(x)$

Fig. 15 - $\mathscr{F}(x_1, x_2)$ for the process $\ell + \ell \rightarrow h$ + anything via 2γ process; $G(x) = 2(1-x)$

Fig. 16 - $\mathscr{F}(x_1, x_2)$ for the process $\ell + \ell \rightarrow h$ + anything via 2γ process; $G(x) = 6.84\ \nu W_2(x)$

Fig. 17 - $\mathscr{F}(x_1, x_2)$ for deep inelastic electroproduction $\ell + h \rightarrow \ell$ + anything

Fig. 18 - Mechanism for the process $\ell + h \rightarrow h$ + anything

Fig. 19 - $\mathscr{F}(x_1, x_2)$ for the process $\ell + h \rightarrow h$ + anything; $G(x) = 2(1-x)$

Fig. 20 - $\mathscr{F}(x_1, x_2)$ for the process $\ell + h \rightarrow h$ + anything; $G(x) = 6.84\ \nu W_2(x)$

Fig. 21 - $\mathscr{F}(x_1, x_2)$ for the process $\gamma + h \rightarrow \gamma$ + anything

Fig. 22 - $\mathscr{F}(x_1, x_2)$ for the process $\gamma + h \rightarrow h$ + anything; $G(x) = 2(1-x)$

Fig. 23 - $\mathscr{F}(x_1, x_2)$ for the process $\gamma + h \rightarrow h + \text{anything}$; $G(x) = 6.84\, \nu W_2(x)$

Fig. 24 - (a) Mechanism for deep inelastic Compton scattering

(b) Possible $O(\alpha)$ mechanism for $\gamma + h \rightarrow h + \text{anything}$

Fig. 25 - $\mathscr{F}(x_1, x_2)$ for the Bethe-Heitler process $\gamma + h \rightarrow \mu + \text{anything}$

Fig. 26 - Drell-Yan mechanism for the process $h + h \rightarrow \ell + \text{anything}$

Fig. 27 - $\mathscr{F}(x_1, x_2)$ for the process $h + h \rightarrow \ell + \text{anything}$

Fig. 28 - Mechanism for the process $h + h \rightarrow \gamma + \text{anything}$

Fig. 29 - $\mathscr{F}(x_1, x_2)$ for the process $h + h \rightarrow \gamma + \text{anything}$

Fig. 30 - Possible $O(\alpha)$ mechanism for the process $h + h \rightarrow \gamma + \text{anything}$

Fig. 31 - (a) Photon exchange mechanism for the process $h + h \rightarrow h + \text{anything}$

(b) Annihilation mechanism for the process $h + h \rightarrow h + \text{anything}$

Fig. 32 - Coulomb contribution to $\mathscr{F}(x_1, x_2)$ for the process $h + h \rightarrow h + \text{anything}$; $G(x) = 2(1-x)$

Fig. 33 - Coulomb contribution to $\mathscr{F}(x_1, x_2)$ for the process $h + h \rightarrow h + \text{anything}$; $G(x) = 6.84\, \nu W_2(x)$

Fig. 34 - Annihilation contribution to $\mathscr{F}(x_1, x_2)$ for the process $h + h \rightarrow h + \text{anything}$; $G(x) = 2(1-x)$

Fig. 35 - Annihilation contribution to $\mathscr{F}(x_1, x_2)$ for the process $h + h \rightarrow h + \text{anything}$; $G(x) = 6.84\, \nu W_2(x)$

Fig. 36 - Total cross-section for W production in Drell-Yan parton-antiparton annihilation model

Fig. 37 - Configuration of partons in phase space immediately after deep inelastic interaction for (a) $e^+e^- \rightarrow$ hadrons, (b) $ep \rightarrow e +$ hadrons, (c) $pp \rightarrow$ hadrons.

Fig. 38 - Configuration of partons in phase space long after deep inelastic interaction for (a) $e^+e^- \rightarrow$ hadrons, (b) $ep \rightarrow e +$ hadrons, (c) $pp \rightarrow$ hadrons.

Fig. 39 - Configuration of partons in phase space after an ordinary hadron-hadron collision.

Fig. 40 - Mechanism for the process $\ell + h \rightarrow \ell +$ anything

Fig. 41 - Mechanism for the process $e + e \rightarrow \gamma + (e+e)$

Fig. 42 - Virtual photon acting as a target for deep inelastic scattering in colliding beam process

Fig. 43 - Two photon mechanism which can produce hadrons at high p_T in colliding beam processes.

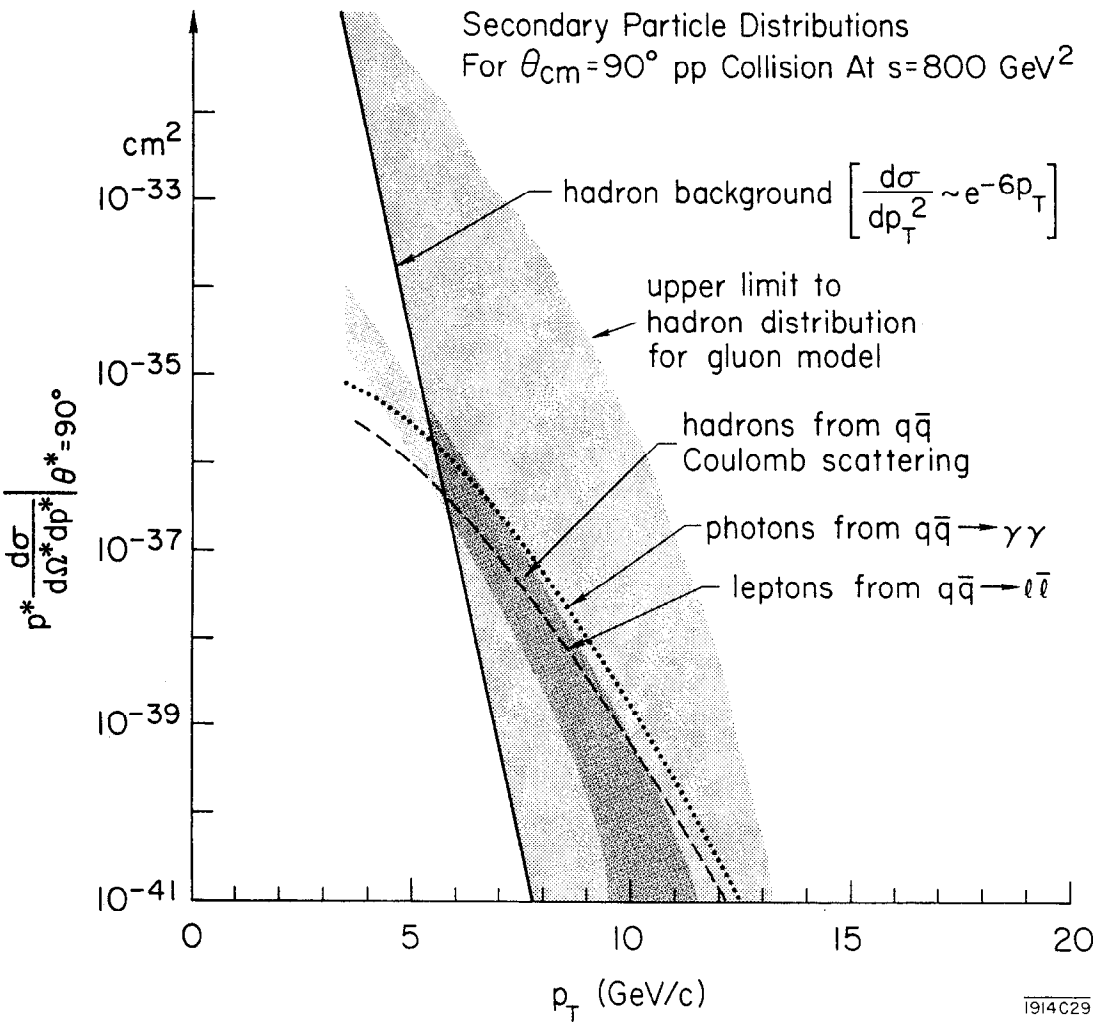
Secondary Particle Distributions
For $\theta_{cm}=90°$ pp Collision At s=800 GeV^2
hadron background $\left[\frac{d\sigma}{dp_T^2} \sim e^{-6p_T}\right]$
upper limit to
hadron distribution
for gluon model
hadrons from $q\bar{q}$
Coulomb scattering
photons from $q\bar{q} \rightarrow \gamma\gamma$
leptons from $q\bar{q} \rightarrow \ell\bar{\ell}$
$p^* \frac{d\sigma}{d\Omega^* dp^*}\Big|_{\theta^*=90°}$
cm^2
10^{-33}
10^{-35}
10^{-37}
10^{-39}
10^{-41}
0
5
10
15
20
p_T (GeV/c)
1914C29

Fig. 1

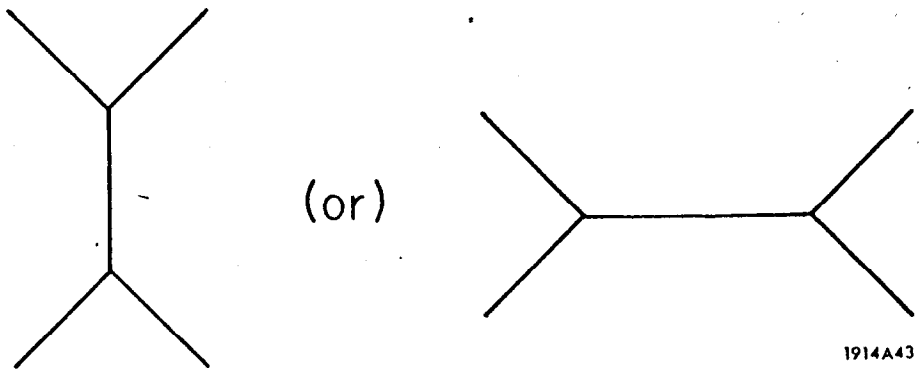

Fig. 2

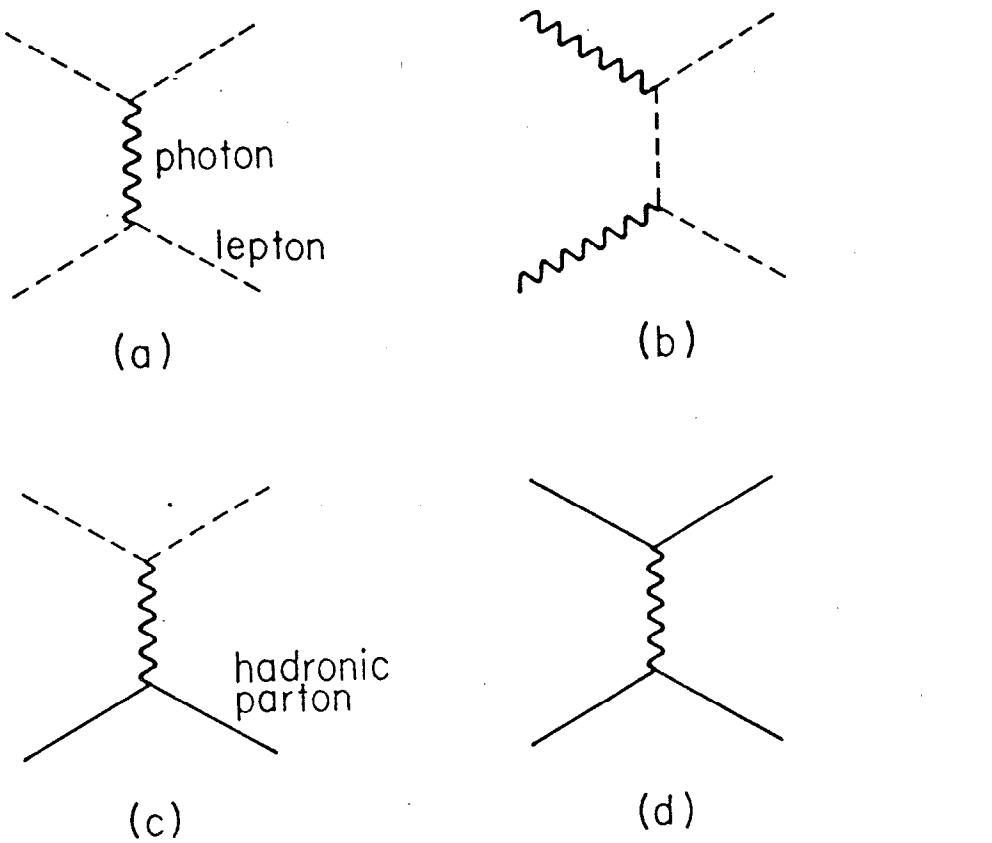

Fig. 3

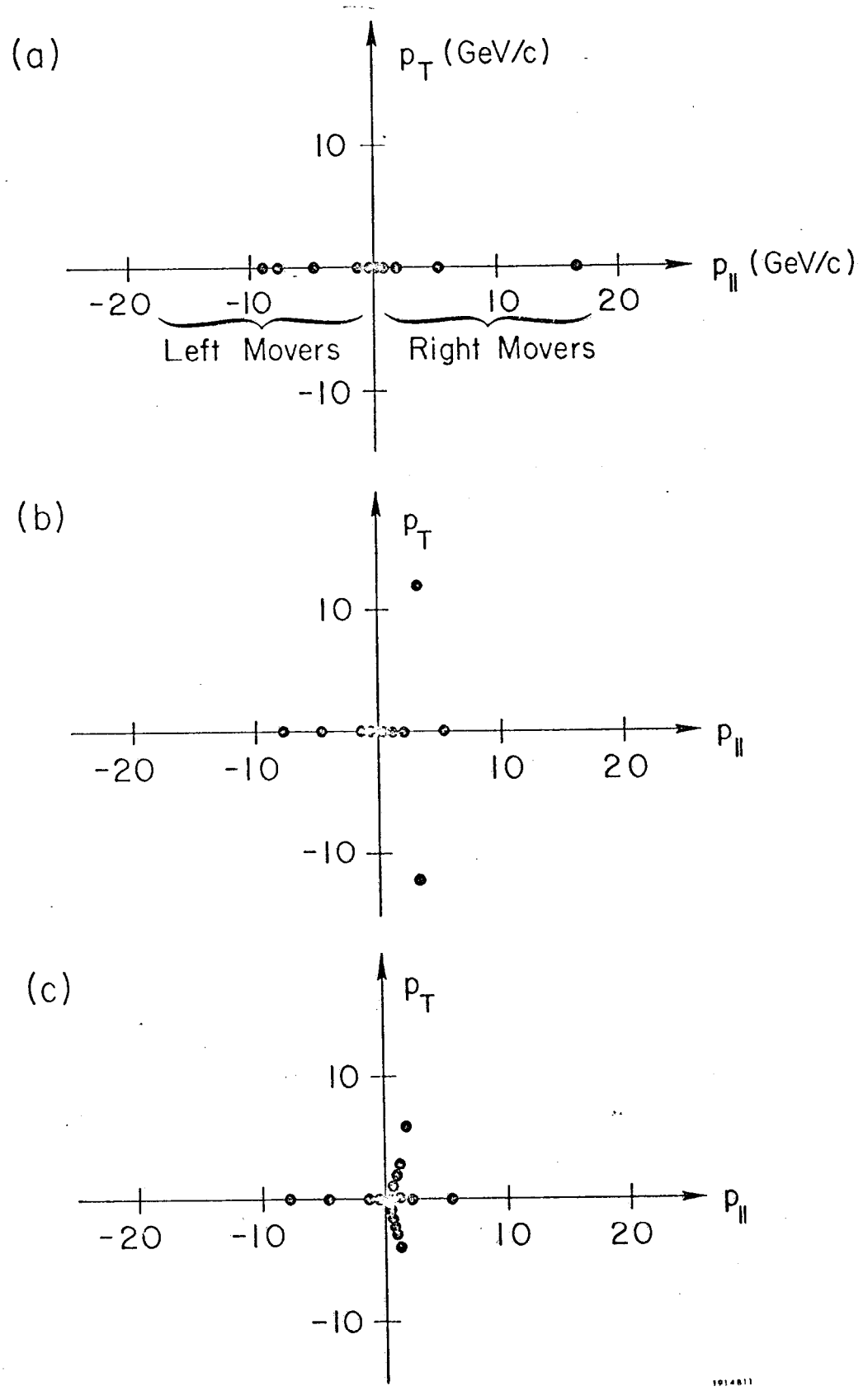
(a)
p_T (GeV/c)
10
-10
-20
-10
10
20
$p_{||}$ (GeV/c)
Left Movers
Right Movers
(b)
p_T
10
-10
-20
-10
10
20
$p_{||}$
(c)
p_T
10
-10
-20
-10
10
20
$p_{||}$

Fig. 4

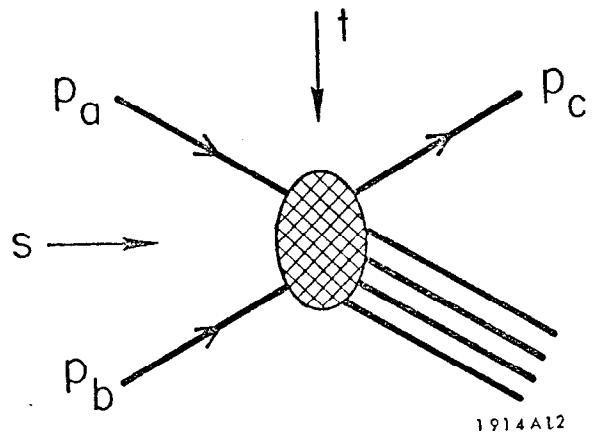

Fig. 5

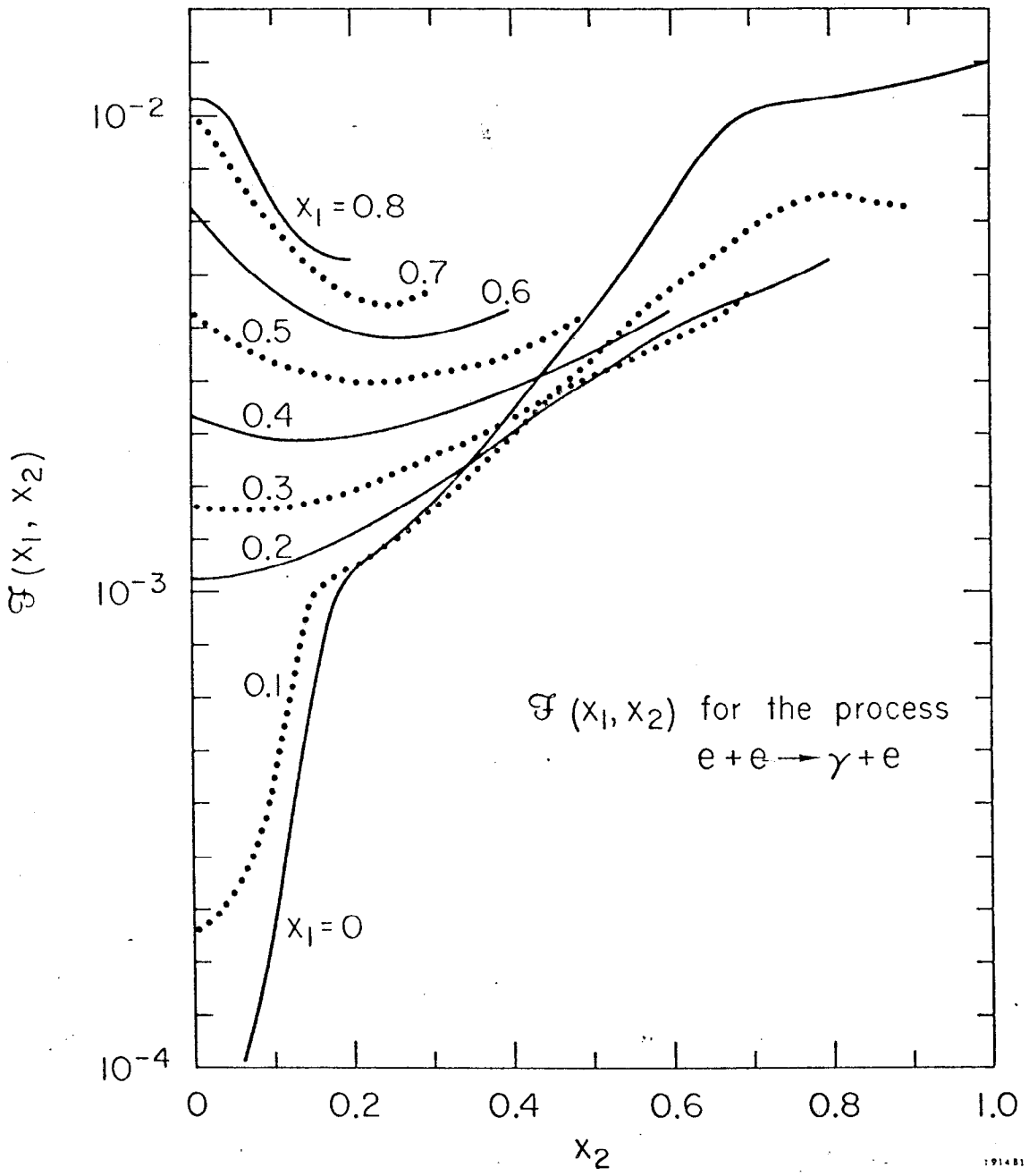
10^{-2}
10^{-3}
10^{-4}
$\mathcal{F}(x_1, x_2)$
$x_1 = 0.8$
0.7
0.6
0.5
0.4
0.3
0.2
0.1
$x_1 = 0$
$\mathcal{F}(x_1, x_2)$ for the process
$e + e \rightarrow \gamma + e$
0
0.2
0.4
0.6
0.8
1.0
x_2
1914B1

Fig. 6

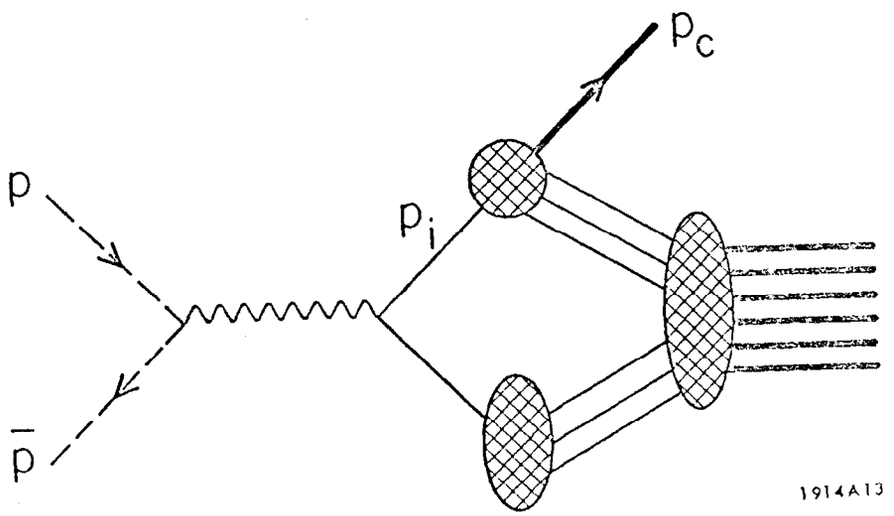

Fig. 7

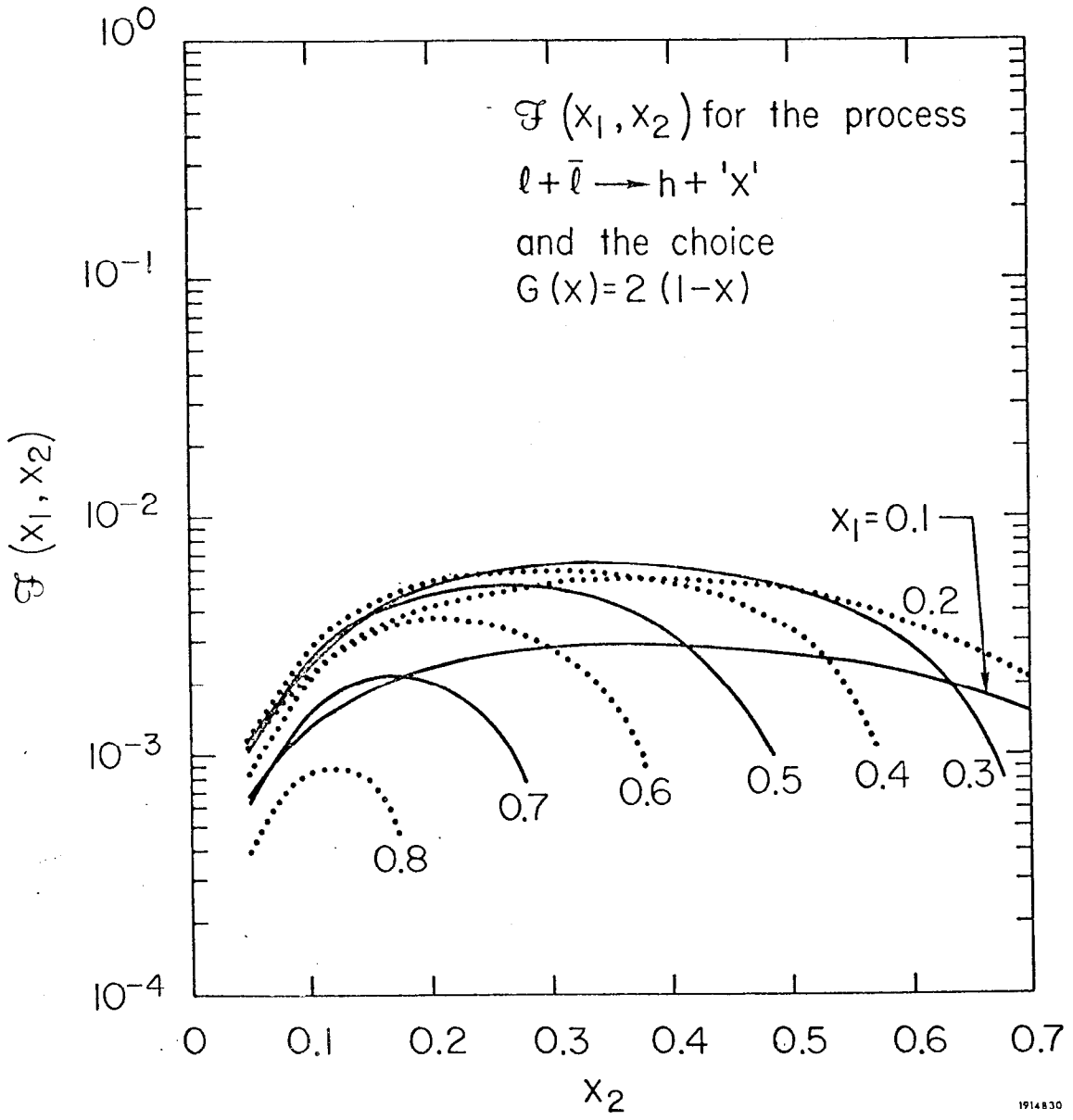
$\mathcal{F}(x_1, x_2)$ for the process
$\ell + \bar{\ell} \rightarrow h + 'X'$
and the choice
$G(x) = 2(1-x)$
$\mathcal{F}(x_1, x_2)$
x_2
$x_1 = 0.1$
0.2
0.3
0.4
0.5
0.6
0.7
0.8
10^0
10^{-1}
10^{-2}
10^{-3}
10^{-4}
0
0.1
0.2
0.3
0.4
0.5
0.6
0.7
1914830

Fig. 8

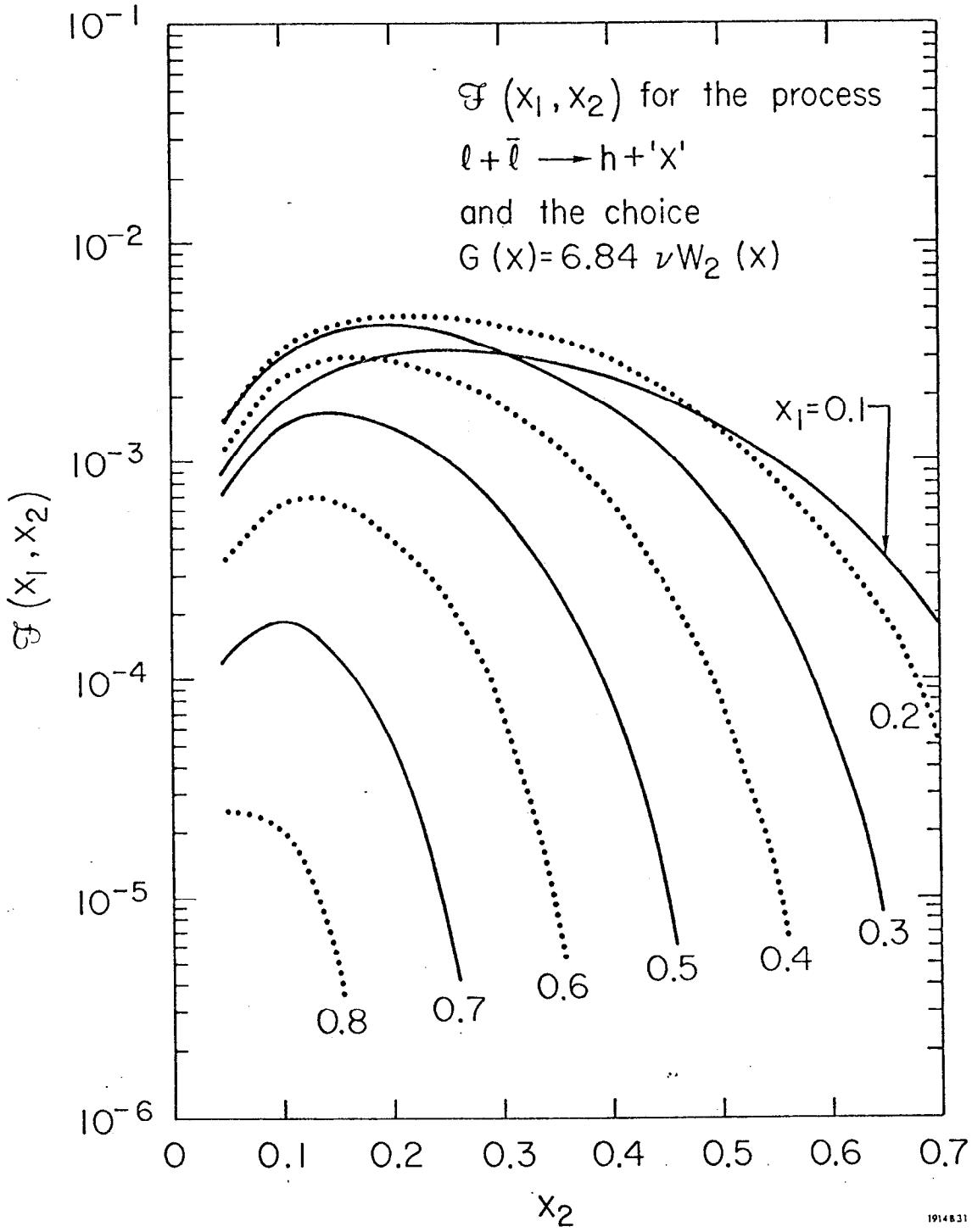
$\mathcal{F}(x_1, x_2)$ for the process
$\ell + \bar{\ell} \longrightarrow h + 'X'$
and the choice
$G(x) = 6.84\ \nu W_2(x)$
$x_1 = 0.1$
0.2
0.3
0.4
0.5
0.6
0.7
0.8
10^{-1}
10^{-2}
10^{-3}
10^{-4}
10^{-5}
10^{-6}
$\mathcal{F}(x_1, x_2)$
0
0.1
0.2
0.3
0.4
0.5
0.6
0.7
x_2
1914B31

Fig. 9

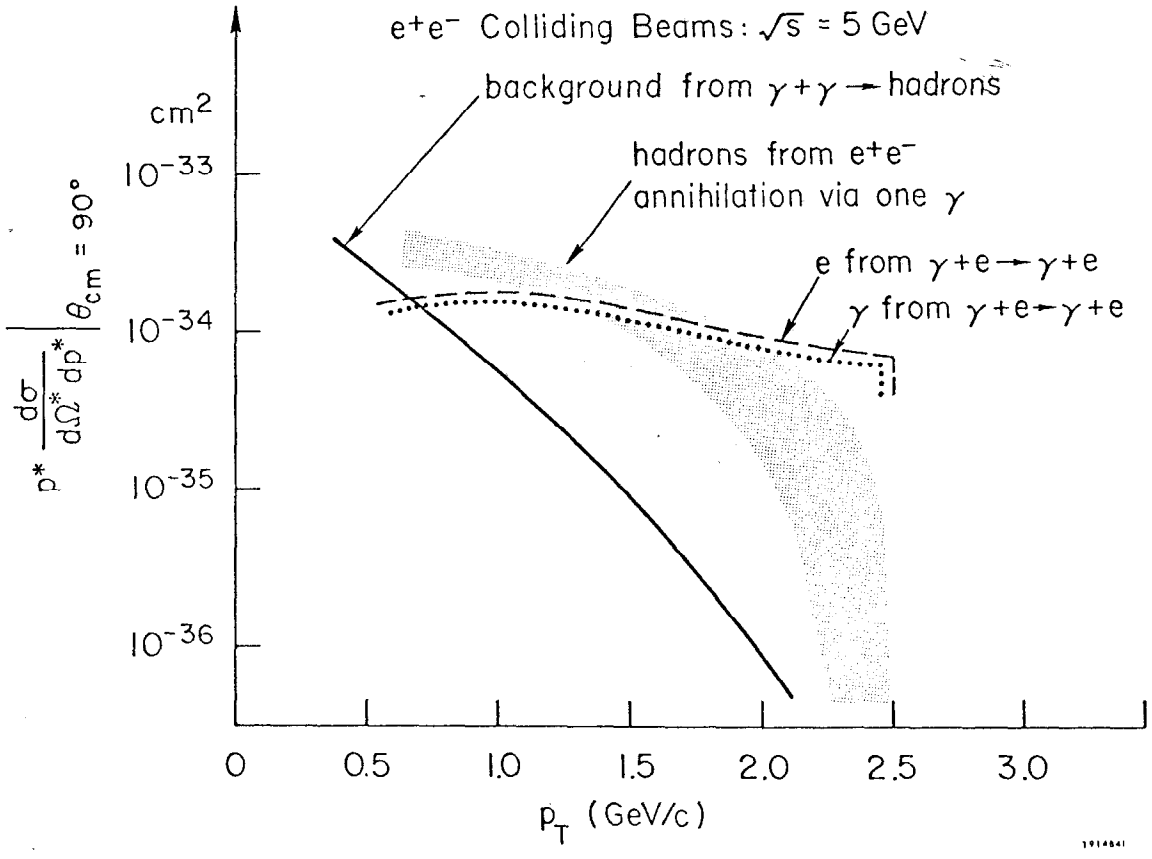
e+e− Colliding Beams: √s = 5 GeV
background from γ+γ → hadrons
hadrons from e+e− annihilation via one γ
e from γ+e → γ+e
γ from γ+e → γ+e
cm2
10−33
10−34
10−35
10−36
p* dσ/dΩ* dp* |θcm = 90°
0
0.5
1.0
1.5
2.0
2.5
3.0
pT (GeV/c)

Fig. 10

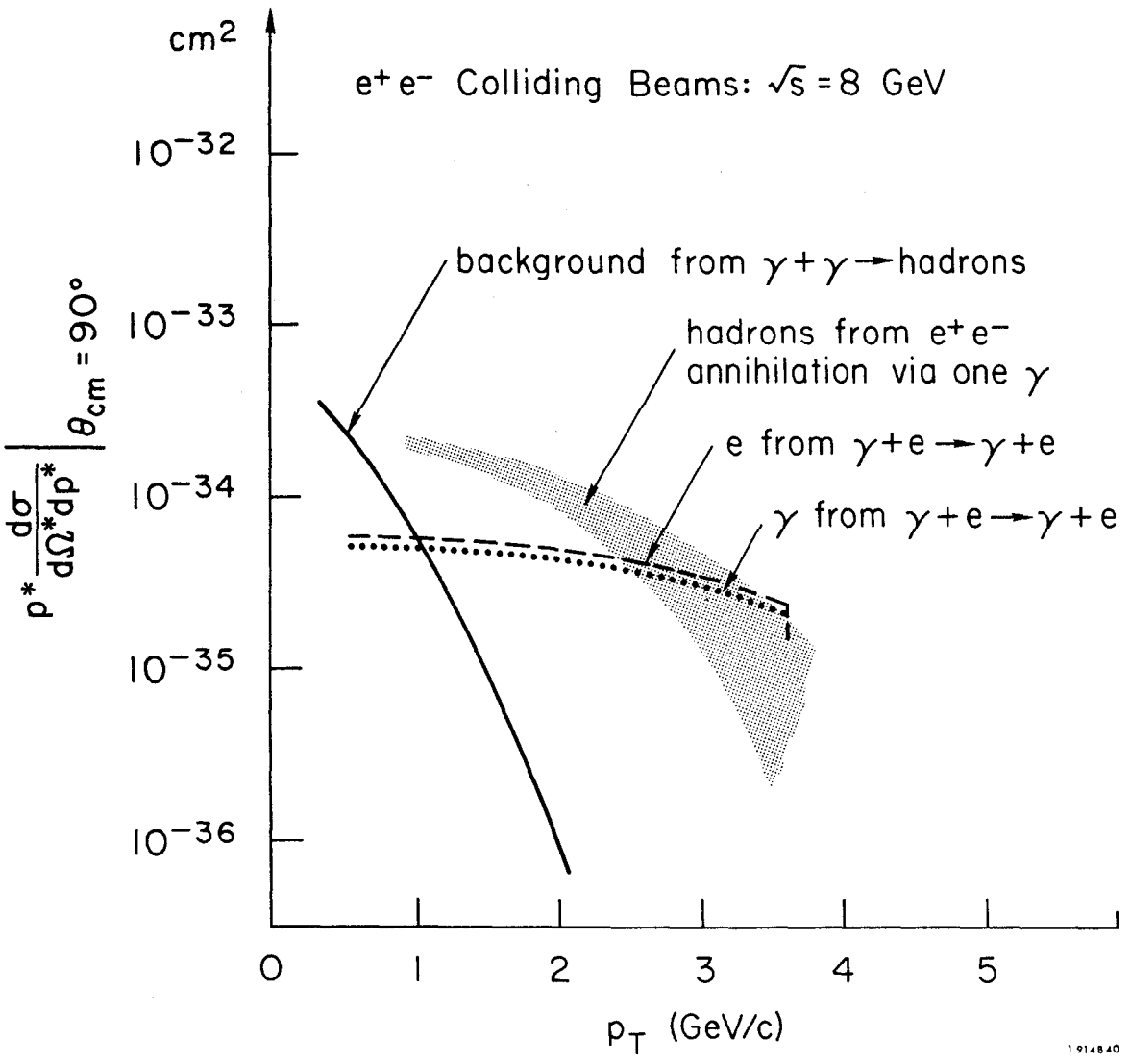
cm2
e+ e− Colliding Beams: √s = 8 GeV
10−32
10−33
10−34
10−35
10−36
background from γ + γ → hadrons
hadrons from e+e− annihilation via one γ
e from γ + e → γ + e
γ from γ + e → γ + e
p* dσ/dΩ*dp* |θcm = 90°
0
1
2
3
4
5
pT (GeV/c)
1 914840

Fig. 11

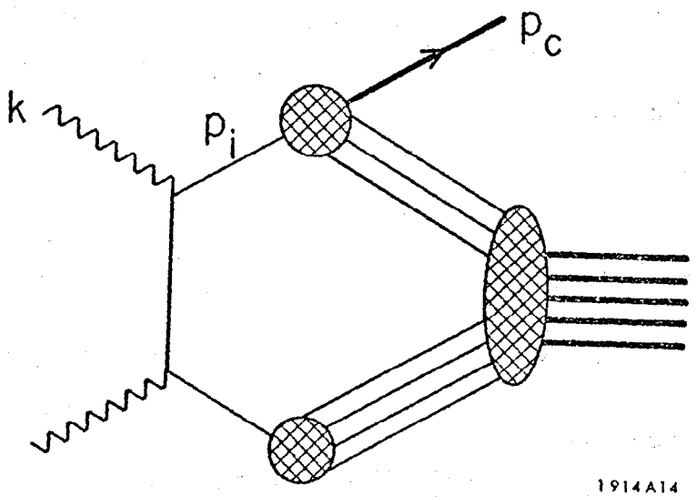

Fig. 12

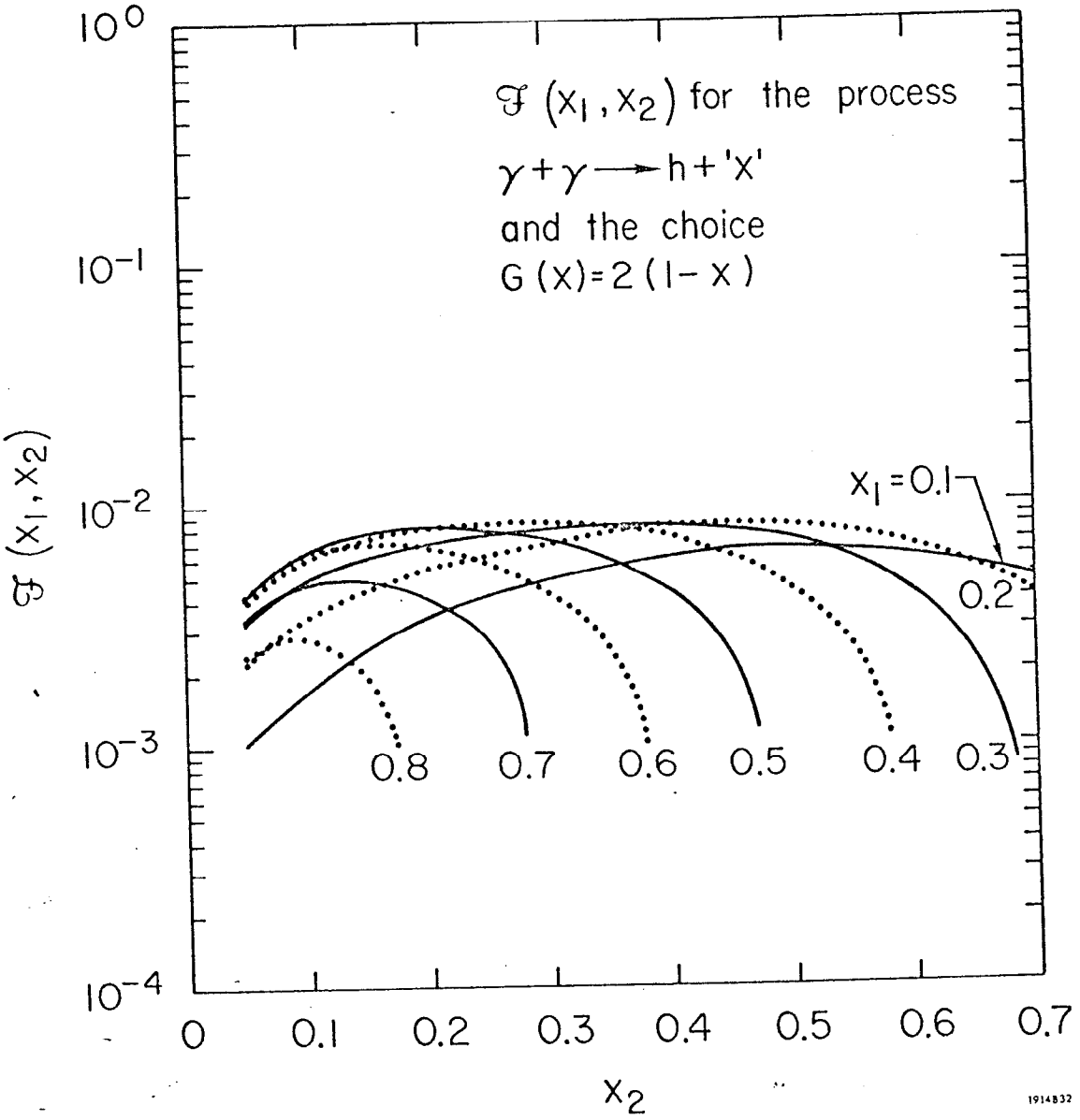
$\mathcal{F}(x_1, x_2)$ for the process
$\gamma + \gamma \longrightarrow h + 'X'$
and the choice
$G(x) = 2(1-x)$
$\mathcal{F}(x_1, x_2)$
x_2
$x_1 = 0.1$
0.2
0.3
0.4
0.5
0.6
0.7
0.8
10^0
10^{-1}
10^{-2}
10^{-3}
10^{-4}
0
0.1
0.2
0.3
0.4
0.5
0.6
0.7
1914B32

Fig. 13

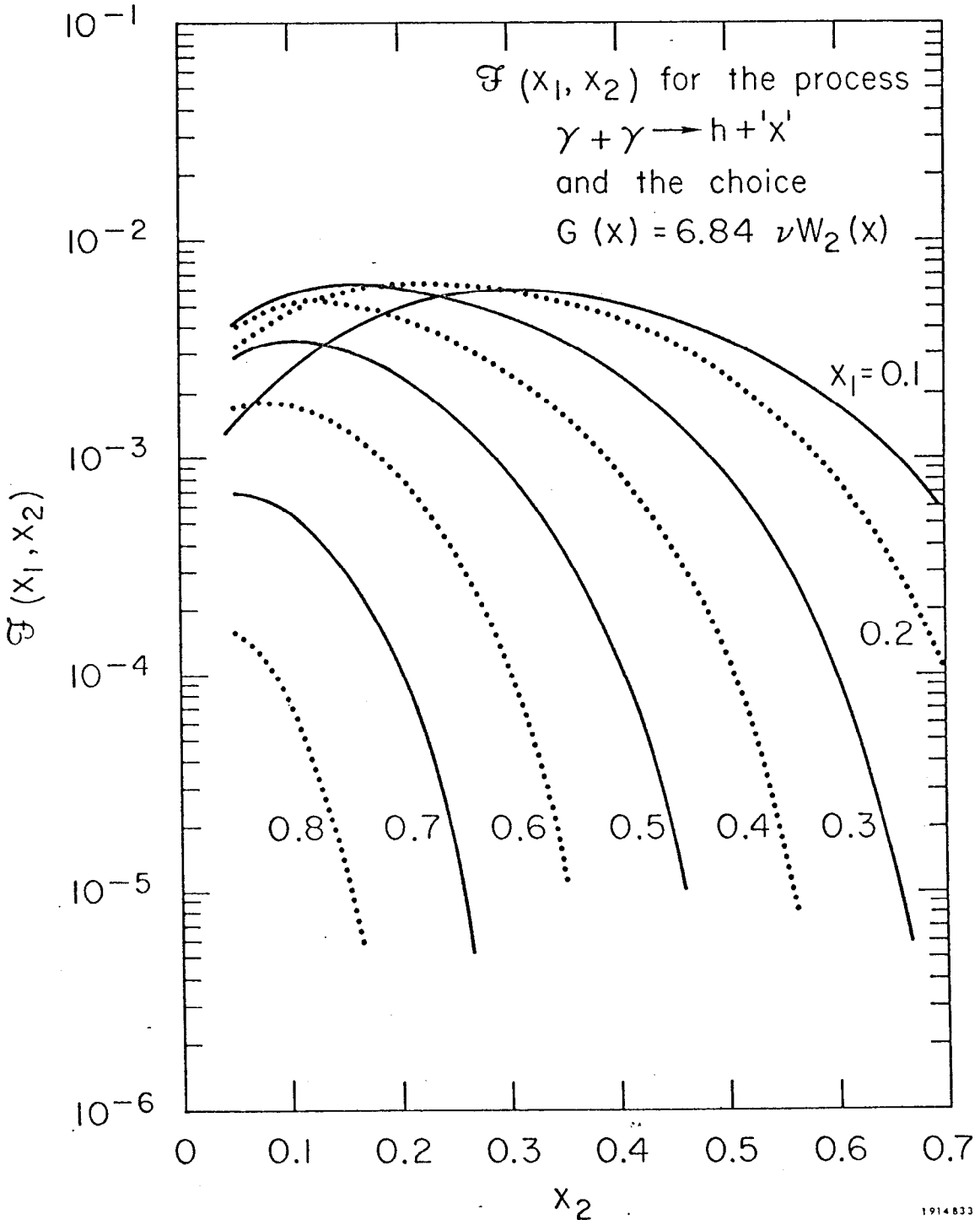
$\mathcal{F}(x_1, x_2)$ for the process
$\gamma + \gamma \rightarrow h + 'x'$
and the choice
$G(x) = 6.84\ \nu W_2(x)$
$x_1 = 0.1$
0.2
0.3
0.4
0.5
0.6
0.7
0.8
10^{-1}
10^{-2}
10^{-3}
10^{-4}
10^{-5}
10^{-6}
$\mathcal{F}(x_1, x_2)$
0
0.1
0.2
0.3
0.4
0.5
0.6
0.7
x_2
1914833

Fig. 14

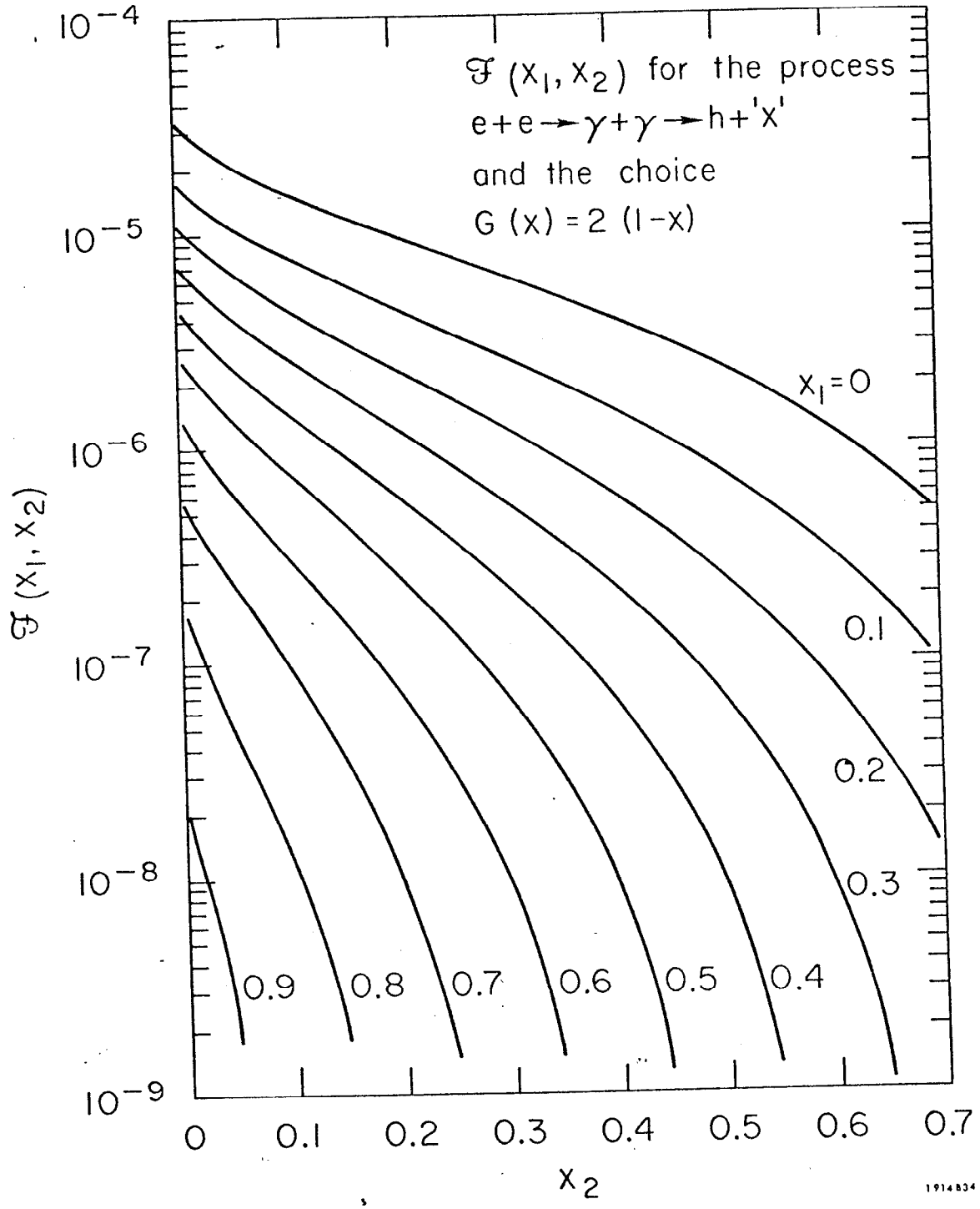
$\mathcal{F}(x_1, x_2)$ for the process
e+e→γ+γ→h+'x'
and the choice
G(x) = 2(1−x)
$\mathcal{F}(x_1, x_2)$
10^{-4}
10^{-5}
10^{-6}
10^{-7}
10^{-8}
10^{-9}
$x_1=0$
0.1
0.2
0.3
0.4
0.5
0.6
0.7
0.8
0.9
0
0.1
0.2
0.3
0.4
0.5
0.6
0.7
x_2
1914834

Fig. 15

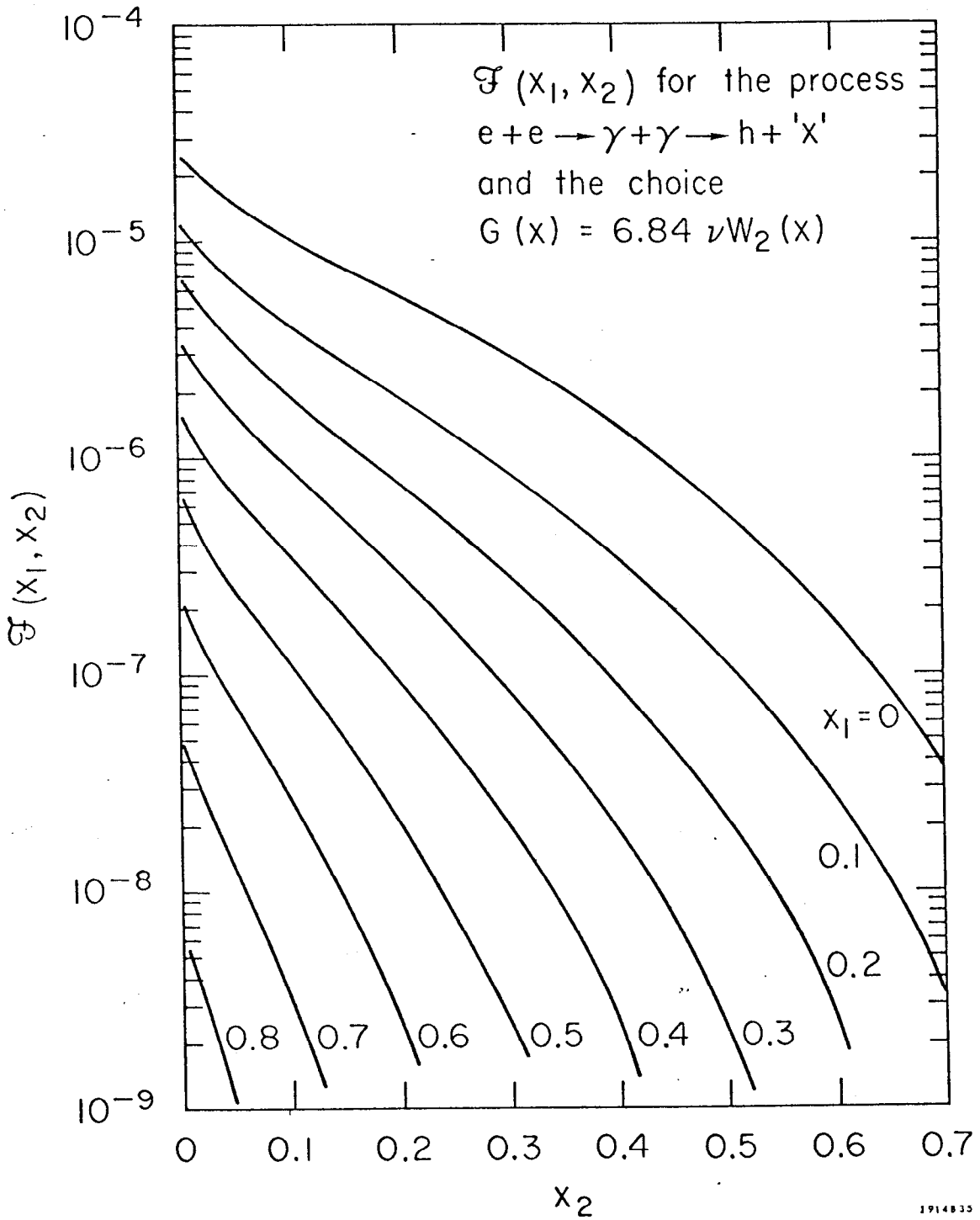
$\mathcal{F}(x_1, x_2)$ for the process
$e+e \rightarrow \gamma+\gamma \rightarrow h+'x'$
and the choice
$G(x) = 6.84\ \nu W_2(x)$
10^{-4}
10^{-5}
10^{-6}
10^{-7}
10^{-8}
10^{-9}
$\mathcal{F}(x_1, x_2)$
$x_1 = 0$
0.1
0.2
0.3
0.4
0.5
0.6
0.7
0.8
0
0.1
0.2
0.3
0.4
0.5
0.6
0.7
x_2
1914B35

Fig. 16

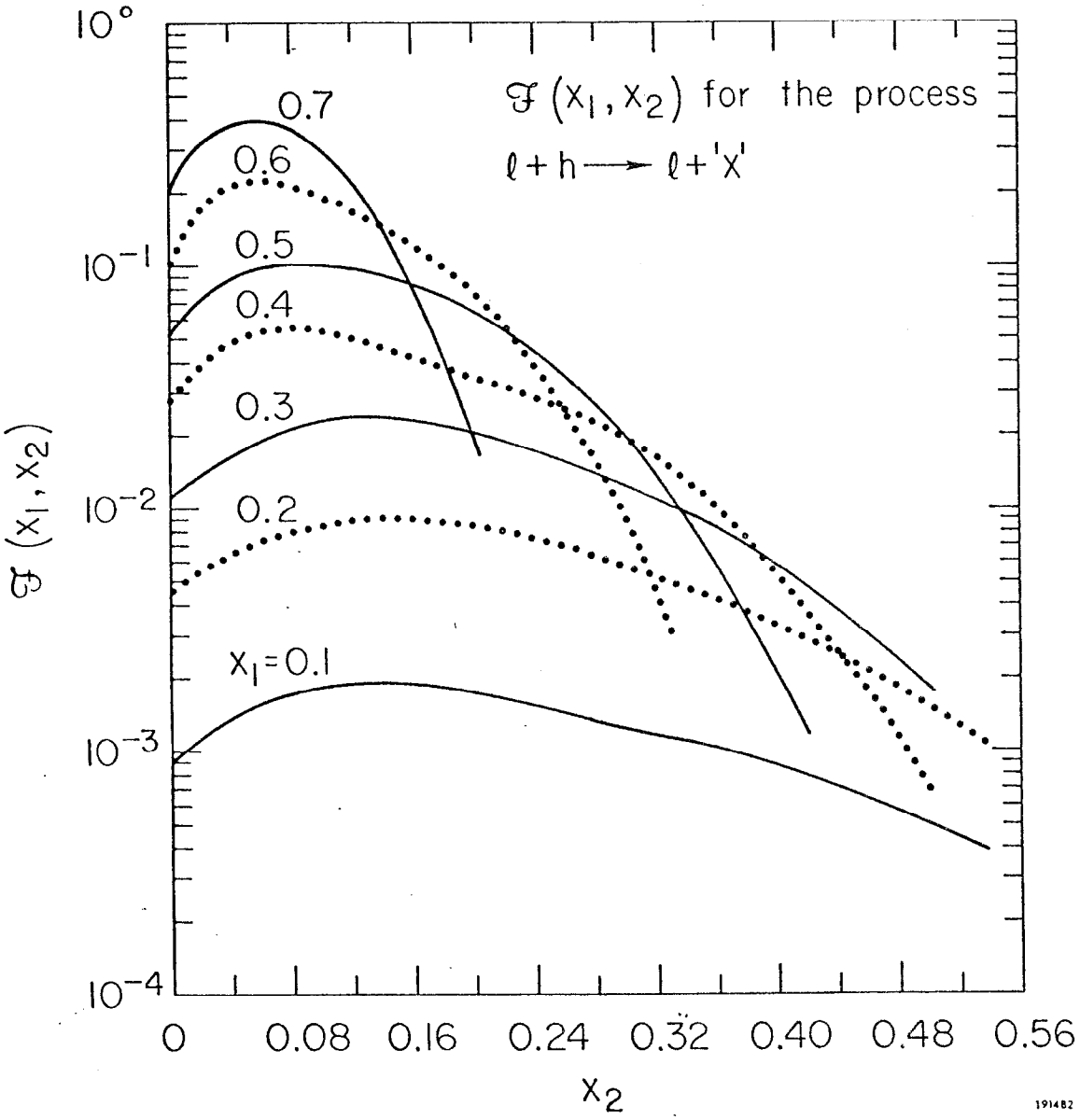
10°
10⁻¹
10⁻²
10⁻³
10⁻⁴
𝔉 (x₁, x₂)
𝔉 (x₁, x₂) for the process
ℓ + h ⟶ ℓ + 'X'
0.7
0.6
0.5
0.4
0.3
0.2
x₁ = 0.1
0
0.08
0.16
0.24
0.32
0.40
0.48
0.56
x₂
1914B2

Fig. 17

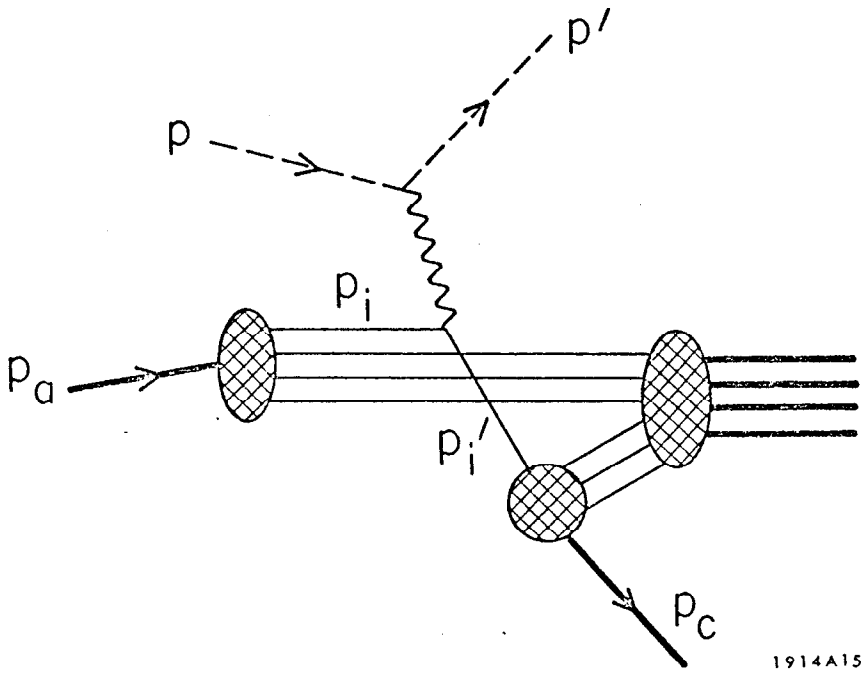

Fig. 18

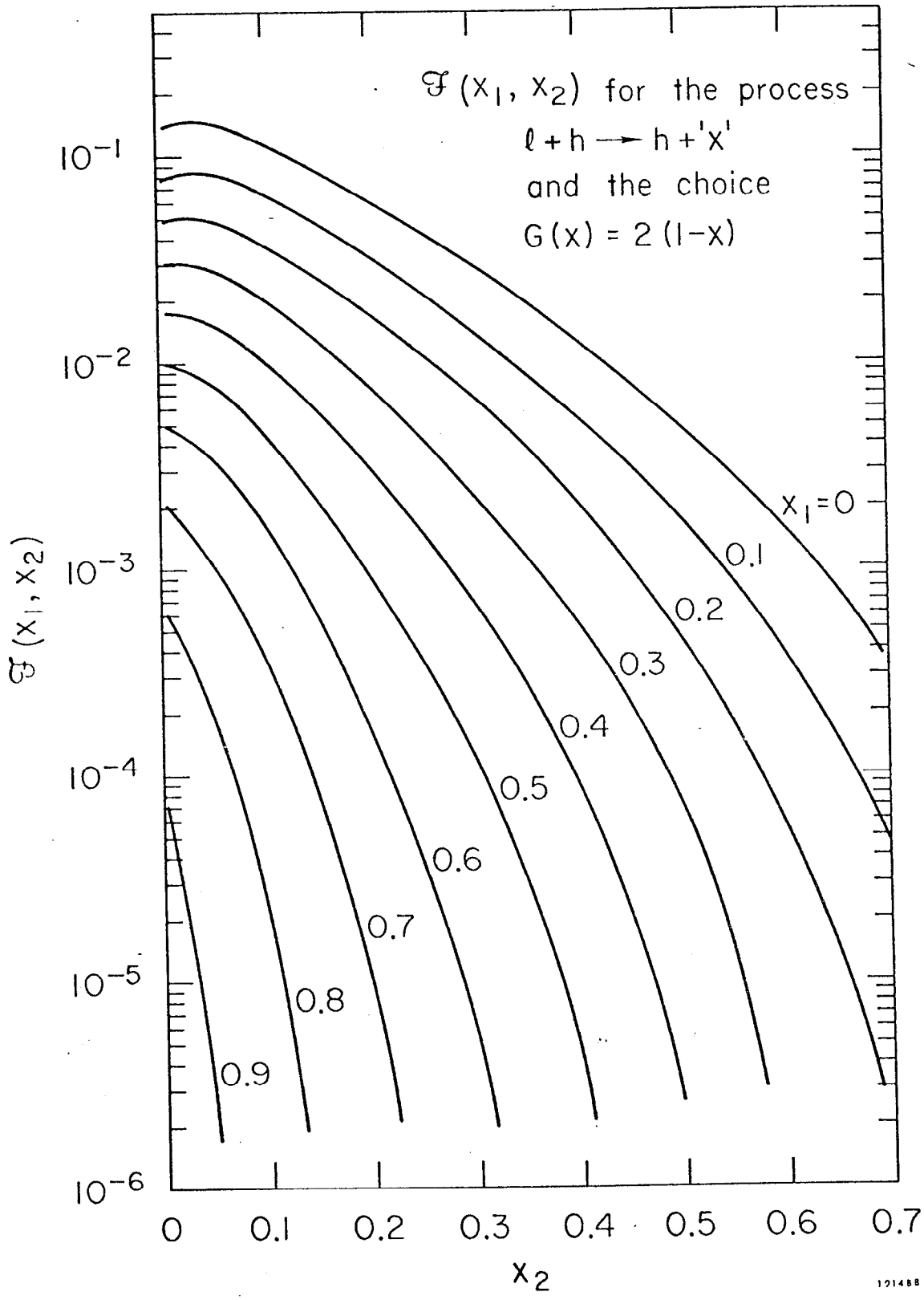
$\mathcal{F}(x_1, x_2)$ for the process
$\ell + h \rightarrow h + 'X'$
and the choice
$G(x) = 2(1-x)$
$x_1 = 0$
0.1
0.2
0.3
0.4
0.5
0.6
0.7
0.8
0.9
10^{-1}
10^{-2}
10^{-3}
10^{-4}
10^{-5}
10^{-6}
$\mathcal{F}(x_1, x_2)$
0
0.1
0.2
0.3
0.4
0.5
0.6
0.7
x_2
121488

Fig. 19

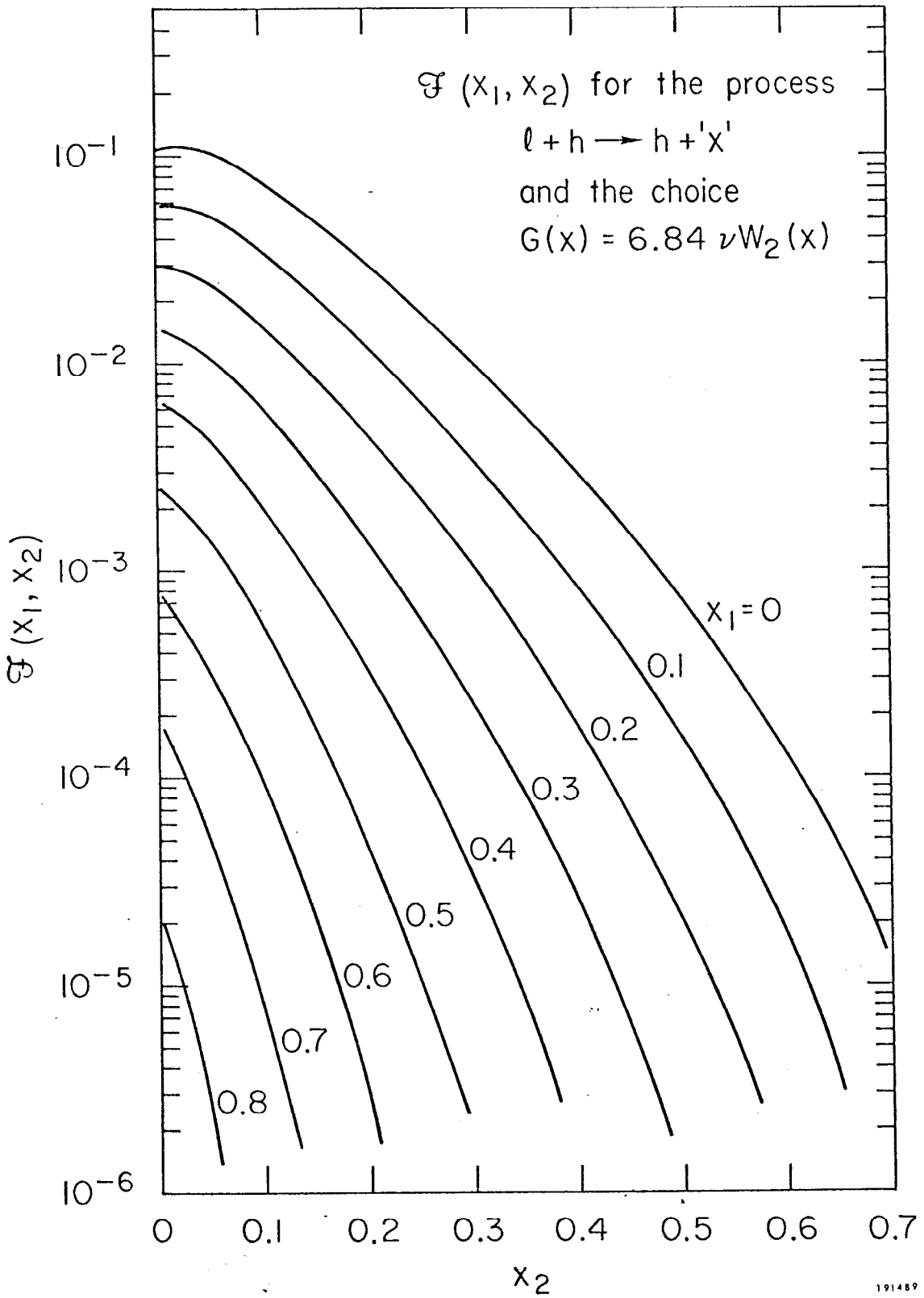
$\mathcal{F}(x_1, x_2)$ for the process
$\ell + h \rightarrow h + 'X'$
and the choice
$G(x) = 6.84\ \nu W_2(x)$
10^{-1}
10^{-2}
10^{-3}
10^{-4}
10^{-5}
10^{-6}
$\mathcal{F}(x_1, x_2)$
$x_1 = 0$
0.1
0.2
0.3
0.4
0.5
0.6
0.7
0.8
0
0.1
0.2
0.3
0.4
0.5
0.6
0.7
x_2
191489

Fig. 20

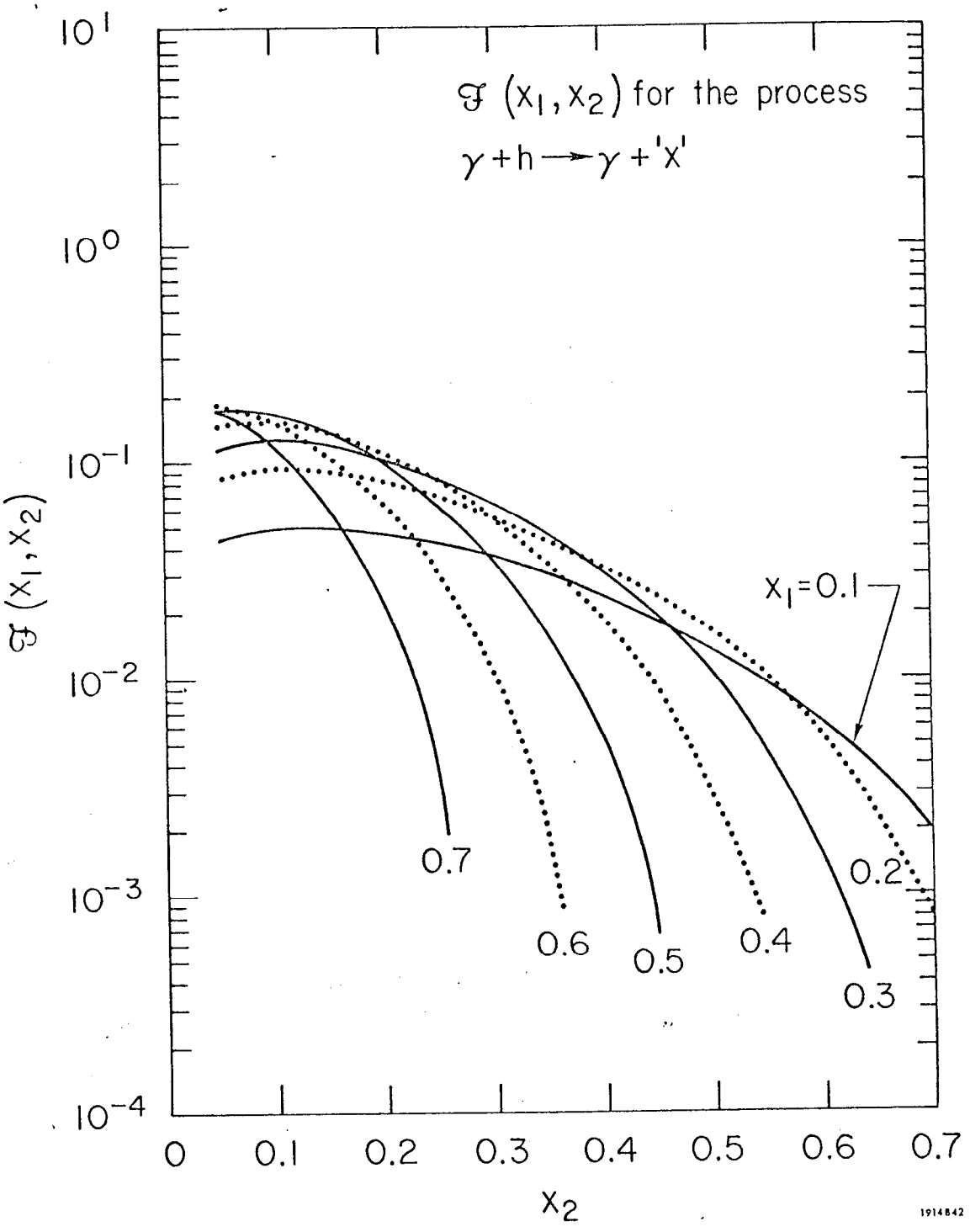
$\mathcal{F}(x_1, x_2)$ for the process
$\gamma + h \rightarrow \gamma + 'X'$
10^1
10^0
10^{-1}
10^{-2}
10^{-3}
10^{-4}
$\mathcal{F}(x_1, x_2)$
$x_1 = 0.1$
0.7
0.6
0.5
0.4
0.3
0.2
0
0.1
0.2
0.3
0.4
0.5
0.6
0.7
x_2
1914B42

Fig. 21

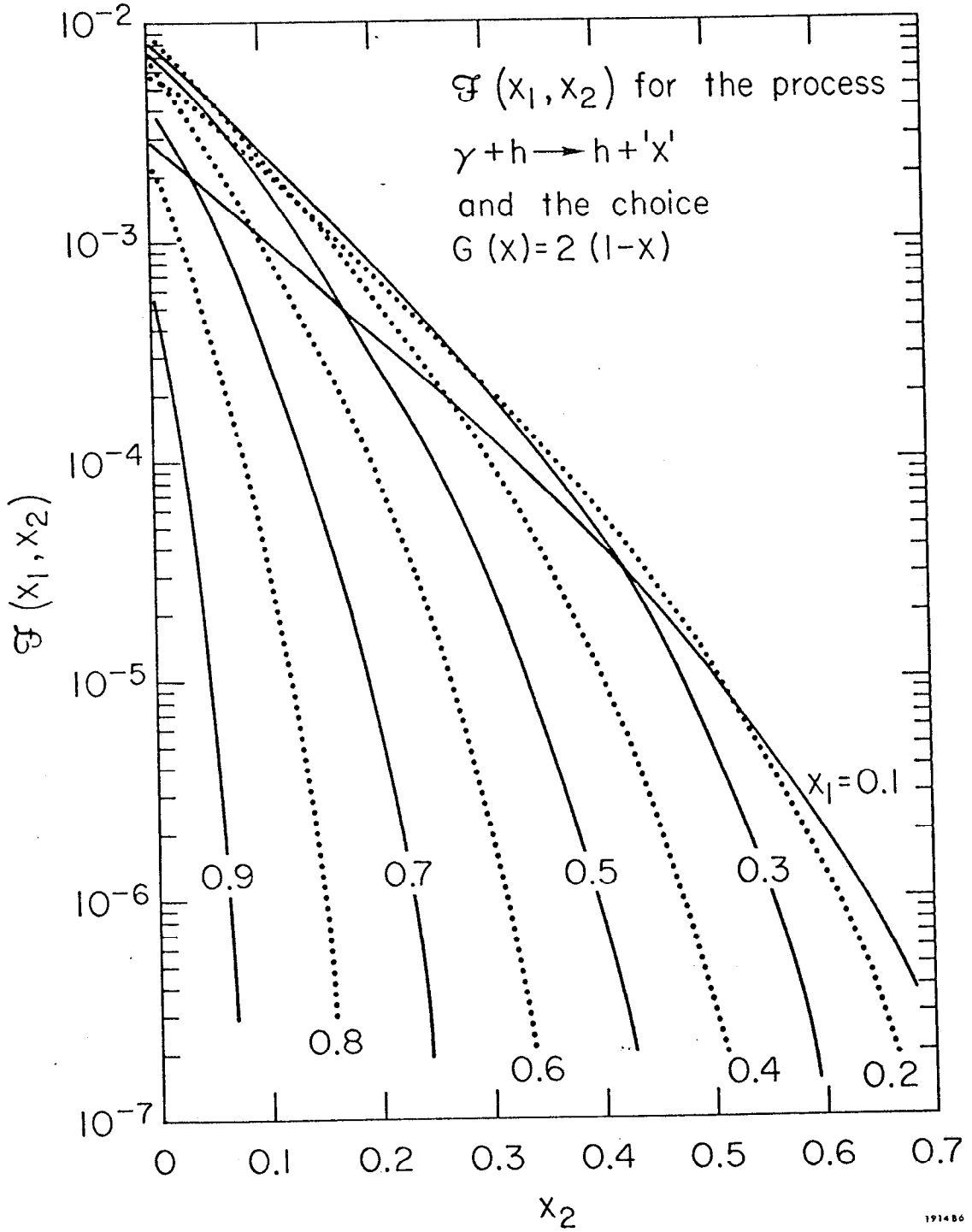
10^{-2}
10^{-3}
10^{-4}
10^{-5}
10^{-6}
10^{-7}
$\mathcal{F}(x_1, x_2)$
$\mathcal{F}(x_1, x_2)$ for the process
$\gamma + h \rightarrow h + 'X'$
and the choice
$G(x) = 2(1-x)$
$x_1 = 0.1$
0.2
0.3
0.4
0.5
0.6
0.7
0.8
0.9
0
0.1
0.2
0.3
0.4
0.5
0.6
0.7
x_2
191486

Fig. 22

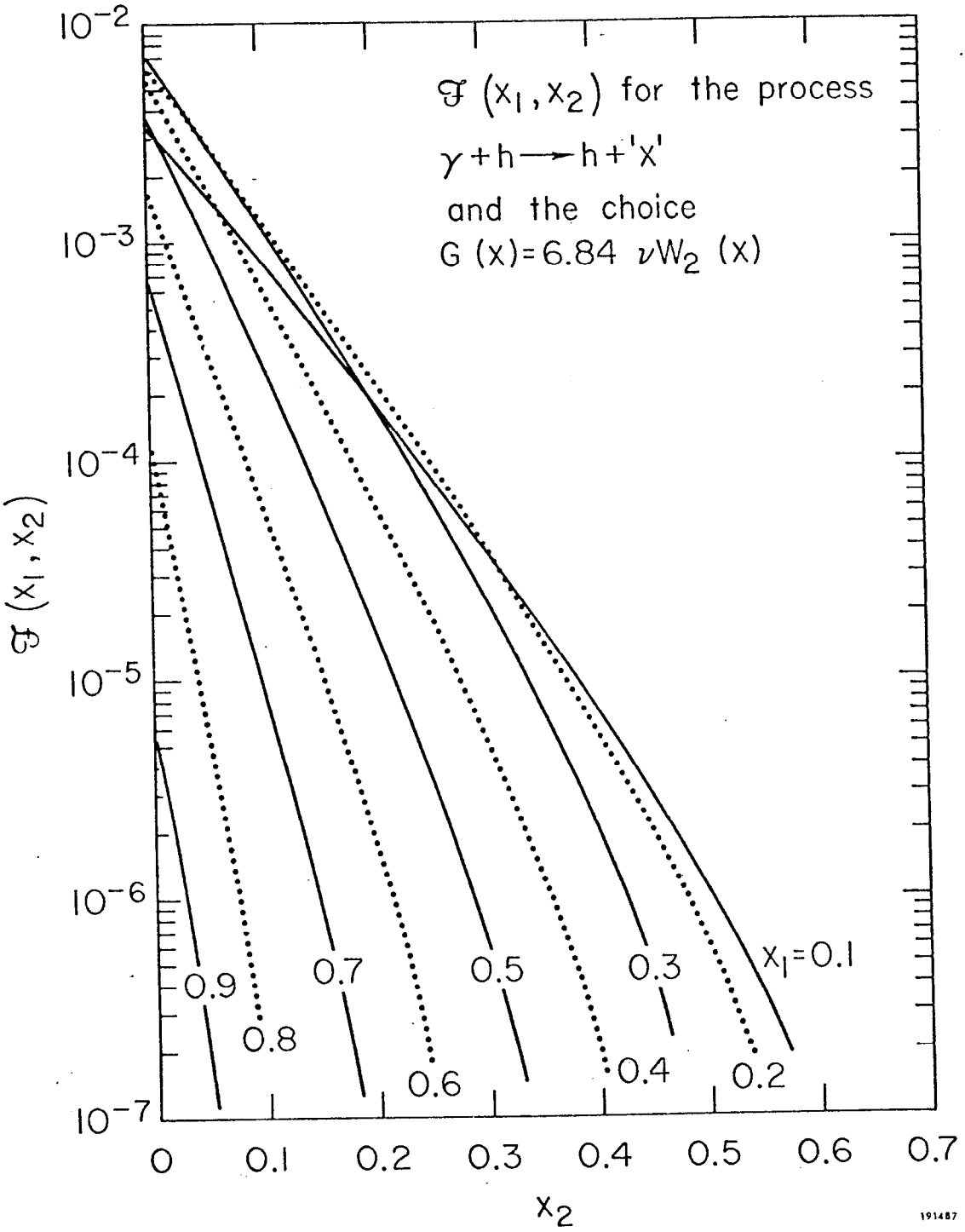
$\mathcal{F}(x_1, x_2)$ for the process
$\gamma + h \rightarrow h + 'X'$
and the choice
$G(x) = 6.84\ \nu W_2(x)$
10^{-2}
10^{-3}
10^{-4}
10^{-5}
10^{-6}
10^{-7}
$\mathcal{F}(x_1, x_2)$
0
0.1
0.2
0.3
0.4
0.5
0.6
0.7
x_2
$x_1 = 0.1$
0.2
0.3
0.4
0.5
0.6
0.7
0.8
0.9
191487

Fig. 23

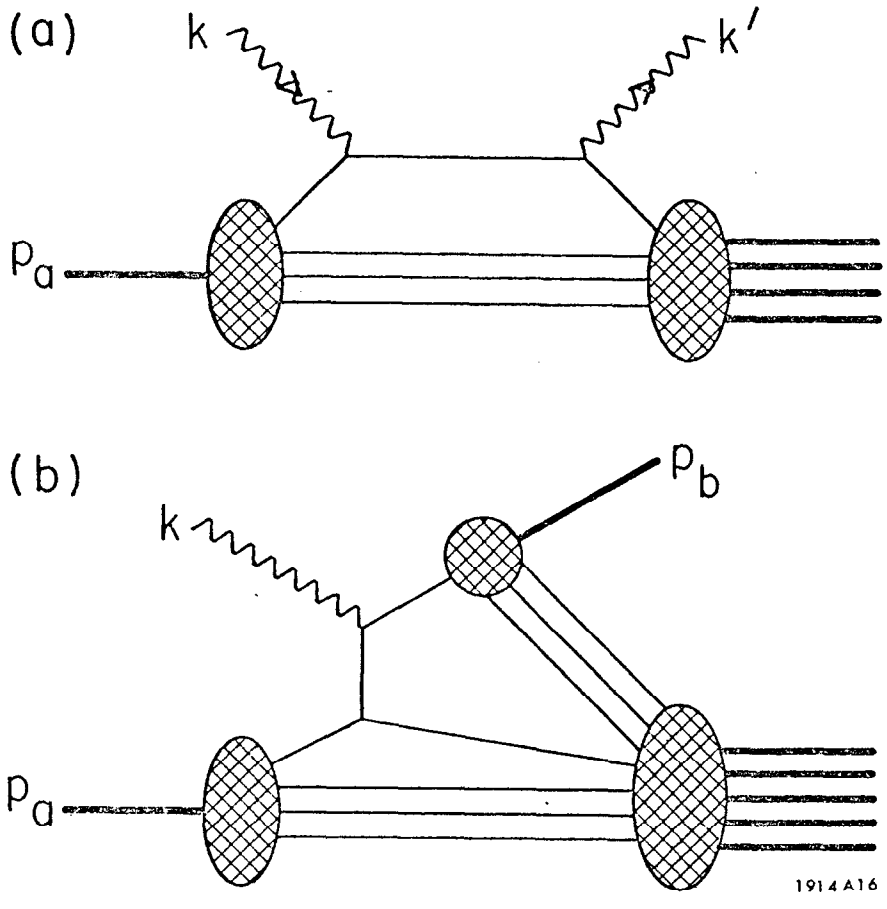

Fig. 24

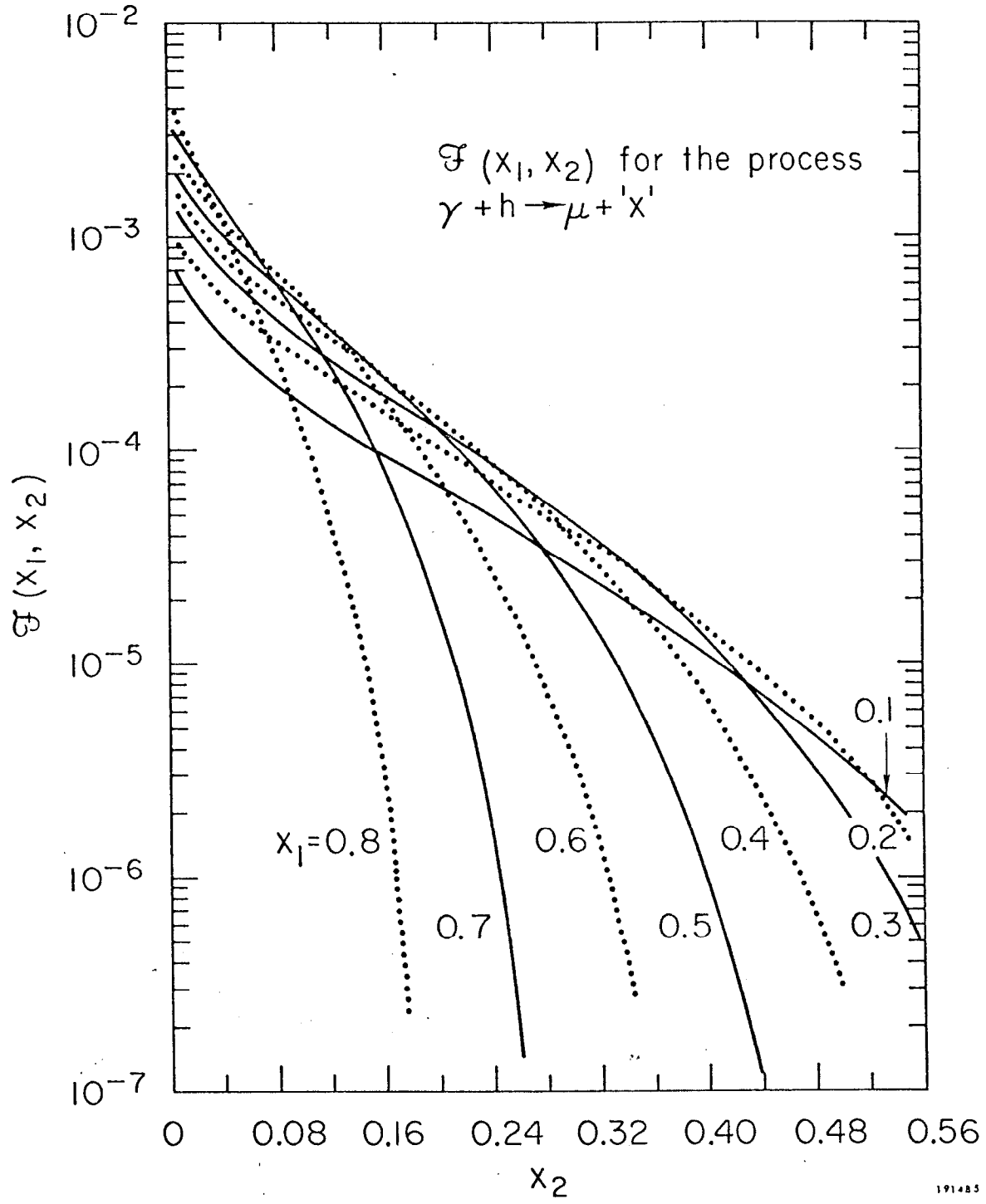
10^{-2}
10^{-3}
10^{-4}
10^{-5}
10^{-6}
10^{-7}
$\mathcal{F}(x_1, x_2)$
$\mathcal{F}(x_1, x_2)$ for the process
$\gamma + h \rightarrow \mu + 'X'$
x_1=0.8
0.7
0.6
0.5
0.4
0.3
0.2
0.1
0
0.08
0.16
0.24
0.32
0.40
0.48
0.56
x_2
191485

Fig. 25

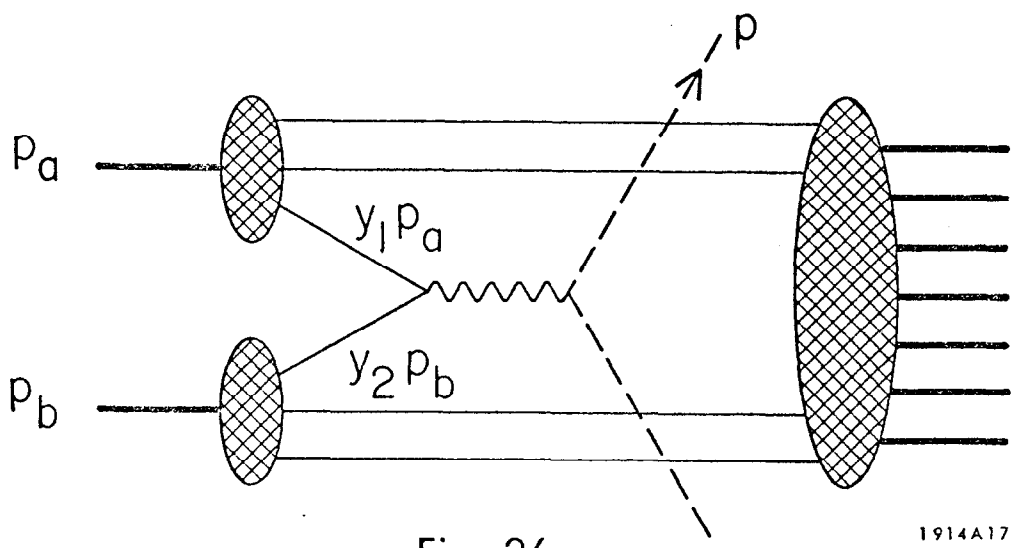

Fig. 26

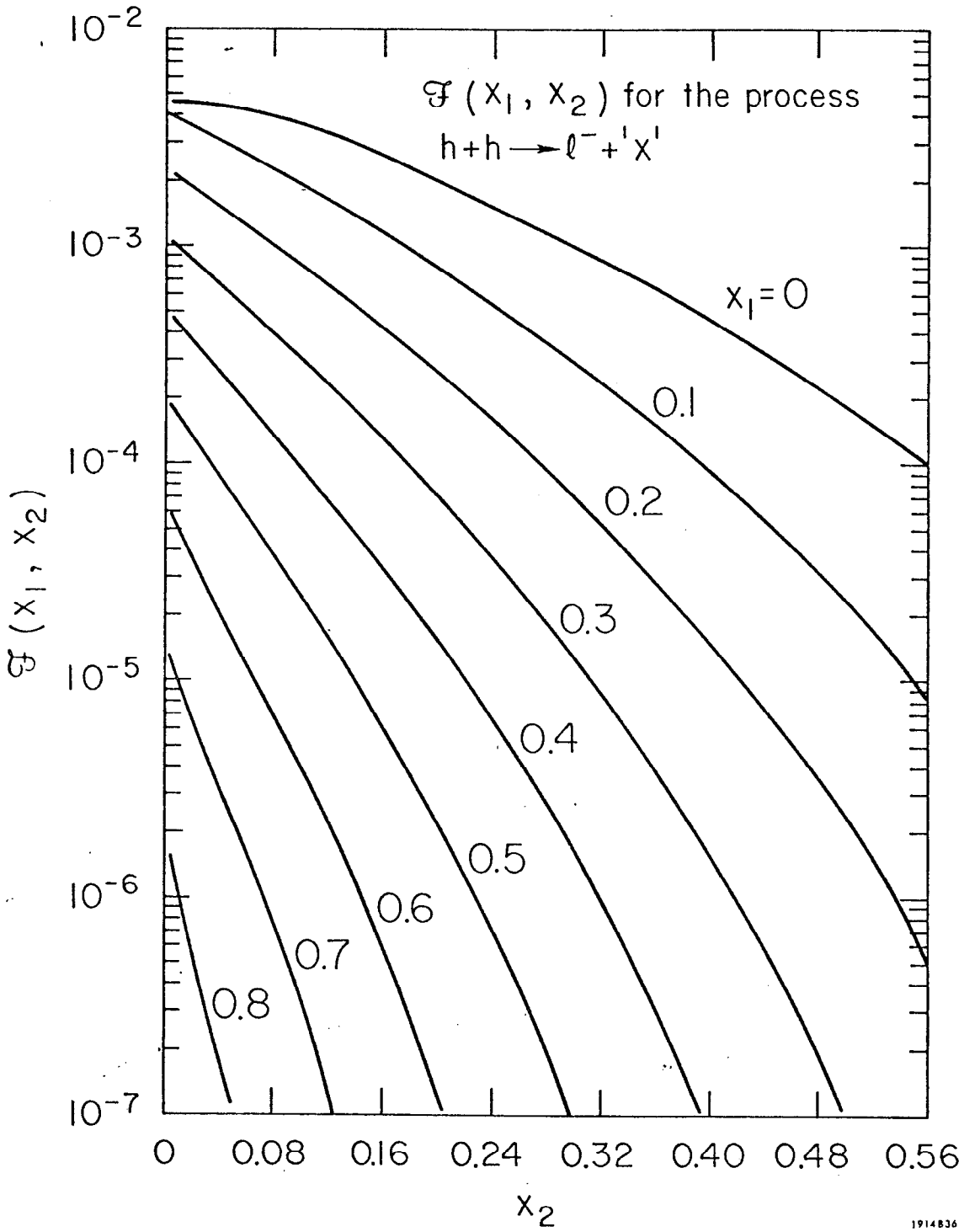
$\mathcal{F}(x_1, x_2)$ for the process
$h+h \rightarrow \ell^- + {}'X'$
$x_1 = 0$
0.1
0.2
0.3
0.4
0.5
0.6
0.7
0.8
10^{-2}
10^{-3}
10^{-4}
10^{-5}
10^{-6}
10^{-7}
$\mathcal{F}(x_1, x_2)$
0
0.08
0.16
0.24
0.32
0.40
0.48
0.56
x_2
1914836

Fig. 27

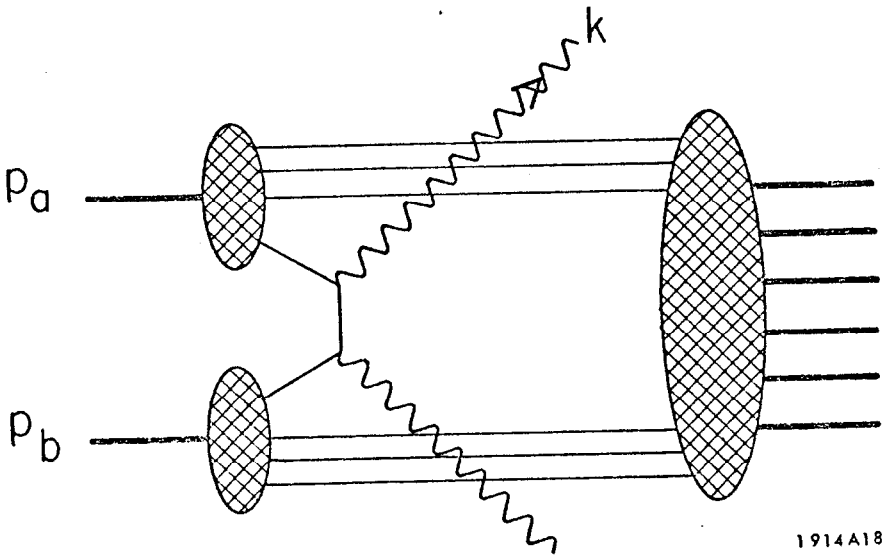

Fig. 28

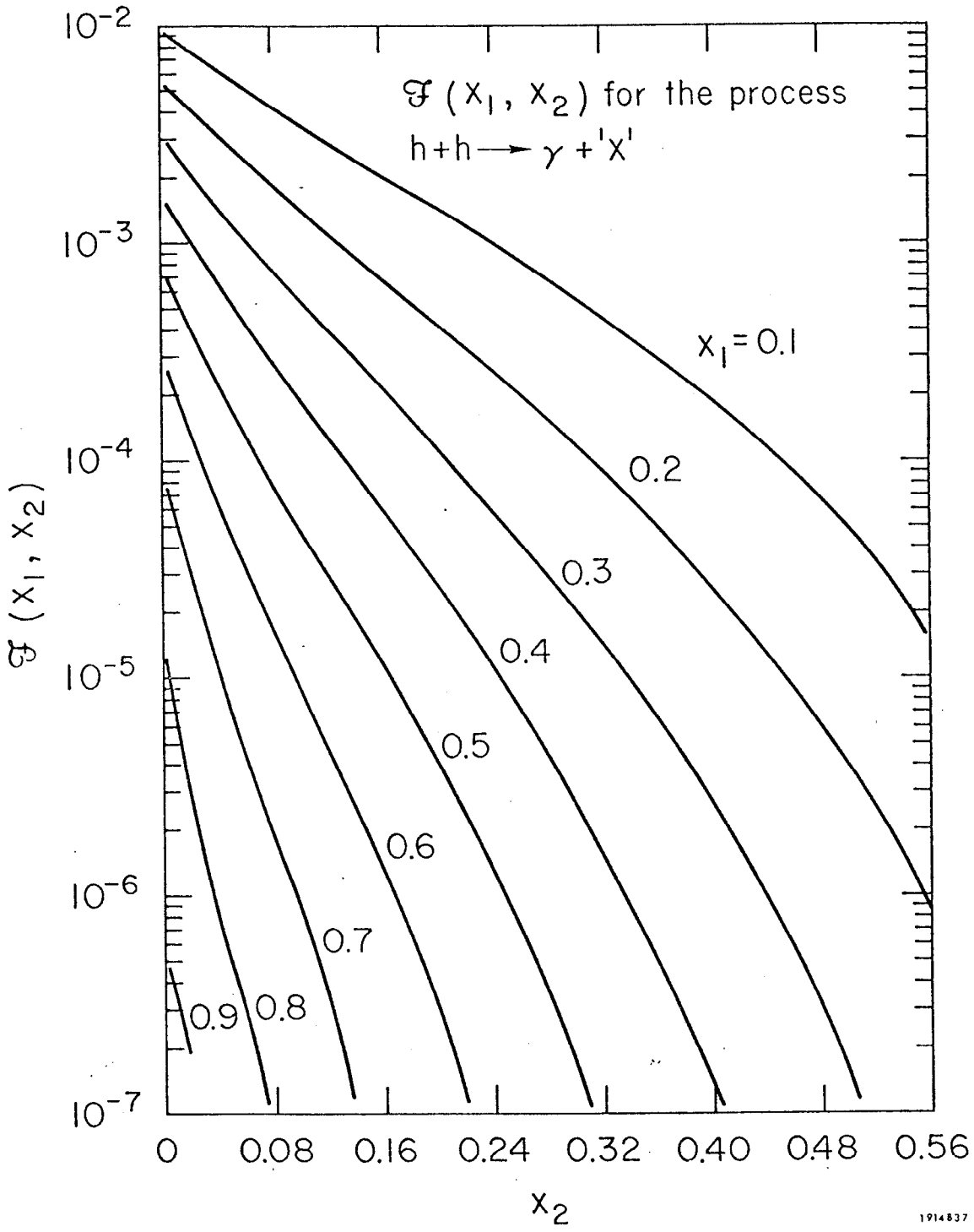
$\mathcal{F}(x_1, x_2)$ for the process
$h+h \rightarrow \gamma + 'X'$
$x_1 = 0.1$
0.2
0.3
0.4
0.5
0.6
0.7
0.8
0.9
10^{-2}
10^{-3}
10^{-4}
10^{-5}
10^{-6}
10^{-7}
$\mathcal{F}(x_1, x_2)$
0
0.08
0.16
0.24
0.32
0.40
0.48
0.56
x_2
1914837

Fig. 29

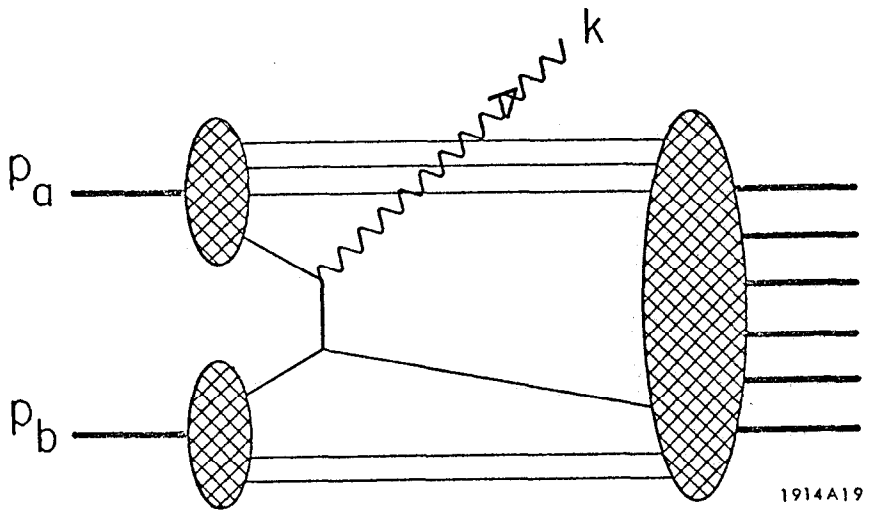

Fig. 30

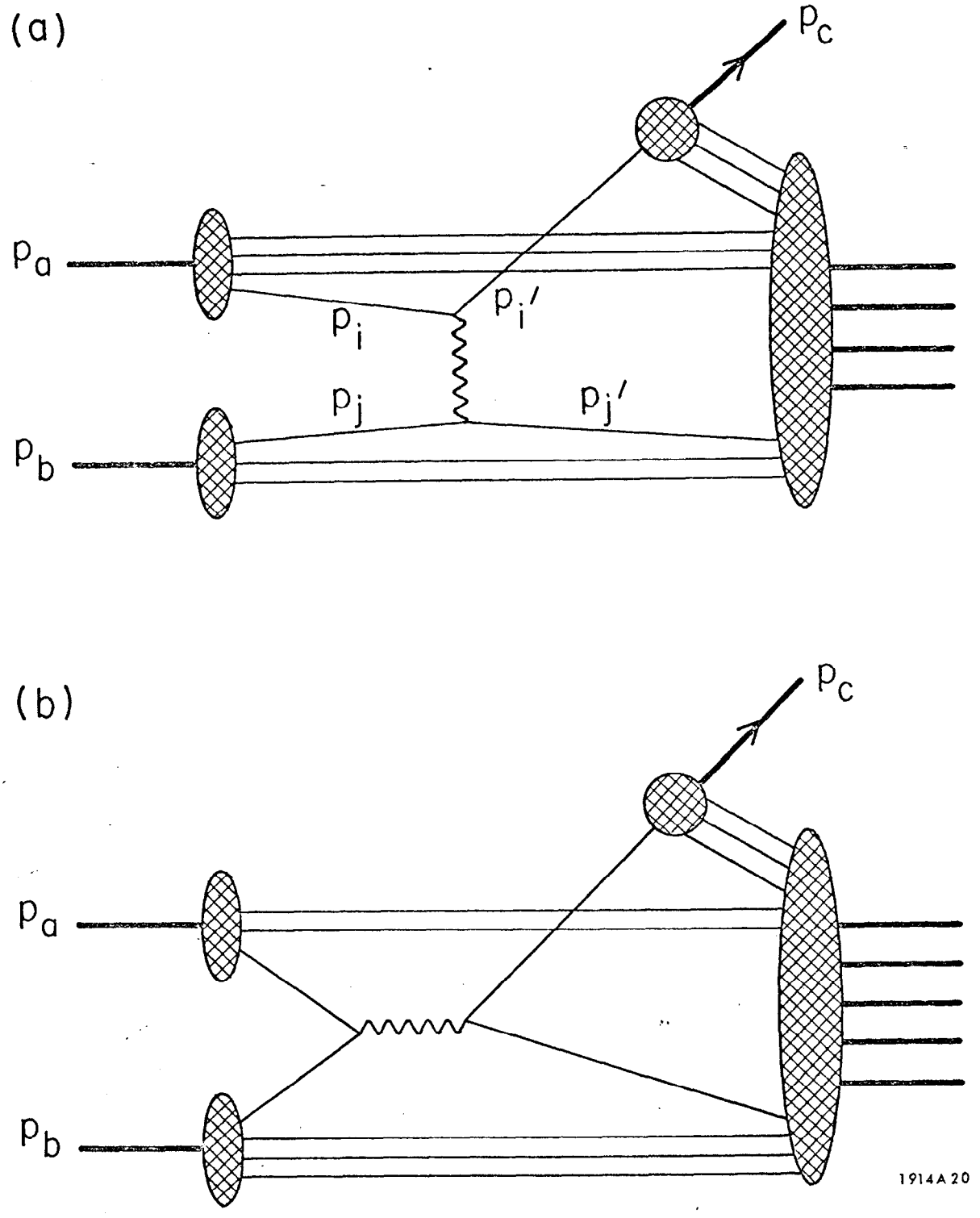

Fig. 31

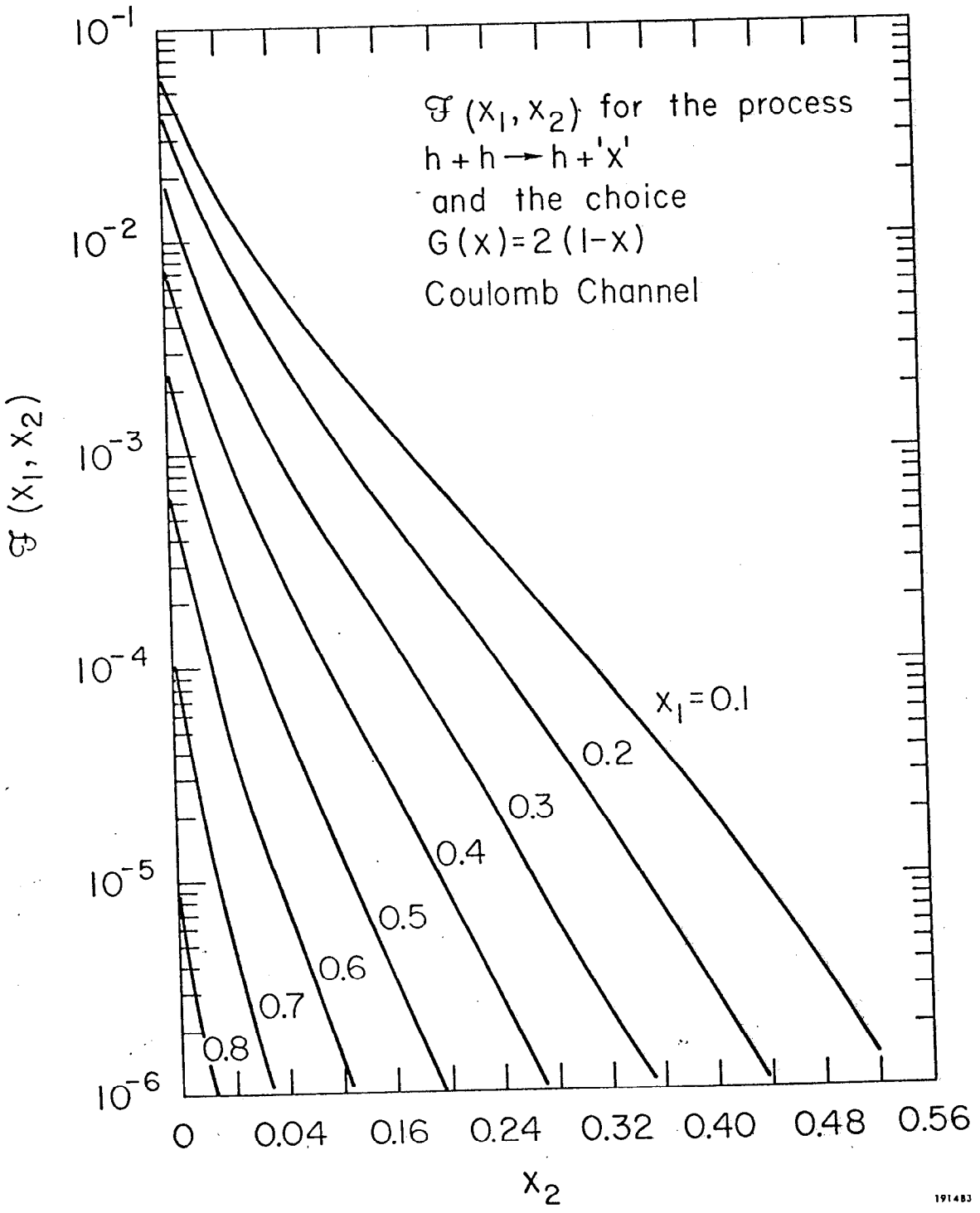
$\mathcal{F}(x_1, x_2)$ for the process
h + h → h + 'x'
and the choice
G(x) = 2(1-x)
Coulomb Channel
$\mathcal{F}(x_1, x_2)$
10^{-1}
10^{-2}
10^{-3}
10^{-4}
10^{-5}
10^{-6}
$x_1 = 0.1$
0.2
0.3
0.4
0.5
0.6
0.7
0.8
0
0.04
0.16
0.24
0.32
0.40
0.48
0.56
x_2
191483

Fig. 32

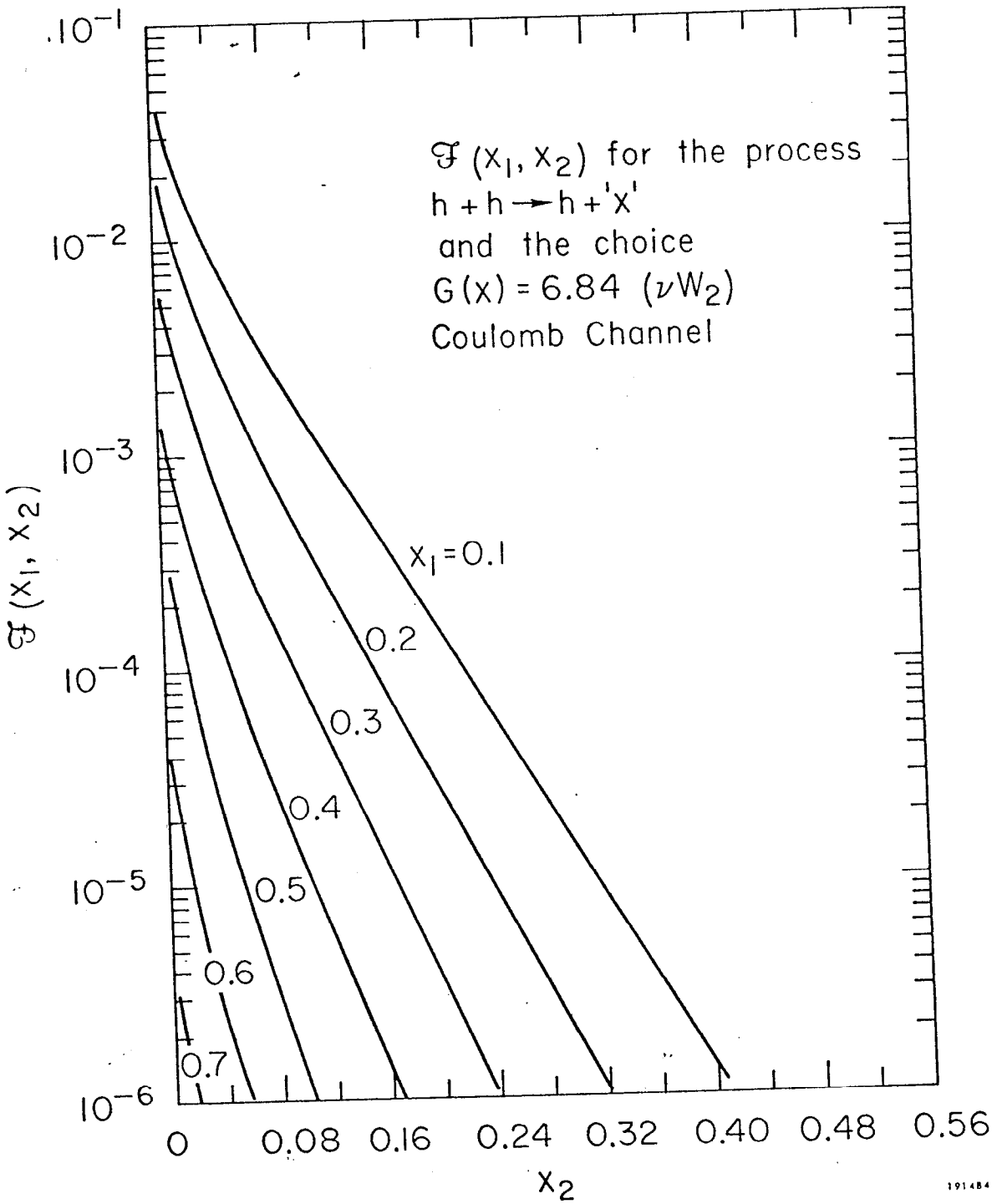
$\mathcal{F}(x_1, x_2)$ for the process
h + h → h + 'x'
and the choice
G(x) = 6.84 (νW_2)
Coulomb Channel
$\mathcal{F}(x_1, x_2)$
x_2
x_1=0.1
0.2
0.3
0.4
0.5
0.6
0.7
10^{-1}
10^{-2}
10^{-3}
10^{-4}
10^{-5}
10^{-6}
0
0.08
0.16
0.24
0.32
0.40
0.48
0.56
191484

Fig. 33

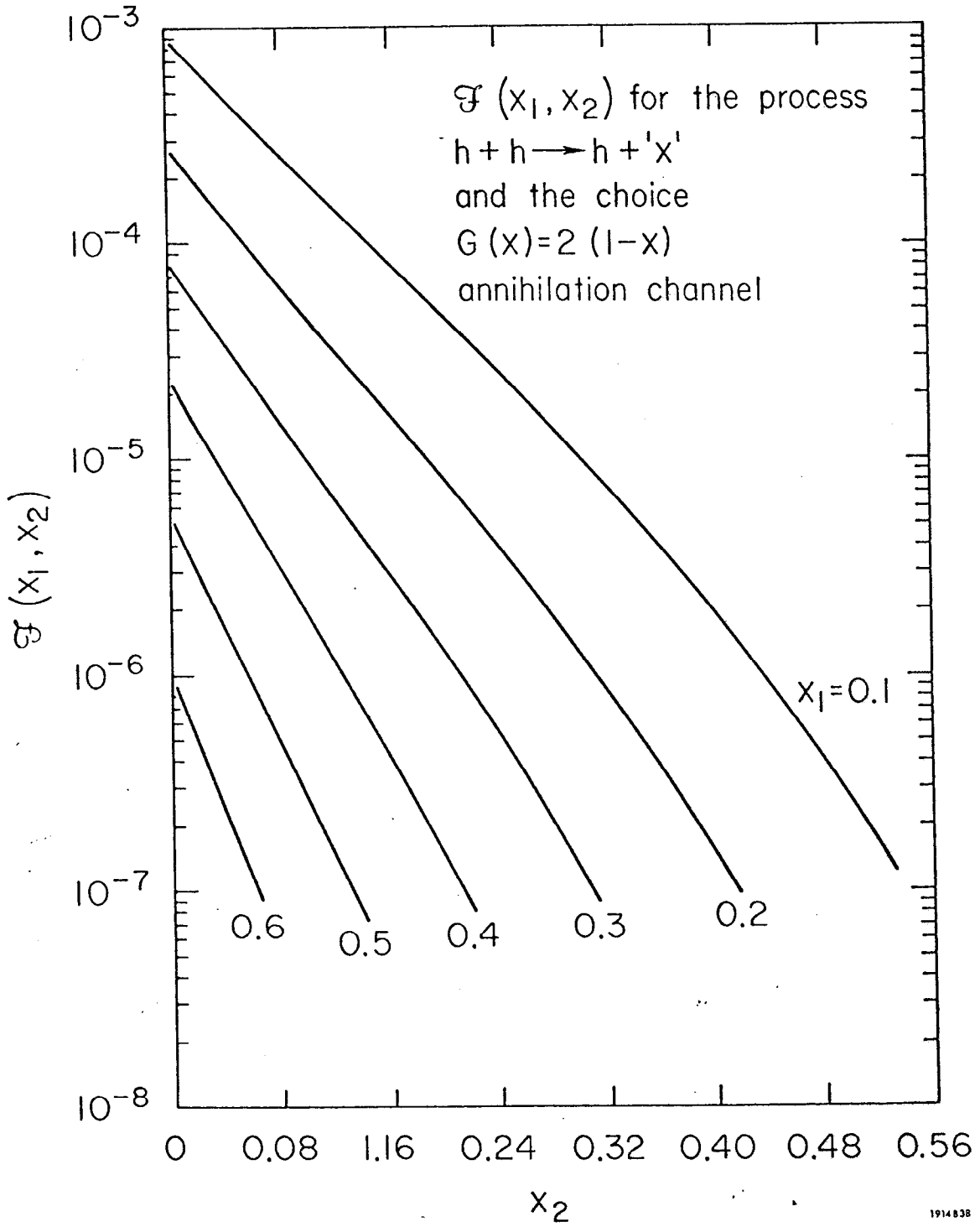
10^{-3}
10^{-4}
10^{-5}
10^{-6}
10^{-7}
10^{-8}
$\mathcal{F}(x_1, x_2)$
$\mathcal{F}(x_1, x_2)$ for the process
h + h → h + 'x'
and the choice
G (x) = 2 (1−x)
annihilation channel
x_1=0.1
0.2
0.3
0.4
0.5
0.6
0
0.08
1.16
0.24
0.32
0.40
0.48
0.56
x_2
1914838

Fig. 34

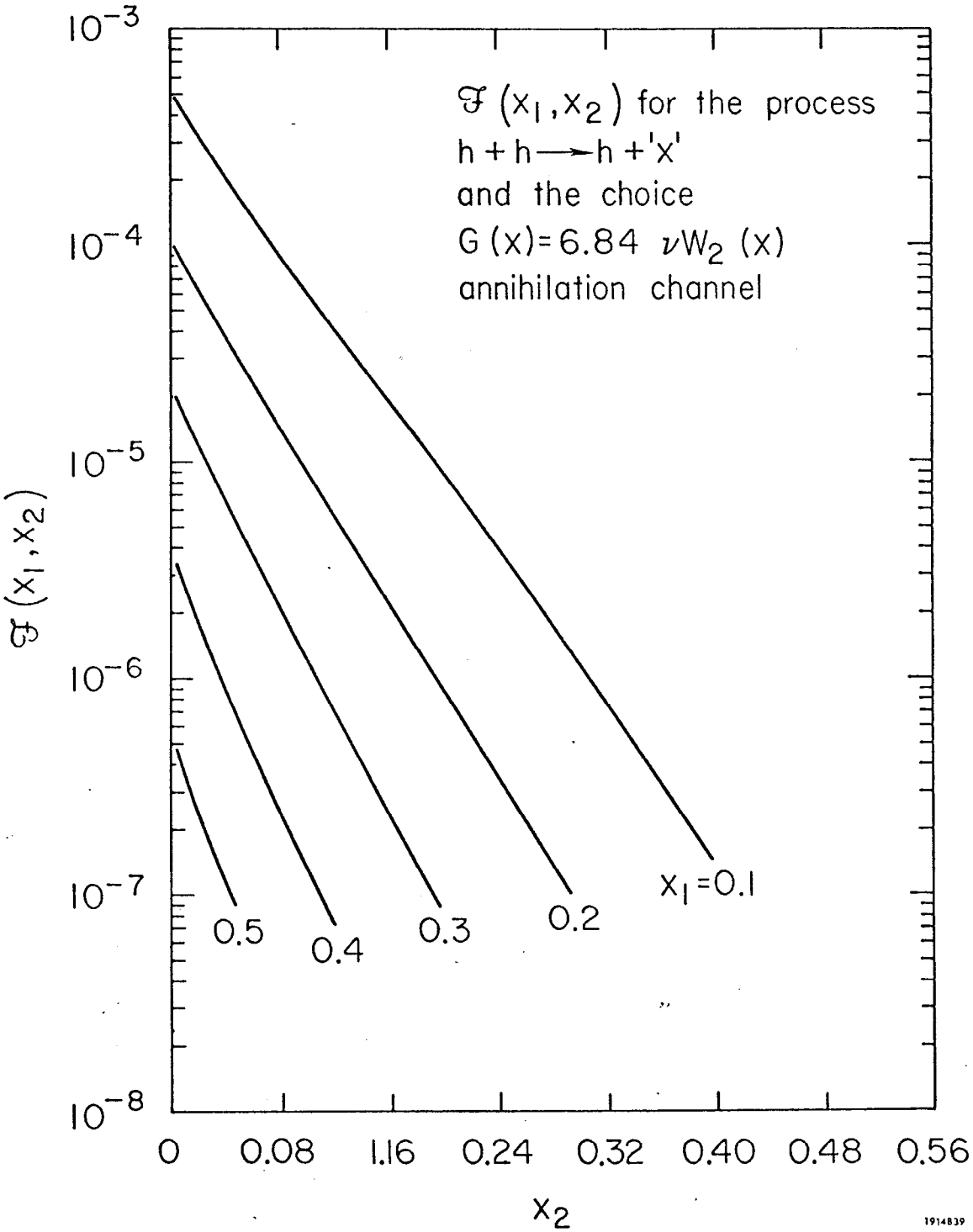
10^{-3}
10^{-4}
10^{-5}
10^{-6}
10^{-7}
10^{-8}
$\mathcal{F}(x_1, x_2)$
$\mathcal{F}(x_1, x_2)$ for the process
h + h ⟶ h + 'x'
and the choice
G (x) = 6.84 νW_2 (x)
annihilation channel
x_1 = 0.1
0.2
0.3
0.4
0.5
0
0.08
1.16
0.24
0.32
0.40
0.48
0.56
x_2
1914839

Fig. 35

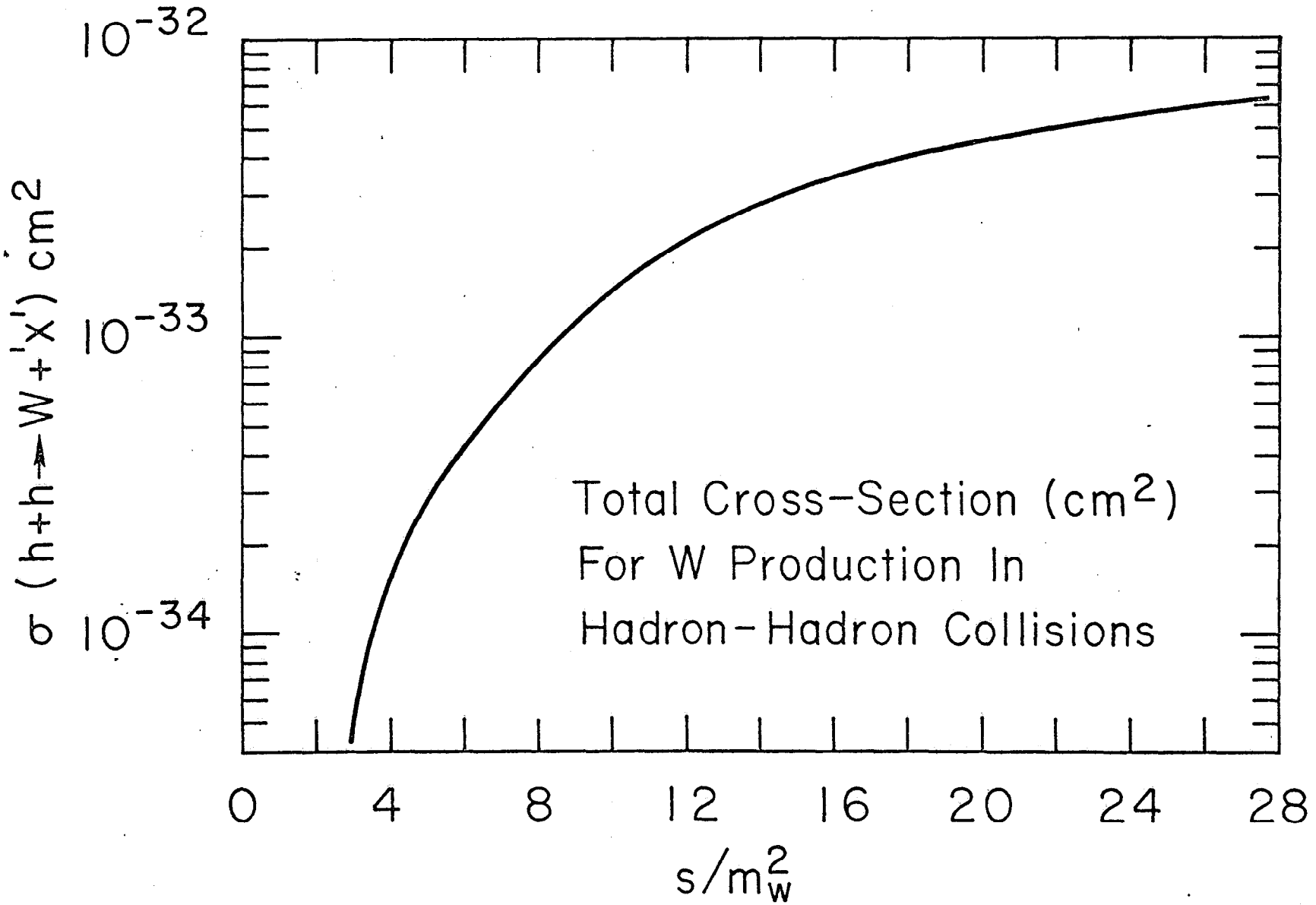

1914B10

Fig. 36

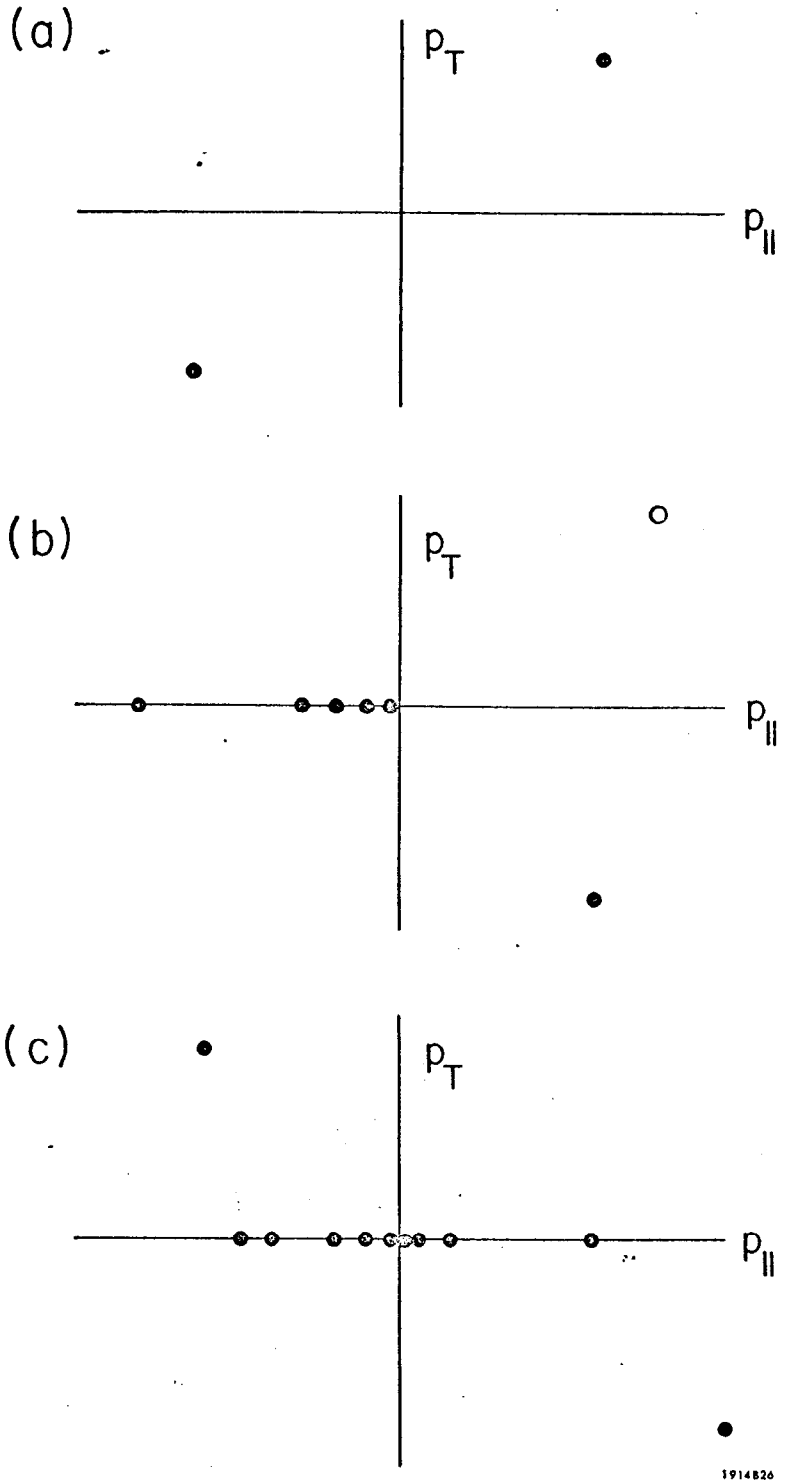

Fig. 37

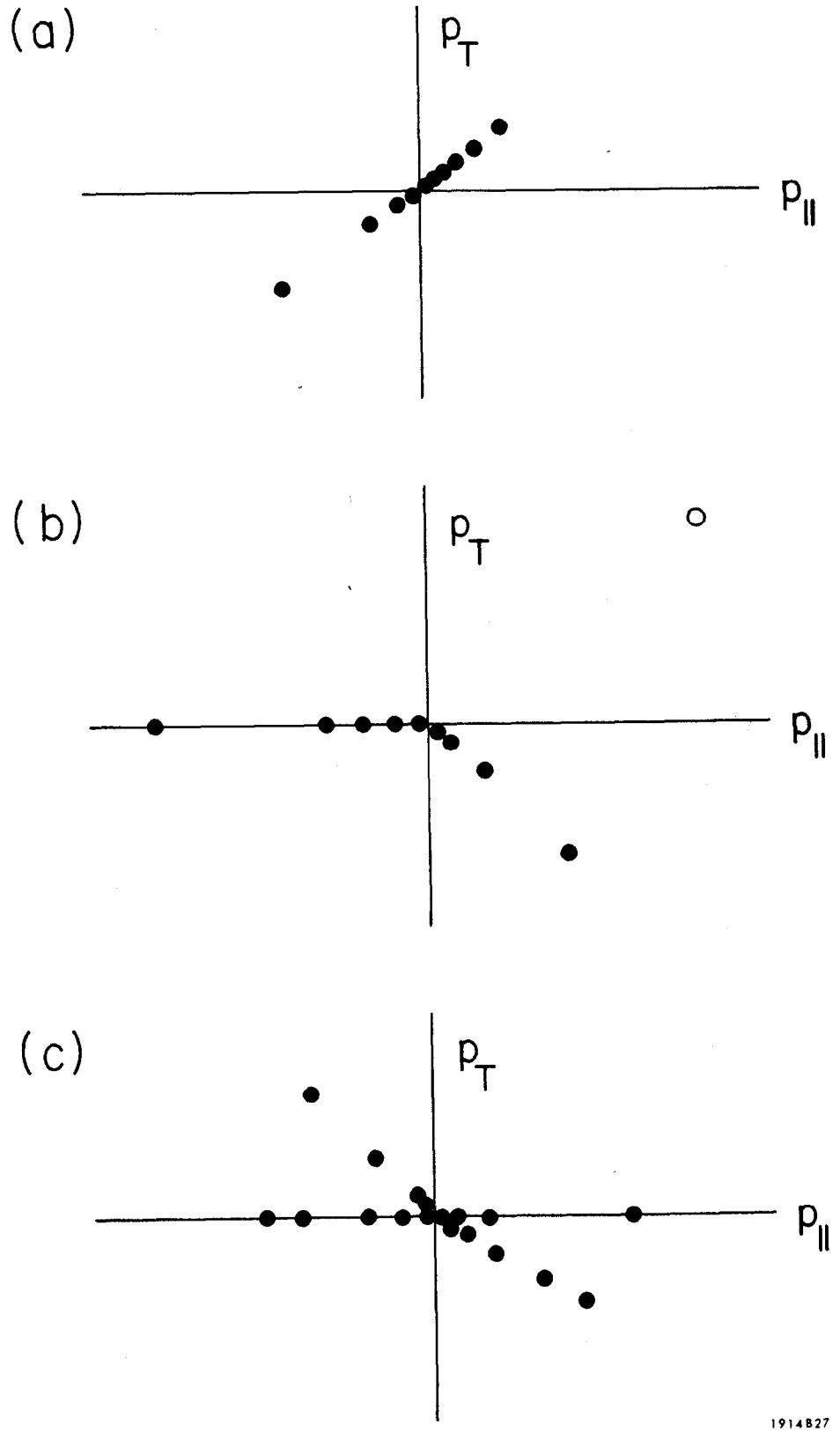

Fig. 38

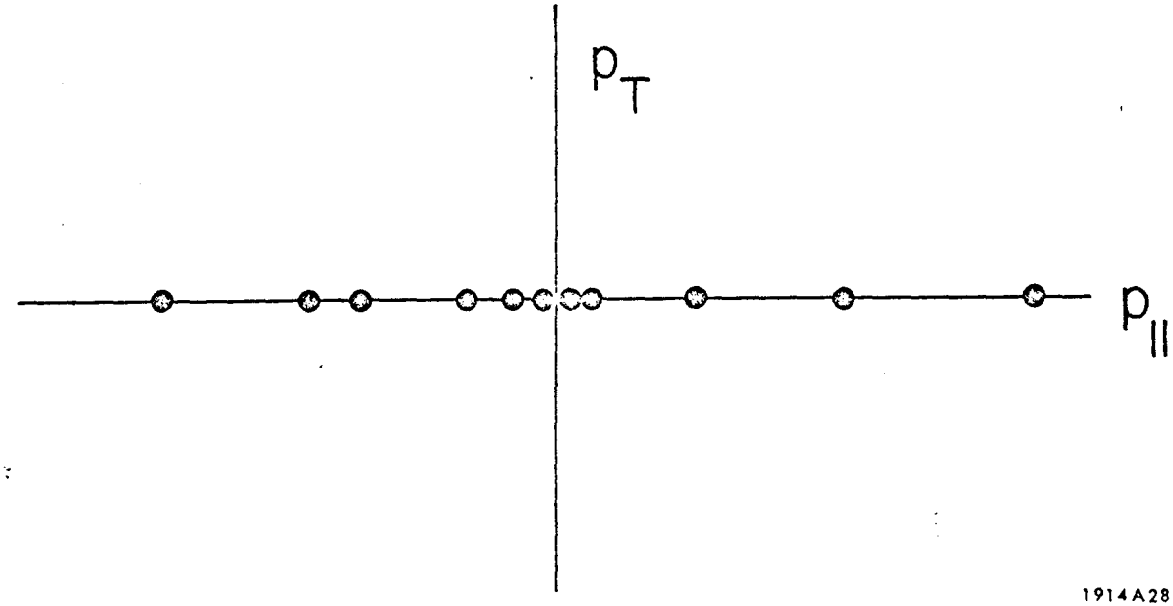

Fig. 39

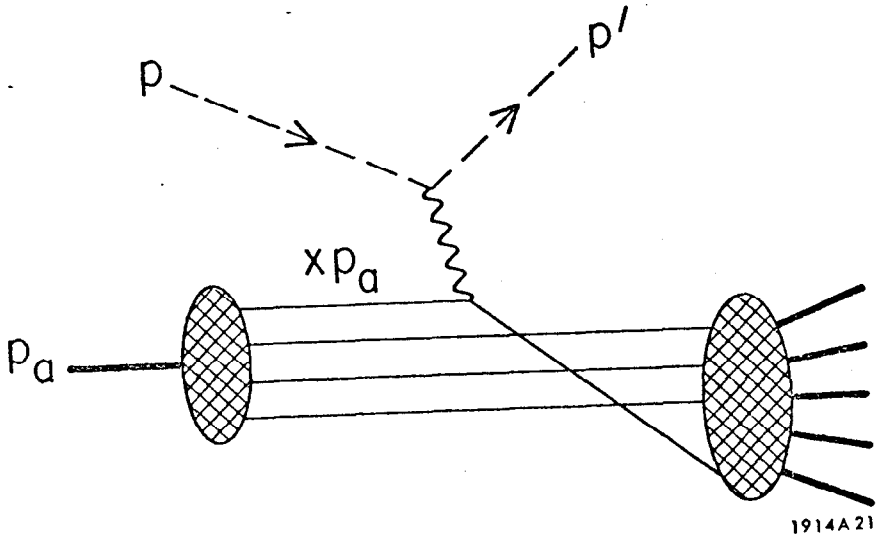

Fig. 40

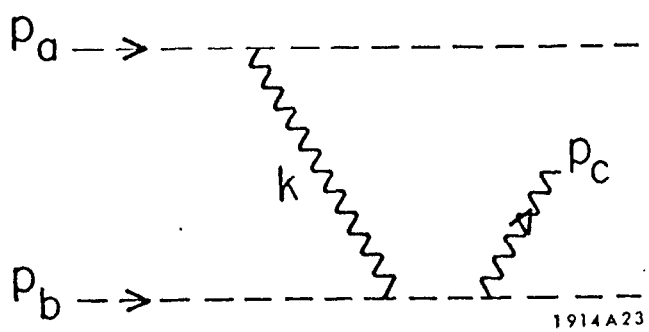

Fig. 41

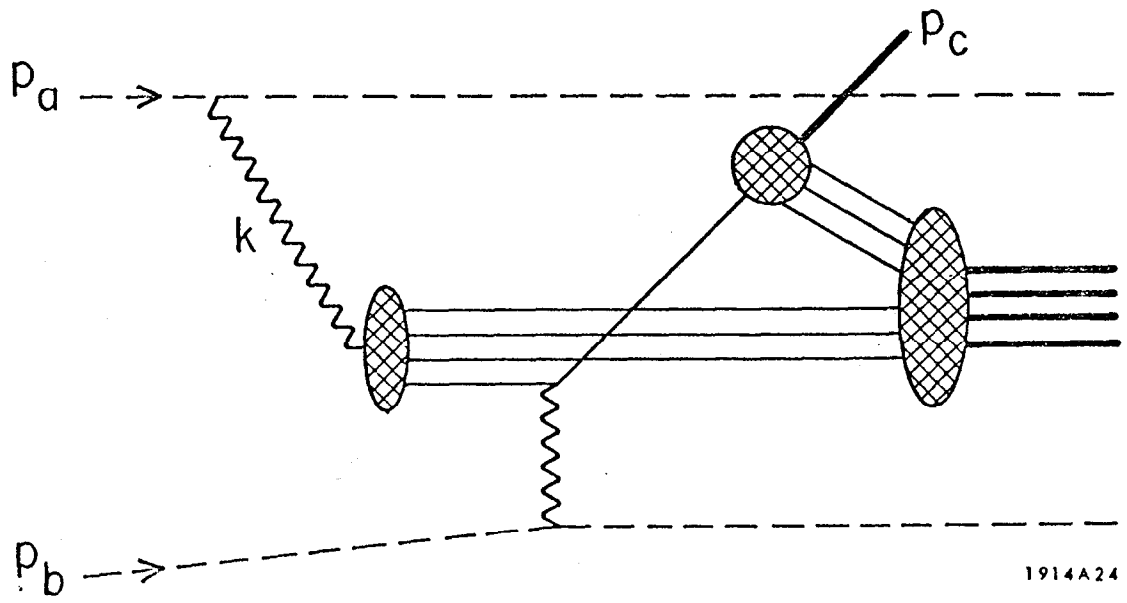

Fig. 42

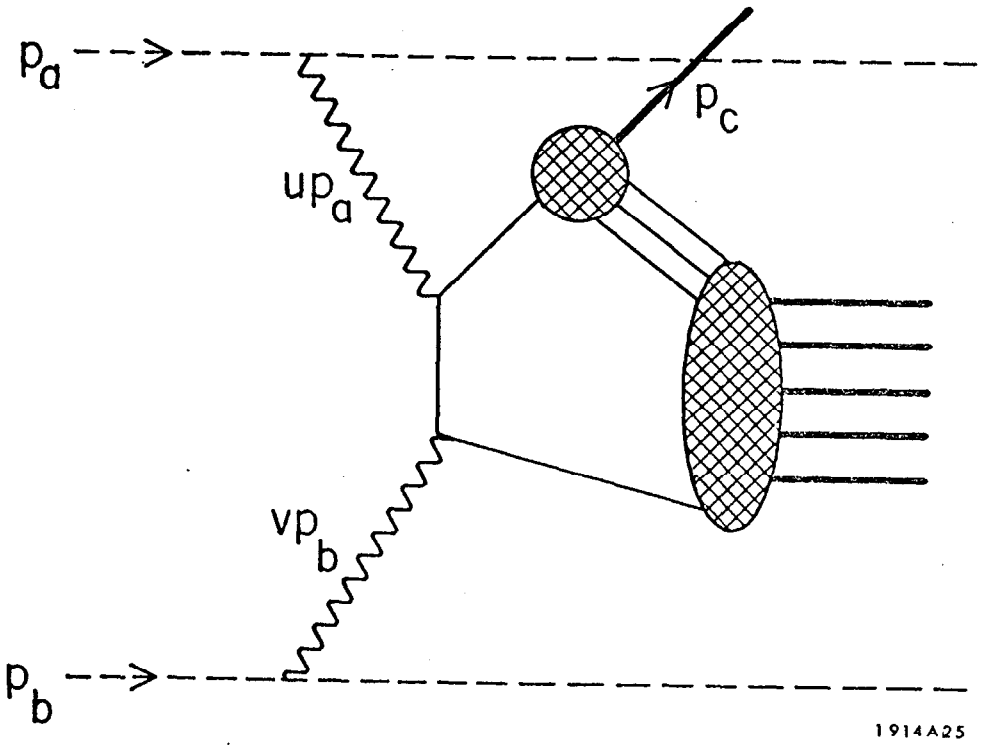

Fig. 43